

KfK 4653
März 1991

KfK Analysis of the SUPER-PHENIX-1 Control Rod Experiments Part 1: The Experimental Results

H. Giese
Institut für Neutronenphysik und Reaktortechnik
Projekt Nukleare Sicherheitsforschung

Kernforschungszentrum Karlsruhe



KERNFORSCHUNGSZENTRUM KARLSRUHE

Institut für Neutronenphysik und Reaktortechnik
Projekt Nukleare Sicherheitsforschung

KfK 4653

KfK Analysis of the SUPER-PHENIX-1 Control Rod Experiments
Part 1: The Experimental Results

H. Giese

Kernforschungszentrum Karlsruhe GmbH, Karlsruhe

Als Manuskript gedruckt
Für diesen Bericht behalten wir uns alle Rechte vor

Kernforschungszentrum Karlsruhe GmbH
Postfach 3640, 7500 Karlsruhe 1

ISSN 0303-4003

KfK Analysis of the SUPER-PHENIX-1 Control Rod Experiments Part 1: The Experimental Results

Abstract

The experimental start-up programme of the French fast breeder reactor SUPER-PHENIX-1 (SPX-1) comprised a considerable number of control rod experiments, the analysis of which represented one of the major activities of the 'SPX-1 task force', consisting of working groups at the CEA, ENEA, UKAEA, BN, INTERATOM and KfK. Both dynamic and static techniques were employed in these experiments and frequently the two types of techniques were used in parallel to check the consistency of their results.

The vast majority of the experiments, however, employed a static technique which is widely used for the assessment of reactor subcriticality and rod worths and which is generally known as the 'Modified Source Multiplication' or 'MSM' technique. While particularly appealing to the experimentalist as once calibrated (e.g. with the help of a rod drop experiment) it only requires the recording of stable subcritical detector count rates, this technique has a severe disadvantage from the analysis point of view: It necessitates calculated correction factors to be applied to the direct experimental results to give reliable answers on the reactor subcriticality. The question therefore arose to what extent these correction factors (and thus the final experimental results of this technique) could depend on the calculation path and on the basic data used for their production.

To clarify whether such a dependence on individual parameters existed, the 'SPX-1 task force' defined a number of control rod configurations for which the different working groups were encouraged to produce MSM correction factors, each group using its own codes, calculation strategies and basic data.

The present report gives a detailed description of the correction factor calculations carried out at KfK and of the experimental results obtained with these factors.

A first comparison with the CEA results shows that the dependence on individual parameters is insignificant, provided that the calculations were adequately adjusted to well reproduce experimental rod worths and subcritical reactivity levels.

Die KfK Auswertung von SUPER-PHENIX-1 Kontrollstabexperimenten Teil 1: Die experimentellen Resultate

Zusammenfassung

Das experimentelle Anfahrprogramm des französischen schnellen Brutreaktors SUPER-PHENIX-1 (SPX-1) beinhaltete u.a. eine beträchtliche Anzahl von Kontrollstabexperimenten, deren Auswertung eine der wesentlichen Aufgaben der 'SPX-1 task force' darstellte. Letztere umfaßt Arbeitsgruppen bei der CEA, ENEA, UKAEA, BN, INTERATOM und der KfK. Bei diesen Experimenten wurden sowohl dynamische als auch statische Meßtechniken eingesetzt, z.T. auch beide Meßtechniken parallel, um die Konsistenz ihrer Ergebnisse zu prüfen.

Die Mehrzahl der Experimente verwendete jedoch eine statische Technik, die häufig zur Ermittlung von Unterkritikalitätsniveaus und von Kontrollstabwirksamkeiten eingesetzt wird und unter dem Namen 'Modifizierte Quellmultiplikation' (MSM) bekannt ist. Obwohl vom experimentellen Standpunkt besonders ansprechend, da sie nach einmaliger Eichung (z.B. durch einen 'Rod-drop') nur noch die Registrierung stationärer unterkritischer Zählraten erfordert, hat diese Methode doch einen entscheidenden Nachteil: Um zuverlässige Aussagen über die Unterkritikalität des Reaktors zu erhalten, müssen an den experimentellen Rohresultaten berechnete Korrekturfaktoren angebracht werden. Es stellte sich somit zwangsläufig die Frage, ob und inwieweit diese Korrekturfaktoren (und damit die experimentellen Ergebnisse dieser Methode) von der zu ihrer Bestimmung verwendeten Berechnungsstrategie und Basisdaten abhängen.

Um zu klären, ob eine solche Abhängigkeit von individuellen Parametern vorliegt, hat die 'SPX-1 task force' angeregt, daß die verschiedenen Arbeitsgruppen für eine bestimmte Auswahl von Kontrollstabkonfigurationen unter Benutzung ihrer eigenen Codes, Berechnungsstrategien und Basisdaten, MSM-Korrekturfaktoren produzieren.

Der vorliegende Bericht gibt eine detaillierte Schilderung der im KfK durchgeführten Korrekturfaktorrechnungen und der mit den erhaltenen Faktoren produzierten experimentellen Resultate.

Ein erster Vergleich mit den bei der CEA erhaltenen Resultaten zeigt, daß die Abhängigkeit der Korrekturfaktoren von individuellen Parametern insignifikant ist, vorausgesetzt, daß die Rechnungen in adäquater Weise an experimentelle Kontrollstabwirksamkeiten und unterkritische Reaktivitätsniveaus angepaßt wurden.

Table of contents

	Page
I. Introduction	1
II. Description of the SUPER-PHENIX-1 core	3
III. The modified source multiplication technique MSM	5
III.1 Short description of the theoretical basis	5
III.2 Problems arising in the context of MSM correction factor calculations	6
IV. MSM measurements in SUPER-PHENIX-1	11
IV.1 The configurations	11
IV.2 Subcritical counting	12
IV.3 The calibration state ('Etalon')	12
V. General remarks on MSM correction factor calculations	15
V.1 Cross section preparation	15
V.2 Types of calculations	16
VI. Production of MSM correction factors for C1D	18
VI.1 The calibration state (Etalon) SCP 929 SAC↓ of C1D	18
Assessment of the numerator of the correction factors G_i	19
Assessment of the denominators of the correction factors G_i	23
VI.2 The selected configurations of C1D	28
The iterative graphical solution	29
The direct graphical solution	30
The analytical solution	30

	Page
VII. Production of MSM correction factors for CMP	34
VII.1 Introductory comments on the different adjustment strategies employed for 2D and 3D calculations	34
VII.2 The calibration state (Etalon) SCP 542 SAC↓ of CMP	37
Assessment of the numerator of the correction factors G_i	38
Assessment of the denominators of the correction factors G_i	40
VII.3 The selected configurations of CMP	43
VIII. Some remarks on uncertainties of experimental results	47
VIII.1 The present state	47
VIII.2 Recent considerations	48
IX. Conclusions	51
Acknowledgements	52
References	53
Appendix 1 : Calculations concerning the C1D Etalon	55
Appendix 2 : Calculations concerning the selected configurations of C1D	71
Appendix 3 : Calculations concerning the CMP Etalon	79
Appendix 4 : Calculations concerning the selected configurations of CMP	87
Figures	109

List of Figures

Page

Figure 1	Core loading of SUPER-PHENIX-1, core version C1D	109
Figure 2	Core loading of SUPER-PHENIX-1, core version CMP	110
Figure 3	Layout of an SCP absorber	111
Figure 4	Schematic construction of a SAC absorber assembly	112
Figure 5	Layout of the SAC absorbers	113
Figure 6	Axial position of the B_4C column of SCP control rods with respect to the fissile loading at 180°C	114
Figure 7	Axial position of the B_4C column of SAC control rods with respect to the fissile loading at 180°C	115
Figure 8	The determination of $\rho_{cal} \cdot C_{cal}$ for the C1D Etalon	116
Figure 9	Correction factor G for SCP 920 B1↓ B2↑ in C1D	117
Figure 10	Correction factor F for SCP↓ SAC↑ in C1D	118
Figure 11	The determination of $\rho_{cal} \cdot C_{cal}$ for the CMP Etalon (2D calculation)	119
Figure 12	The determination of $\rho_{cal} \cdot C_{cal}$ for the CMP Etalon (3D calculation)	120

I Introduction

Control rod experiments formed a substantial part of the SUPER-PHENIX-1 (SPX-1) start-up programme. Such experiments were made in both the first critical core with minimum excess reactivity and the fully loaded core. The two core versions are frequently referred to as the 'CID' core (coeur de 1^{ère} divergence) and the 'CMP' core (coeur de montée en puissance). While in the CID core relatively few experiments were made, devised predominantly to confirm the fulfillment of safety requirements, measurements in CMP also covered numerous physics aspects.

Different experimental techniques have been employed in the course of these measurements, based on both dynamic and static neutron flux response upon reactivity insertion.

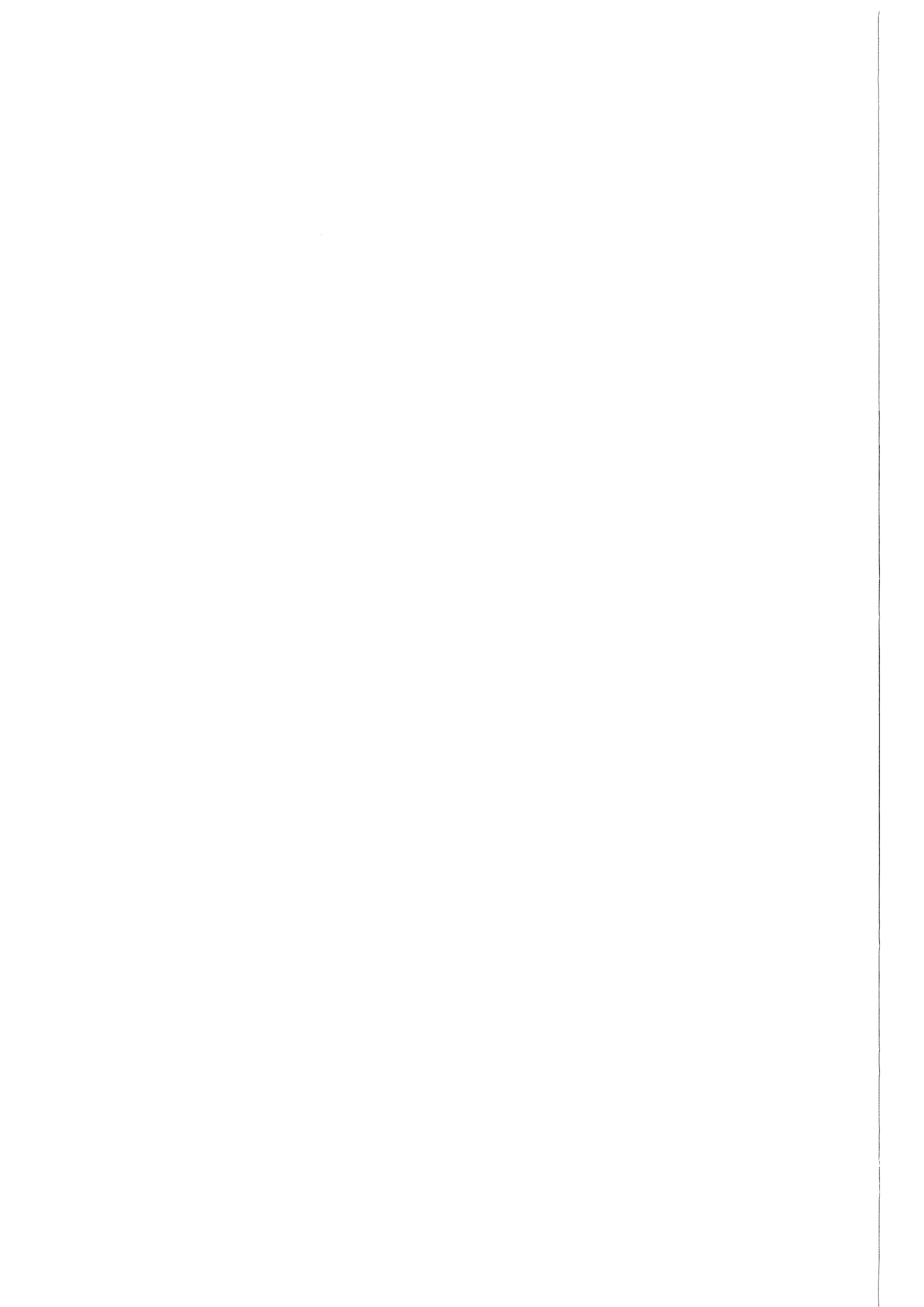
Dynamic techniques included 'Rod drop', 'Balancement' (i.e. reactivitywise compensating insertion of one rod and withdrawal of another for differently interacting rod couples) and stepwise insertion and withdrawal of a single rod around its critical insertion depth. The analysis of these experiments is finished and has been documented by CEA (References / 1 and 2 /).

The majority of the measurements was made using a static technique, the so-called Modified Source Multiplication method (MSM) / 6 / in which the subcriticality of the reactor is deduced from static detector count rates. While representing the most attractive technique in view of its experimental simplicity, the analysis is impeded by the necessity of calculated corrections to be applied to the direct experimental results. Different calculation strategies can be chosen to assess these corrections and the question arose whether these would eventually lead to the same corrections and thus to the same corrected experimental results.

To clarify this point of essential importance, the SPX-1 analysis task force has agreed on its meeting of October 27th, 1987 on a list of control rod arrays for the CID and CMP core loading versions for which MSM-correction factors should be produced by the CEN-Cadarache, by KfK and possibly by other partners participating in the SPX-1 analysis. Each of these groups was advised to use their own standard data banks and calculation methods.

The final objective of these activities was to arrive at the definition of a unique set of experimental results, to be used in the future by all partners participating in the SPX-1 analysis as a standard reference.

The present report gives a detailed description of the KfK approach to produce MSM correction factors, and of the experimental results obtained with the use of this approach.



II Description of the SUPER-PHENIX-1 core

Cross section views of the fissile loading of the first critical core C1D with minimum excess reactivity and of the fully loaded core CMP are shown in Figures 1 and 2. The reactor comprises a two zone plutonium fuelled conventional core, surrounded axially and radially by uranium blankets and steel reflectors and has a 120° periodicity. At 20°C, the hexagonal element pitch over the flats is 17.9 cm, resulting in an average area per subassembly of 277.4832 cm². The nominal core height is 100 cm. As the control rod experiments to which the present analysis refers were performed at the standard handling temperature of 180°C it appears useful to also indicate the dimensions corresponding to this temperature.

With axial and radial linear expansion factors of 1.00114 and 1.00269 / 13 / for the transition from 20°C to 180°C the dimensions at 180°C become:

Pitch:	17.9482 cm
Area per subassembly:	278.9781 cm ²
Core height:	100.1140 cm

The core region comprises 190 inner core subassemblies and 168 outer core subassemblies with corresponding enrichments of about 16 at.% and 19 at.% Pu/Pu + U. Cylindricalised core radii at 180°C are 133.932 cm for the inner zone and 188.468 cm for the outer zone, respectively.

The following singularity types are present in the core region:

- . 18 diluent assemblies.
- . 33 dummy fuel elements present only in the first critical core C1D.
These elements were all located in the inner core zone.
- . 21 SCP control rods representing the main control system.
(SCP = 'système de commande principale')
- . 3 SAC control rods representing the secondary shut down system.
(SAC = 'système d'arrêt complémentaire')

The internal structure of the SCP and SAC control rod absorbers is presented in Figures 3 to 5.

SCP control rods (Fig.3) comprise an outer hexagonal and an inner cylindrical steel tube, the latter containing a cluster of 31 steel pins filled with boroncarbide of 90 at.% ¹⁰B enrichment. The gaps between this cluster and the surrounding cylindrical steel tube are filled with 8 steel pins of adequate shape. The gaps between all pins and between inner and outer steel tube are filled with sodium.

The length of an SCP absorber from the first to the last boroncarbide pellet is 114.5 cm at 20°C, and expands to 114.63 cm at 180°C.

SAC control rods comprise a train of three individual absorber units running in a hexagonal outer steel tube. These absorber units, the upper two of which are identical, are connected to each other and to the driving mechanism by universal joints. A schematic drawing of the absorber assembly is shown in Figure 4.

The length of the upper and central absorber unit at 20°C is 30 cm, that of the lower unit is 16.8 cm.

The upper and central units contain 4 absorber pins each. At 20°C, the diameter of the boroncarbide pellets over the lower 25 cm of these pins is 4.7 cm. Over the remaining 5 cm at the top of each pin it is 4.5 cm (Figures 4 and 5).

The lower unit contains 8 absorber pins. At 20°C, the diameter of the boroncarbide pellets in these pins is 2.2 cm over the lower 11.8 cm and 2.0 cm over the top 5 cm (Figures 4 and 5).

The corresponding dimensions at 180°C can be derived by using the axial and radial expansion factors quoted above.

As for the SCP control rods, boroncarbide is used as an absorber with a ¹⁰B enrichment of 90 at.%.

Figures 6 and 7 show the axial location of the absorber parts of SCP and SAC with respect to the fissile core region when the control rods are said to be fully raised and fully inserted. The dimensions given in Figures 6 and 7 refer to the realistic temperature at the time of the experiments, i.e. 180°C.

When SCP is said to be fully raised, its lower end (i.e. the bottom of its lowest boroncarbide pellet) is located 0.2 cm above the upper core/blanket interface, and when the rod is fully inserted the lower end is 1.4 cm below the lower core/blanket interface.

The SCP insertion levels ('Cotes') found in documentation have to be interpreted as the distance in [mm] by which the absorber has been raised from full insertion. The indication SCP 542 (critical insertion in CMP) therefore means that the lower absorber end is located 52.8 cm above the lower core boundary or that the absorber is inserted into the core by 47.3 cm.

The overall length of a SAC absorber is 97.08 cm (from the first to the last boroncarbide pellet) and thus less than the core height. When the rod is fully raised, the lower end of the absorber is located 6.8 cm above the upper core/blanket interface to avoid excessive burnup during plant operation, and when the rod is fully inserted its lower end is located 1.06 cm above the lower core/blanket interface.

The neutron flux can be monitored by:

- The reactor operation instrumentation consisting of three clusters of under-vessel detectors located in the positions marked GDN (GDN = 'guide des neutrons', see Figures 1 and 2). Each cluster comprises two ³He detectors, two ²³⁵U fission chambers and one ionisation chamber.
- Three ²³⁵U fission chambers of 12 cm length located at 3 axial positions in a central channel of the core centre subassembly. To provide sufficient space for this channel, 19 fissile pins had been removed from this subassembly and replaced by a cylindrical steel tube. The mechanical setup that was inserted into the central channel to hold the chambers at the desired axial position is normally referred to as the 'BOUPHY' (BOUPHY = 'bouchon physique').

During the majority of the experiments, two chambers 'touched' the core/axial breeder interface from the core side, while the third chamber was centered on the core midplane.

III The modified source multiplication technique MSM

III.1 Short description of the theoretical basis

The 'Modified Source Multiplication Method' MSM / 6 / is based on the fact that according to the monokinetic point reactor model the count rate of any detector recording the neutron flux of a subcritical reactor with a driving neutron source is directly proportional to the strength of that neutron source and to the detector efficiency and inversely proportional to the subcriticality of the reactor. This means that the product of count rate and subcriticality is a constant:

$$\rho \cdot C = \text{const.} \quad (1)$$

Once the constant is known, any subcritical state of the reactor can easily be identified by a simple static count rate measurement. The constant is assessed by putting the reactor to a well defined subcritical level ρ_{cal} , the so-called calibration state or 'Etalon', and by recording the associated detector count rate C_{cal} .

An unknown subcriticality ρ_u of the reactor is thus obtained from the associated count rate C_u as

$$\rho_u = \frac{\rho_{cal} \cdot C_{cal}}{C_u} \quad (2)$$

For realistic reactors, however, and in particular in the case of control rod experiments in such reactors, the situation is complicated by the fact that frequently the point reactor model is not strictly valid, so that the product of subcriticality and detector count rate is no longer constant but varies with the individual subcritical control rod array. This variation is a consequence of changes in detector efficiency and in the effective strength of the inherent neutron source when passing from the calibration array to the control rod array in question. Depending on the magnitude of these variations, equation (2) will only be able to give a more or less approximate answer on the subcriticality of the reactor.

To obtain a correct answer, one is obliged to apply to the reactivity value obtained from equation (2) a correction factor **F** which accounts for the array dependent change of $\rho \cdot C$ relative to the calibration configuration. This so-called MSM correction factor **F** cannot be determined by experiments but has to be assessed by calculations. To avoid possible confusion between calculated and measured quantities, the latter will in the further course of this report always be identified by a pre-superscript 'e', i.e. ${}^e\rho$ and eC , while the calculated quantities will be simply referred to as ρ and C .

The correct experimental subcriticality is therefore obtained from the following equation:

$$\rho^{MSM} = \frac{{}^e\rho_{cal} \cdot {}^eC_{cal}}{{}^eC} \cdot \mathbf{F} \quad (3)$$

The correction factor **F** has the form:

$$\mathbf{F} = \frac{\rho \cdot C}{\rho_{cal} \cdot C_{cal}} \quad (4)$$

with the calculated detector count rate $C = \langle \Sigma_{det} \cdot \Phi^{inh} \rangle$. Σ_{det} is the macroscopic cross section of the active detector layer. As isotopic densities of the detector layer cancel out in the count rate ratio of Eq.(4), most analyses use microscopic instead of

macroscopic detector cross sections. In the present case σ_f of ^{235}U was always used for σ_{det} , since until now only the count rates of the central ^{235}U fission chamber have been analysed (see Sec. IV.2).

Φ^{inh} is the flux solution of an inhomogeneous (source-mode) calculation. The pointed brackets symbolize integration over energy and over the volume of the active detector layer.

One should note that the result of equation (2), representing the uncorrected (point-reactor) subcriticality of the reactor as obtained directly from the experiments is often referred to as ${}^e\rho^{MSA}$, the superscript MSA originating from the french 'multiplication de source approchée'.

Equation (3) can therefore be abbreviated as

$$\rho^{MSM} = {}^e\rho^{MSA} \cdot \mathbf{F} \quad (5)$$

For reasons of simplicity, the expression ${}^e\rho^{MSA}$ will frequently be encountered in the context of uncorrected experimental results discussed later in this report.

The principal disadvantage of the MSM-method is thus that results of calculations interfere with experimental results and that therefore the uncertainty of the latter can become a question of calculational precision. To what extent calculation uncertainties influence the MSM result depends clearly on the particular situation. If for a given control rod array the reactor behaves similar to a point reactor, i.e. the detector efficiency and effective source strength vary little with respect to the Etalon and hence \mathbf{F} differs little from unity, e.g. by 1%, even an error of 50% on $(\mathbf{F}-1)$ would entail an error of only 0.5% on the experimental result. Although such 'insensitive' situations are also encountered in SPX-1, there are others where correction factors were found to differ by as much as 50% from unity. In these cases, an error in $(\mathbf{F}-1)$ of 50% would have a strongly deteriorating influence on the experimental result.

This illustrates that a reliable determination of the MSM-correction factors is a task of essential importance in the course of the analysis of subcritical multiplication experiments, in particular in those cases where these factors differ substantially from unity. The following section will therefore discuss the specific problems encountered with the production of MSM correction factors, and indicate the strategy presently chosen at KfK to overcome these problems.

III.2 Problems arising in the context of MSM correction factor calculations

In order to keep computing costs within tolerable limits, calculations used for the production of MSM correction factors are usually run on a relatively low 'level', i.e. in diffusion theory with condensed cross sections (3 to 6 energy groups) and coarse meshes in the order of 10 cm. Different aspects, as e.g. the sometimes substantial number of control rod arrays to be analysed, budget constraints and simplicity of the calculation input frequently lead to a preference of 2D rather than 3D calculations.

Results obtained from such standard calculations are thus affected by condensation and mesh size errors on one hand, and by the neglect of transport and axial effects (in 2D calculations) on the other. In view of the numerous approximations introduced, it is little surprising that in most cases a comparison e.g. of the reactivity levels established in such calculations with the associated experimental situations shows a rather poor agreement. In particular two deficiencies of such calculations are of relevance in the present context:

1. A reactivity scale offset:

Using standard cross sections, the production of which will be described later in Sec. V.1, KfK calculations performed in either 3D or in 2D geometry with a global axial buckling value of 5.41 m^{-2} as suggested by CEA for the SPX-1 analysis, showed a negative reactivity scale offset; i.e. the reactor was predicted to be more subcritical than found in the experiments.

2. A faulty prediction of control rod worths:

Using the same standard cross sections, KfK calculations were found to substantially overpredict control rod worths.

These deficiencies are a consequence of the above indicated low calculation level but to a certain extent they also reflect the influence of basic cross section data inaccuracies and of inevitable geometrical modelling approximations.

Consequently the question arises whether the above indicated deficiencies - and possibly others - are likely to have a deteriorating influence on the MSM correction factors and thus on the corrected experimental results, and if so, what remedial action should be taken.

Following a logical line of reasoning, one would obviously demand that the calculations should as closely as possible reproduce both, the experimental reactivity scale and control rod worths, as otherwise one would not expect to obtain the correct calculated detector count rates ' C_{cal} ' and ' C ' which appear in the correction factors. While the influence of control rod worths on detector count rates is directly evident, that of the reactivity scale might seem less obvious. To make this point more transparent, it may be recalled that the present problem involves inhomogeneous, i.e. fixed source driven calculations. While in the case of homogeneous calculations, a shift of the reactivity scale (e.g. by global scaling of DB^2 or $\nu\Sigma_f$) would only lead to a general renormalisation of the neutron fluxes - without changing the flux shape itself -, the inhomogeneous flux solution depends on the proximity of the critical state. While at large subcriticalities, the flux shape is dominated by the spatial distribution of the fixed (static) neutron source, at small subcriticalities i.e. when approaching the critical state, it is progressively more influenced by the spatial distribution of the fission source and resembles therefore more the flux shape of the homogeneous solution.

Following the first impetus, one would therefore call for high precision calculations to ensure optimum correspondance of experiments and calculations. One has to be aware of the fact, however, that irrespective of the calculational precision the above mentioned potential basic data inaccuracies and inevitable modelling approximations could still prevent exact agreement of calculations and experiments. Precise calculations would therefore, apart from being rather complicated and costly, only partially solve the problem. A different approach had thus to be found.

A closer look at the MSM factor formula shows that the accuracy demanded for the calculations is really much less stringent than would intuitively be presumed. As correction factors represent a ratio of two products $\rho \cdot C$, errors of the same magnitude affecting both the numerator and the denominator, will cancel out in the ratio and will therefore have no deteriorating influence on the correction factors. This means that the individual count rates or the products $\rho \cdot C$ and $\rho_{cal} \cdot C_{cal}$ may contain substantial errors. Only the relative change of the product $\rho \cdot C$ when passing from the calibration array to a given control rod configuration must be correctly calculated! It is therefore the 'ratio-nature' of the MSM correction factors that mitigates the impact of calculation deficiencies.

Experience has shown that the diffusion approximation, a condensation of the cross sections to few energy groups and a wide mesh spacing tend to produce similar errors in $\rho \cdot C$ for a wide range of control rod configurations. In many cases it was thus

found that in spite of the observed reactivity scale shift and the faulty rod worth prediction, due to the 'ratio-nature' of the correction factors, relatively simple diffusion theory calculations could serve for the production of these factors without the risk of introducing excessive errors into the experimental results. A typical example for this situation is the first CEA analysis of the CID experiments which will be detailed in Sec. VI.

Obviously, this does not mean that any type of simplified calculation will produce satisfactory correction factors for any control rod configuration. The situation becomes more problematic for control rod arrays in which the errors produced by the diffusion approximation, cross section condensation and coarse mesh size are significantly different for the Etalon and for the investigated configuration. Amongst these arrays are in particular those that produce strongly distorted flux distributions, like e.g. the stuck-rod situation in which all except one or two control rods are shut down and in which as a consequence of steep flux gradients, the mesh size error is significantly greater than for the Etalon case.

Total errors introduced by the standard calculation scheme into the products $\rho \cdot C$ and $\rho_{cal} \cdot C_{cal}$ might in such cases differ by several percent, and it is this difference between the errors in the two products which is then reflected in the correction factors. The question therefore arose, under which conditions one could even in these more complicated cases still employ the same type of relatively simple calculations and obtain satisfactory results (i.e. errors on correction factors rarely larger than 1%).

Investigations have shown that this is possible, provided that certain parameters in these calculations are adequately modified to (artificially) improve the correspondence of calculations and experiments. Such parameter modifications which have also been employed by the present KfK analysis comprise:

1. An adjustment of the calculated to the experimental core reactivity in a situation, where absorbers are not inserted into the core but raised into the upper axial blanket. A faulty prediction of control rod worths would therefore have no influence on the calculated core reactivity. (It will be seen later (Sec. VII.1) that this is true strictly only in the case of 2D calculations.) The core reactivity of such a situation is frequently referred to as the 'core excess reactivity'.

The core reactivity adjustment procedure chosen in the present KfK analysis was somewhat different, depending on whether the correction factor calculations were performed in 2D or in 3D geometry. In the case of the 2D calculations this adjustment was made by buckling variation, in the case of 3D calculations it was made by $\nu\Sigma_f$ variation.

As a side remark it is mentioned that for the BOL core of SPX-1 (CMP-loading) the core excess reactivity with all control rods fully raised was in the order of +3700 pcm. (1 pcm = $10^{-5}\Delta(1/k)$) Obviously, this state of the reactor could not be established in the experiments because of its large positive reactivity. As the core excess reactivity was thus not amenable to a direct measurement, it had to be determined from the shut-down reactivity in combination with the S-curve of the control rod system (see Sec. VII.3).

2. An adjustment of the calculated to the measured control rod worths by adequate modification (in our case a reduction) of the absorber cross sections.

In the KfK analysis the rod worth adjustment was made by replacing the standard absorber cross sections by a mixture of these cross sections with those of the control rod sodium follower. The resulting cross sections will be referred to as 'diluted' absorber cross sections. By varying the proportions of the cross

section mixture, i.e. the 'dilution' of the absorber cross sections, the calculated rod worths could be adjusted to the experimental values. As the experimental values were a-priori unknown, special procedures had to be employed in this context, the details of which will be described later in this report (see Sec. VI.2).

To those readers who are not familiar with the subject, the purpose of the first adjustment (1.) will not seem directly evident as in the context of the subcritical experiments the necessity of an agreement of the (positive) calculated and experimental core reactivity of this situation is difficult to see. The idea behind this adjustment is to separate as far as possible local and global effects on k_{eff} and thus to arrive at a closer agreement of experiments and calculations. This is easily understood with the help of a simple example:

Supposing that for a 2D correction factor calculation one had chosen the critical condition of the core as the point of first adjustment, it would have been impossible to judge whether the diluted absorber cross sections used to simulate critical control rod insertion were realistic in terms of reactivity insertion into the core or whether a faulty reactivity effect provoked by an error e.g. in the axial buckling or in the ν -value (in $\nu\Sigma_f$) was fortuitously compensated by the use of incorrectly diluted absorber cross sections. This would have the following consequences:

- Subsequent control rod movements (e.g. SAC insertion in SPX-1 to establish the Etalon, see Sec. IV.3) would be made in a reactor whose flux distribution is deteriorated by the presence of SCP control rods with a faulty reactivity worth; i.e. the neutron flux deformation could be too weak or too strong depending on whether the SCP reactivity worth was under- or overpredicted.
- In those cases where a subcritical control rod array comprises one or more fully raised or fully inserted SCP control rods (e.g. rod drop configurations in CID), the reactivity difference obtained when moving these rods from critical insertion, i.e. when replacing the diluted absorber by a sodium follower or by a full density absorber is obviously also unrealistic.

To avoid these difficulties, the present adjustment strategy starts with a global adjustment of the core reactivity excluding the influence of control rods and continues with a local adjustment of the absorber cross sections.

The remaining question is how faulty one of these adjustments might be without causing impermissible errors in F, or in other words which amount of misadjustment can be permitted so that the calculated MSM factors still remain reasonably reliable. A comprehensive answer to this question cannot be given as a generally applicable theoretical treatment of this problem is not available. It is known, however, that the answer depends on the particular reactor and on the individual control rod array. It is for this reason that in the course of the present analysis, frequently a series of calculations with minor parameter variations has been run for a given control rod array. The correction factor changes observed for these variations allowed to judge the uncertainties introduced by faulty calculation adjustment. This was done with particular care for the Etalon situations, as the subcriticalities of these form the basis for the assessment of all other arrays.

It should be noted for completeness that, obviously, different strategies can be chosen to improve the agreement between correction factor calculations and experimental reality than the artificial adjustment of the calculations described above and used by KfK.

An alternative possibility which largely avoids the sometimes rather cumbersome procedure of calculation adjustment is to produce adequately modified control rod absorber cross sections. In the procedure recently employed by the CEN-Cadarache, these cross sections were prepared in such a way that they contain implicit heterogeneity, transport, energy group condensation and mesh-size corrections (References / 3,4 and 5 /). The same procedure was used for the control rod sodium followers and for the diluent subassemblies. A use of such cross sections in 3D diffusion theory calculations was found to lead to an improved reproduction of the critical state and to control rod worths that differ relatively little from the experimental results. Calculation deficiencies originating from other sources than the cross sections of these subassembly types (e.g. an inaccurate value of ν in the production term $\nu\Sigma_f$) were obviously not removed by the use of the MONSTRE method and some residual discrepancies were observed between the MONSTRE based calculations and the experimental results. These residual inaccuracies, however, were in general small and an a-posteriori adjustment of the calculations could be often considered unnecessary.

This method is doubtlessly more elegant than the one presented in this report, but a set of nuclear data and computer codes which allow a sufficiently close representation of the experimental conditions is at present not available at KfK.

IV MSM measurements in SUPER-PHENIX-1

IV.1 The configurations

Control rod experiments in SPX-1 using the MSM-method comprised a substantial number of arrays, covering the insertion of single rods, various rod pairs showing different interactions, inner and outer ring triplets, complete rings, withdrawal of one or more rods from shut-down and many others.

For the present analysis, the SPX-1 analysis task force has defined a list of control rod configurations which covers a broad variety of cases with very different MSM correction factors.

For the C1D-core:

1. SCP 929, SAC ↓ (Calibration state 'Etalon-C1D')
2. SCP 920, B1 ↓ B2 ↑
3. SCP 922, B9 ↑ B10 ↓, B1 918
4. SCP ↓, SAC ↑
5. SCP ↓, SAC ↓
6. SCP 600, SAC ↑
7. SCP 600, SAC ↓
8. SCP 915, B2,B4,B6 ↓
9. SCP 918, B10,B15,B20 ↓

For the CMP core:

1. SCP 542, SAC ↓ (Calibration state 'Etalon-CMP')
2. SCP 542, B10 ↓
3. SCP 542, B2 ↓
4. SCP 542, SAC1 ↓, SAC2,SAC3 ↑
5. SCP 542, B1,B2 ↓
6. SCP 542, B10,B17 ↓
7. RI ↓, RE 542
8. RI 900, RE ↓
9. SCP 519, B2 ↓
10. SCP 519, B7 ↓
11. SCP 519, B8 ↓
12. SCP 520, B9 ↓
13. SCP 521, B10 ↓
14. SCP 522, B11 ↓
15. SCP 465, B2,B4,B6 ↓
16. SCP 486, B10,B15,B20 ↓
17. SCP ↓, SAC ↑
18. SCP ↓, SAC ↓
19. SCP ↓, B12 ↑

B1,B2 etc. are individual rods of the SCP system, SAC1,SAC2, and SAC3 are those of the SAC system (see Figures 1 and 2). RI and RE are the inner and outer ring of the SCP system, respectively. The indications ↑ and ↓ signify a fully raised and a fully inserted rod respectively. An explanation of how the numbers indicating partial insertion of the SCP rods have to be interpreted was already given in Sec. II. Whenever the insertion state of the SAC rods is not explicitly indicated, they are fully raised.

IV.2 Subcritical counting

Subcritical count rates were recorded on the ^3He chambers of the 3 GDN under-vessel detector clusters and on the 3 uranium fission chambers located at different axial heights in the central channel. In principle, 6 independent results would therefore have been available for each configuration, but only one count rate - that of the central counter - was finally used in the analysis. This had the following reason:

The experiments were performed in a 'fresh core'. The inherent neutron source was therefore still rather small so that in the subcritical range, for the majority of the control rod arrays the under vessel detectors showed very small count rates, and thus very poor counting statistics. The only exception from this situation was encountered in a series of experiments, where starting from total shut-down, control rods were raised exclusively in one 120° sector of the core. This particular approach to criticality led to a strong local flux peak in the area surrounding the raised rods and produced sufficient count rates in the GDN detector located in their vicinity. These experiments, however, were not yet analysed at KfK. The GDN results were therefore excluded from the present analysis.

For the majority of the control rod arrays, MSM correction factor calculations were performed in 2D geometry representing the core midplane only. In these cases no neutron flux information was available for detector positions above or below the core midplane and thus no correction factors could be derived for the off-centre detectors.

As far as the calculations in 3D geometry are concerned, a comparison of measured and calculated axial fission rate profiles of ^{235}U in the critical CMP core had revealed significant errors ($> 10\%$) in the vicinity of the upper and lower core/blanket boundaries, i.e. near the location of the off-centre BOUPHY detectors. It was therefore preferred to also exclude the results of these two detectors from the present analysis and to base the interpretation solely on the count rates obtained from the central ^{235}U fission chamber.

IV.3 The calibration state (Etalon)

As indicated in Sec. III, measurements using the MSM technique require the establishment of a subcritical calibration state or Etalon in which both subcritical level ${}^e\rho_{cal}$ and detector count rate ${}^eC_{cal}$ are known. For the SPX-1 control rod experiments, the Etalon configuration was defined as:

SCP-Z_c SAC ↓.

i.e. main regulating system SCP at critical insertion, secondary system SAC fully inserted. The critical insertions Z_c of the SCP system in CID and CMP were 'Cotes' 929 and 542 respectively. At 180°C , these 'cotes' are equivalent to absorber insertion depths into the core of 8.61 cm and 47.31 cm. respectively. As under normal operating conditions the SAC rods are fully raised, the value of the subcriticality of the Etalon state is equivalent to the worth of the SAC rods with SCP at critical insertion. Provided, of course, that the insertion of SAC was really made into the critical reactor. For completeness it should be mentioned that in the SPX-1 experiments this was never exactly the case, but the insertion took place into a reactor that was ≈ 8 pcm subcritical.

The subcriticality ${}^e\rho_{cal}$ of the Etalon state is usually obtained by performing an inverse kinetics analysis of the dynamic flux response recorded during a rod drop

experiment, in the case of SPX-1 thus a drop of the complete SAC system into the near critical reactor. The associated detector count rate ${}^e C_{cal}$ is taken when sufficient time has elapsed after the drop and the flux has reached its new asymptotic level.

The difficulty encountered with the use of this procedure is that the standard reactor kinetic equations, normally employed for the analysis of rod drop experiments, are based on the point reactor approximation. The results obtained with these equations are therefore reliable only as long spatial effects play a subordinate role. While in small reactors the deviation from point reactor kinetics is frequently negligible, this is normally not true for large power reactors and the use of point kinetics can seriously deteriorate the result of the rod drop analysis. Different codes have been developed to overcome this problem by extending the standard inverse kinetics algorithm in such a way that it will account for spatial effects in an approximate manner. The code version used for the SPX-1 analysis is based on the so-called *Carpenter*-method, a thorough description of which is given in Ref./ 6 /. The range of applicability of this code is, however, limited to reactivity insertions of the order of 3\$, i.e. of ≈ 1000 pcm in SPX-1. As the SPX-1 Etalon subcriticality is of the same order of magnitude, there were doubts as to whether the use of *Carpenter's* analysis algorithm would produce a reliable result. Only for exploratory reasons, this analysis was nevertheless carried out. The result obtained was (fortuitously ?) close to the one found in the improved analysis path described below. It was, however, not used in the further course of the analysis.

To avoid the questionable use of *Carpenter's* algorithm for the analysis of a direct SAC rod drop experiment, the Etalon subcriticality was determined using an implicit method, based on a series of rod drops involving smaller reactivity insertions which were amenable to an evaluation with the *Carpenter*-method. The inverse kinetics analysis of each of these rod drops, which comprised single rod, rod pair and rod triplet insertions, led to a certain subcriticality ${}^e \rho_i$ and an associated detector count rate ${}^e C_i$ after the drop. The suffix 'i' refers to the particular rod drop.

As the detector count rate ${}^e C_{cal}$ of the Etalon state was known, the Etalon subcriticality could now easily be determined by inverse application of the MSM formula:

$$\rho_{cal,i}^{MSM} = \frac{{}^e \rho_i \cdot {}^e C_i}{{}^e C_{cal}} \cdot G_i \quad (6)$$

or

$$\rho_{cal,i}^{MSM} = \rho_{cal,i}^{MSA} \cdot G_i \quad (7)$$

Analogous to Sec. III, the correction factors G_i have the form

$$G_i = \frac{\rho_{cal} \cdot C_{cal}}{\rho_i \cdot C_i} \quad (8)$$

For each individual rod drop one obtained therefore one individual value for the Etalon subcriticality. Its final value $\bar{\rho}_{cal}^{MSM}$ was obtained as the mean value of all individual results.

It is readily seen that equations (6) through (8) represent a simple inversion of equations (3) through (5), discussed in Sec. III. While in Sec. III, the Etalon subcriticality was considered to be known and the subcriticality of other control rod arrays was established on the basis of its knowledge, in the present case, the known subcriticality of a control rod array provides the basis to assess the Etalon subcriticality.

As a concluding remark in this context one should add that the laborious procedure of assessing the subcriticality of the Etalon state SCP-Z_c SAC↓ via a series of individual rod drops can obviously be avoided by simply defining the reactor state after one of the individual drops as the Etalon. This would have substantially simplified the whole analysis of the experiments.

The incentive for the presently chosen approach of 'synthesizing' the Etalon subcriticality from a series of experiments arose from the fact that the results of the rod drop experiments were readily available. These rod drops had been primarily carried out as part of a series of experiments destined to test the consistency of rod worths measured using different experimental techniques (Rod-drop, 'Balancement', MSM). With the individual results available, the additional effort of calculating a suitable set of MSM correction factors was considered acceptable in view of the merit of a reduced uncertainty on the Etalon subcriticality achieved by averaging over the individual $\rho_{cal,i}^{MSM}$ results.

V General remarks on MSM correction factor calculations

V.1 Cross Section Preparation

The cross sections used in KfK calculations were those prepared by Belgonucléaire (BN) and described in / 7 /.

All cross sections are based on the KFKINR001 26 group adjusted data library / 8 /. Cell-averaged cross sections were prepared using the collision probability code KAPER4 / 9 / in 3 different versions:

- * The heterogeneous version for the:
 - inner and outer core cell

- * The homogeneous version for the:
 - radial and axial blanket,
 - radial and axial reflector,
 - neutron guide tubes, and
 - structural parts of the SAC control rods.

- * The SUPERCELL-version for the:
 - dummy fuel elements,
 - diluents,
 - control rod followers (providing modified diffusion coefficients / 10 /),
 - and the three types of control rod absorbers (SCP, upper and lower SAC).

The simplified onedimensional models that have been used for the production of cell averaged cross sections for the different control rod absorbers were described in / 11 /.

Some modifications were introduced at KfK into the cross section set prepared by BN:

As the composition specification of the dummy fuel assemblies was modified after BN had finished the cross section preparation, the cross sections for this element type were newly prepared at KfK on the basis of the revised specification / 14 /.

As some inconsistencies had been discovered in the compositions of SAC absorbers and articulations between earlier and more recent documentation (/ 14 /), it was considered prudent to also rerun the cross section preparations for the different SAC absorber constituents.

For the calculations described hereafter, the so produced 26 group cross section set was condensed to 4 energy groups, using flux spectra from a 3D diffusion theory calculation of SPX-1. In this calculation, all SCP control rods were inserted to the critical level of the CMP core (SCP 542). It should be noted, that SAC cross sections were condensed using the flux spectra of the SCP control rods. This was done for reasons of consistency with earlier calculations where condensation spectra were obtained from an RZ model of SPX-1. As in this model the three SAC rods appeared as a very thin annulus, the flux spectra were not considered to be typical of an absorber medium, and the condensation of the SAC absorbers was performed using the spectra of the somewhat thicker SCP annuli.

For the simulation of partially inserted control rod absorbers in 2D calculations as well as for the adjustment of calculated control rod worths to corresponding measured worths in 2D and 3D calculations (see next section), SCP absorber cross sections were mixed in varying proportions with the SCP sodium-follower cross sections. Cross sections produced in this way are frequently referred to as 'diluted SCP cross sections'.

V.2 Types of calculations

All calculations run at KfK used the finite difference hexagonal diffusion theory code D3E (/ 12 /). The majority of the calculations was run using a full plan core centre plane 2D representation. As mentioned before, partially inserted SCP absorbers were simulated in this type of calculation by the use of so-called diluted cross sections, i.e. mixed SCP absorber and sodium follower cross sections.

Part of the calculations were repeated in 3D geometry to judge the deteriorating influence of the use of a 2D model on MSM correction factors for different control rod arrays.

It should be noted that, concerning the representation of fully raised and of fully inserted control rod absorbers, certain simplifications were introduced into the 3D calculations to minimize the number of axial meshes. As indicated in Sec. II, the lower end of an SCP absorber is located 0.2 cm above the upper core/blanket interface when the absorber is said to be fully raised and 1.4 cm below the lower core/blanket interface when the absorber is said to be fully inserted. The corresponding levels of the SAC absorbers are 6.8 cm above the upper core/blanket interface and 1.06 cm above the lower core/blanket interface, respectively.

Instead of using these exact axial levels, the calculations simply assumed that the lower ends of the absorbers were level with either the upper or the lower core/blanket interface. Supplementary test calculations have shown that these simplifications have neither a significant influence on calculated rod worths nor on the MSM correction factors, obtained from these calculations.

In contrast to these simplifications introduced for fully raised and fully inserted absorbers, partial insertions of control rod absorbers (occurring for SCP rods only), were always correctly modelled in the 3D calculations.

All calculations were run in 4 energy groups with a radial M1 mesh (i.e. 7 points per subassembly, equivalent to a sidelength of the basic triangle of ≈ 10 cm). Axial meshes in 3D calculations ranged from 2 cm in the core region to 10 cm in the axial blanket and reflector.

Subcritical (source-driven) flux distributions, necessary to calculate the detector count rates which are required for the production of MSM correction factors (see Sec. III), were obtained through (inhomogeneous) source mode calculations. These were initiated using the associated real and adjoint flux solutions for the corresponding homogeneous problem.

The source input used for the source mode calculations was individualised for each fissile subassembly as prescribed by CEA specifications / 13,14 /. Source strengths of neutrons originating from spontaneous fission and from (α,n) processes were provided separately with their associated spectral distributions.

The following 4 energy group microscopic cross sections were used for the assessment of the central BOUPHY detector count rates:

Energy group	Neutron energy range	$^{U-235}\sigma_f$ [barn] = σ_{det}
1	1.4 MeV - 10.6 MeV	1.245
2	400 KeV - 1.4 MeV	1.187
3	21.5 KeV - 400 KeV	1.658
4	thermal - 21.5 KeV	4.565

The exact geometry and isotopic composition of the BOUPHY chambers being unknown, these cross sections were taken from a heterogeneous KAPER cell calculation of the inner core cell of SPX-1. The flux spectra used for the cross section condensation to 4 energy groups were the heterogeneous KAPER cell spectra. The condensation was performed by a module implemented in KAPER itself.

The calculated subcriticality of the reactor which is also required for the production of MSM correction factors, was always obtained from the well known expression (in operator writing):

$$\rho = - \frac{\langle S\Phi^+ \rangle}{\langle \Phi^+ P\Phi^{inh} \rangle}$$

where

S is the strength of the inherent neutron source,

P is the production operator,

Φ^+ is the adjoint flux solution of the homogeneous problem, and

Φ^{inh} is the direct flux solution of the inhomogeneous problem.

In this case the pointed brackets symbolize integration over energy and over the full reactor volume.

It seems noteworthy that the subcriticality obtained with this formula was always in perfect agreement (within 1pcm) with the reactivity $\rho = 1 - 1/k_{eff}$ resulting from the eigenvalue of the associated homogeneous flux calculation. This agreement testifies the perfect convergence of the inhomogeneous calculations!

VI Production of MSM correction factors for C1D

VI.1 The calibration state (Etalon) SCP 929 SAC↓ of C1D

The first series of MSM factor calculations served to establish the subcriticality of the calibration array SCP 929 SAC↓. Although not suggested by the task force, this campaign of calculations was resumed as the correction factors used in the original CEA analysis of the C1D experiments originated from design level calculations that had not been adjusted to the actual experimental reactivity level and rod worths. The quality of these factors was therefore considered questionable.

The Etalon subcriticality was established on the basis of 14 rod drops. As described in Sec. IV.3, each of these drops produced one value for the Etalon subcriticality. Table I below presents a survey of the rod drop configurations that were used for this purpose, the detector count rates eC_i recorded after each drop, the subcriticality ${}^e\rho_i$ of the reactor after the drop, and the uncorrected (point reactor model) Etalon subcriticalities $\rho_{cal}^{MSA} = ({}^e\rho_i \cdot {}^eC_i) / {}^eC_{cal}$. Reactivities are always given in [pcm], detector count rates in [counts/second = c/s]. The subcritical detector count rate ${}^eC_{cal}$ recorded in the Etalon configuration was 876 c/s.

Table I Results of rod drops in C1D

Configuration after drop	eC_i	${}^e\rho_i$	$\rho_{cal,i}^{MSA}$
1. SCP 920, B1 ↓ B2 ↑	2380	305.4	829.7
2. SCP 921, B1 ↑ B2 ↓	2420	302.6	835.9
3. SCP 922, B9 ↓ B10 ↑, B1 918	3935	206.5	927.6
4. SCP 922, B9 ↑ B10 ↓, B1 918	4141	200.8	949.2
5. SCP 921, B10 ↑ B17 ↓, B1 887	3391	245.9	951.9
6. SCP 921, B2 ↑ B18 ↓, B1 918	3696	228.6	964.5
7. SCP 929, SAC1 ↓, SAC2,3 ↑	3209	252.6	925.3
8. SCP 921, B1,B2 ↓	1231	490.8	689.7
9. SCP 922, B2,B10 ↓	1683	426.5	819.4
10. SCP 921, B2,B18 ↓, B1 914	1258	585.0	840.1
11. SCP 921, B9,B10 ↓	2563	316.0	924.6
12. SCP 920, B10,B17 ↓, B1 895	1670	512.0	976.1
13. SCP 915, B2,B4 ↓, B6↑	1069	580.2	708.0
14. SCP 918, B10,B15,B20 ↓	1317	680.1	1022.5

In the start situation prior to the execution of the rod drops, either two (conf. 1 through 12), or three control rods (conf. 13 and 14) were fully raised, requiring different compensating insertions of the SCP system to keep the reactor close to criticality. The only exception from this procedure is found in conf. 7, where one of the SAC rods was dropped. As under operating conditions the SAC rods are already fully raised, the drop could be executed directly from the normal critical situation SCP 929 SAC \uparrow , without the necessity of preceding rod movements.

In the majority of the cases, the start-off reactivity level was held at about -8 pcm. In order to avoid the rather tedious procedure of trimming all SCP rods to the same insertion depth (curtain position) to maintain this start-off reactivity level through all the experiments, reactor drift was on some occasions compensated by slightly changing the insertion depth of only **one** SCP rod: B1. As, however, the small difference between the insertion depth of B1 and the remaining SCP bank was not expected to have a significant influence on the flux distribution, the present analysis calculations simply assumed that B1 too was at bank insertion.

It is recalled that the insertion levels ('Cotes') of SCP rods indicate the distance in [mm] by which the control rods were raised from full insertion.

Control rods with an \downarrow sign are those that have been dropped from the fully raised state to arrive at the indicated configuration.

Concerning the subcriticalities $^e\rho_i$ given in Table I, it should be mentioned that they were obtained from the values quoted in earlier SPX-1 documentation (/ 1 /), by applying a correction of -3.95% to account for the β_{eff} updating from 380 to 365 pcm / 16 /. It is important to note that these subcriticalities do not directly represent the reactivity worths of the dropped rods, but a superposition of these worths with the start-off subcriticality of -8 pcm.

One observes that the uncorrected MSA results are widely dispersed showing a total scatter of $1022.5 - 689.7 = 332.8$ pcm.

The determination of the correction factors G_i with

$$G_i = \frac{\rho_{cal} \cdot C_{cal}}{\rho_i \cdot C_i}$$

is performed in two separate steps. The first step is concerned with the calculation of the numerator and includes some parametric investigations, while the second step focusses on the calculation of the denominator.

Assessment of the numerator of the correction factors G_i

MSM correction factors for C1D were produced using exclusively 2D calculations. This decision was taken as experience gained in the CMP core analysis, which was historically performed before work on the C1D experiments had started, showed no major differences in correction factors derived from 2D and 3D calculations. This is particularly true for the relatively simple control rod arrays established in C1D.

All calculations were run in 4 energy groups and used an M1 mesh grid (7 points per subassembly).

As was already indicated in Sec. III.2, the principal difficulty encountered in the context of an MSM factor assessment is in that the experimental reactivity levels to which the calculations should be adjusted are still unknown. In the present case the adjustment is facilitated by the fact that the SPX-1 start-up experiments had already been analysed at the CEA / 1 /. The results of this first analysis will therefore serve as a basic guess and guideline.

According to Sec. III.2, the first adjustment of the calculations is performed for a configuration in which the absorbers have little or no influence on the reactivity. This is the case in the so-called 'follower-core' where all control rod absorbers are fully raised. The reactivity of this configuration, which is usually referred to as the 'core excess reactivity', as quoted in CEA documentation of the first analysis of the C1D core is +335 pcm / 1 /. Allowing the β_{eff} updating from the initially used value of 380 pcm to the present value of 365 pcm, the old value of the excess reactivity was expected to drop accordingly by 3.95% to a new value of +321.8 pcm.

The first task of the calculations was therefore to reproduce this reactivity value, which was achieved by using a global axial buckling of $5.38 m^{-2}$. The excess reactivity of +318.7pcm obtained from this calculation was considered to be in satisfactory agreement with the anticipated value.

The next task was to find appropriate absorber cross sections for the SCP control rods to simulate critical insertion and for the SAC control rods to properly reproduce the measured SAC worth. We proceeded in the following way:

Critical insertion of the SCP system (SCP 929) was found to be sufficiently well simulated by a 1% absorber which produced a k_{eff} value of 1.00005. A 1% absorber means a mixture of the macroscopic cross sections of an SCP absorber and an SCP sodium follower in a ratio of 1 : 99.

Concerning the SAC adjustment, the original analysis resulted in an Etalon subcriticality of 965 pcm. Reducing this value by 3.95% (β_{eff} change), an initial estimation of $\rho_{cal}^{MSM} = 927$ pcm was obtained.

As mentioned before, this subcriticality represents a superposition of a SAC worth of 919 pcm and of -8 pcm by which the reactor was already subcritical before SAC insertion.

Lacking diluted absorber cross sections whose use would exactly reproduce the anticipated $\Delta\rho_{SAC} = 919$ pcm, cross sections of a 32.5, 35.0 and 37.5% SCP absorber were tentatively used for SAC. The results obtained from these calculations are given in Table II below and in Figure 8.

Reactivities $\rho = 1 - 1/k_{eff}$ are always given in [pcm]. Count rates are in arbitrary units.

Table II 2D-calculation of $\rho_{cal} \cdot C_{cal}$ for C1D

Configuration	ρ_{cal}	$\Delta\rho_{SAC}$	C_{cal}	$\rho_{cal} \cdot C_{cal}$
1. SCP 929, SAC ↑(Follower)	+5.1	0.0	---	---
2. SCP 929, SAC ↓(32.5% abs.)	-895.7	-900.8	0.1928	172.65
3. SCP 929, SAC ↓(35.0% abs.)	-933.5	-938.6	0.1846	172.29
4. SCP 929, SAC ↓(37.5% abs.)	-969.0	-974.1	0.1775	171.95

An examination of the results of Table II reveals the following points:

1. The product $\rho \cdot C$ changes very little with the worth of SAC and thus with the Etalon subcriticality: 0.4% rel. with a SAC worth change of 8%.
2. The subcriticalities ρ_{cal} established in calculations No. 2, 3, and 4 are not solely caused by the reactivity worth of SAC, which is given in the $\Delta\rho_{SAC}$ column but represent a superposition of the SAC worth with a small mis-alignment of the reactivity scale by +5.1 pcm for the critical configuration 1.

Although the required calculated relationship between the product $\rho_{cal} \cdot C_{cal}$ and the subcriticality of the reactor provoked by SAC insertion had now been established, there were still two points left that needed to be clarified:

1. It was said before, that ≈ 8 pcm of the experimental subcriticalities did not originate from the different rod insertions but that the reactor was kept at that level before the start of each experiment. As the precise origin of that subcriticality can not be identified, it can not be modelled into the calculations and it must be assumed (which is probably realistic) that its influence on the product $\rho_{cal} \cdot C_{cal}$ is negligible.
2. It had to be decided, whether the interpolation of $\rho_{cal} \cdot C_{cal}$ for the anticipated SAC worth of 919 pcm should be performed on the subcriticality ρ_{cal} or on the $\Delta\rho_{SAC}$ values of Table II. Although the second choice would seem more plausible as the 919 pcm refer to the SAC worth, one has to prove that the reactivity scale mismatch at critical has no significant influence on $\rho_{cal} \cdot C_{cal}$.

In the present case, the minute mismatch of the reactivity scale could obviously be anticipated to have a negligible impact on the results. Nevertheless it appeared interesting to clarify this point and to judge the quantitative influence of a reactivity scale shift caused by buckling modification. Some test calculations were therefore run in which the buckling value was changed by $\pm 0.1 m^{-2}$.

In the same phase of the analysis, another set of test calculations was run, in which the absorber dilution used to simulate the critical insertion of SCP was modified. The initially used 1% absorber was replaced alternatively by 3 other absorber concentrations. The reactivity scale shift provoked by these 3 modifications was compensated by an adequate change of the axial buckling so that the critical situation was always well reproduced.

It should be noted that these changes in absorber concentration imply that the reactivity difference between the critical situation and the state with all absorbers fully raised, i.e. the all-follower state will also be changed. As the critical state has been fixed by adequate buckling tuning, these parameter changes effectively modify the calculated core excess reactivity.

The results of these two series of test calculations are given in Table III. For reasons of simplicity, the subscript 'cal' and the 'C' column have been omitted in this table.

Table III Parametric studies for C1D in 2D geometry

Configuration	ρ	$\Delta\rho$	$\rho \cdot C$
<i>1. As Table II, but axial buckling changed from 5.38 m⁻² to 5.48 m⁻²</i>			
1. SCP 929, SAC ↑(Follower)	-215.7	---	---
2. SCP 929, SAC ↓(35.0% abs.)	-1150.4	934.7	171.96
<i>2. As Table II, but axial buckling changed from 5.38 m⁻² to 5.28 m⁻²</i>			
1. SCP 929, SAC ↑(Follower)	+226.0	---	---
2. SCP 929, SAC ↓(35.0% abs.)	-716.6	942.6	172.65
<i>3. Critical insertion of SCP was now simulated by a 0.5% absorber (above it was a 1% absorber) and the buckling was changed to B² = 5.44 m⁻²</i>			
1. SCP 929, SAC ↑(Follower)	+27.0	---	---
2. SCP 929, SAC ↓(35.0% abs.)	-909.2	936.3	172.53
3. SCP 929, SAC ↓(37.5% abs.)	-944.7	971.7	172.19
<i>4. Critical insertion of SCP was now simulated by a 1.5% absorber and the buckling was changed to B² = 5.315 m⁻²</i>			
1. SCP 929, SAC ↑(Follower)	-3.6	---	---
2. SCP 929, SAC ↓(35.0% abs.)	-944.3	940.7	172.07
3. SCP 929, SAC ↓(37.5% abs.)	-979.8	976.7	171.72
<i>5. Critical insertion of SCP was now simulated by a 2.5% absorber and the buckling was changed to B² = 5.21 m⁻²</i>			
1. SCP 929, SAC ↑(Follower)	-0.2	---	---
2. SCP 929, SAC ↓(35.0% abs.)	-945.5	945.3	171.95
3. SCP 929, SAC ↓(37.5% abs.)	-981.1	980.9	171.60

The results of these exploratory calculations show that for the Etalon configuration SCP 929 SAC↓ of C1D, the product $\rho \cdot C$ is very insensitive to reactivity scale shifts provoked by buckling variation. In fact, this product changes by only 0.4% (!) for a reactivity scale shift of ≈ 450 pcm.

Consequently, no significant error will be introduced into the analysis, if the $\rho_{cat} \cdot C_{cat}$ values of Table II are interpolated on the basis of $\Delta\rho_{SAC}$ under neglectation of the reactivity scale shift. The value obtained for a SAC worth of 919pcm is 172.4.

Table III shows furthermore that even a change of the absorber concentration used to simulate critical SCP insertion from 0.5% to 2.5% entailing a worth change relative to a sodium follower from 157.8 to 691.4 pcm (factor 4.4 !) has only a negligibly small influence on $\rho \cdot C$.

Assessment of the denominators of the correction factors G_i

Now that the calculated product $\rho_{cal} \cdot C_{cal}$ has been established, the individual denominators $\rho_i \cdot C_i$ of the correction factors G_i have to be calculated.

In this case, the subcritical levels ρ_i produced by the various rod drops were known (c.f. Table I), but a problem arose from the fact that neither for the different SCP bank insertion levels of Table I nor for the dropped rods, suitably diluted absorber cross sections were available in the analysis cross section block to reproduce the correct reactivity levels.

In principle, this problem could have obviously been overcome by producing the adequately diluted cross sections and linking them to the main cross section block. To preclude the risk of errors in multiple cross section processing and also to investigate the influence of variations in absorber cross sections on calculated rod worths and on correction factors, it was preferred to use a different strategy. For each control rod array of Table I, two series of calculations were run:

- For the first series, the cross sections used to simulate the SCP bank insertion were chosen so that the experimentally critical situation before the drop, mostly involving 2 or 3 fully raised control rods, was slightly overcritical.
- For the second series, the next higher concentrated absorber cross sections available in the cross section block were used, resulting for the start situation in a slightly subcritical level.

Using the closest reproduction possible within the constraints of the available cross section block, experimental reality was thus approached from the positive and from the negative side of the reactivity scale.

For each of the two simulations of the critical SCP 'bank' insertion, a selection of differently diluted absorber cross sections from the standard cross section block was used for the dropped control rod (rods), to cover a certain range around the associated reactivity value quoted in Table I.

The desired result $\rho_i \cdot C_i$ and consequently the correction factor G_i for a given configuration 'i' was then obtained by double interpolation of the calculated values. A first interpolation was made between the two series of calculations to reproduce the effect of the critical SCP insertion. On the resulting $G_i = G_i(\rho)$ relationship (approximately linear) a second interpolation was made to obtain G_i for the correct rod worth.

To facilitate the comprehension of this procedure, a detailed description will be given for the first configuration of Table I : SCP 920, B1↓, B2↑. The experiment had started with a situation, in which rods B1 and B2 (see Figure 1) were fully raised and all remaining SCP rods had been somewhat deeper inserted than in the standard critical 'bank' insertion SCP 929, to compensate the small positive reactivity obtained when B1 and B2 were raised from bank insertion. Rod B1 was then dropped from the fully raised state, leading to the configuration SCP 920, B1↓, B2↑.

The results of the two series of calculations, performed for this array are given in Table IV. In the first series of calculations, the critical insertion level 920 of SCP was simulated by a 1% absorber, in the second series by a 1.5% absorber. Given for each series of calculations are the calculated reactivities ρ of the experimentally critical start situation SCP 920, B1↑, B2↑ and for the investigated configuration SCP 920, B1↓, B2↑ using differently diluted absorber cross sections for rod B1.

Table IV 2D-Calculation of "G" for SCP 920, B1↓, B2↑

First series: SCP 920 simulated by a 1% absorber

Configuration	ρ	$\Delta\rho$	$\rho \cdot C$	G
1. SCP 920, B1↑(Follower) B2↑(")	+37.1	0.0	---	
2. SCP 920, B1↓(42.5% abs.) B2↑(Follower)	-250.5	-287.6	159.78	1.0795
3. SCP 920, B1↓(45.0% abs.) B2↑(Follower)	-257.6	-294.7	159.17	1.0836
4. SCP 920, B1↓(57.5% abs.) B2↑(Follower)	-287.3	-324.4	156.57	1.1016
5. SCP 920, B1↓(60.0% abs.) B2↑(Follower)	-292.3	-329.4	156.12	1.1048
6. SCP 920, B1↓(62.5% abs.) B2↑(Follower)	-297.1	-334.2	155.70	1.1078
7. SCP 920, B1↓(65.0% abs.) B2↑(Follower)	-301.6	-338.7	155.29	1.1107

Second series: SCP 920 simulated by a 1.5% absorber

Configuration	ρ	$\Delta\rho$	$\rho \cdot C$	G
1. SCP 920, B1↑(Follower) B2↑(")	-99.1	-0.0	---	
2. SCP 920, B1↓(42.5% abs.) B2↑(Follower)	-390.6	-291.5	160.21	1.0766
3. SCP 920, B1↓(45.0% abs.) B2↑(Follower)	-397.9	-298.6	159.61	1.0807
4. SCP 920, B1↓(57.5% abs.) B2↑(Follower)	-427.8	-328.7	157.01	1.0985
5. SCP 920, B1↓(60.0% abs.) B2↑(Follower)	-432.8	-333.7	156.56	1.1017
6. SCP 920, B1↓(62.5% abs.) B2↑(Follower)	-437.7	-338.6	156.13	1.1047
7. SCP 920, B1↓(65.0% abs.) B2↑(Follower)	-442.2	-343.1	155.72	1.1076
8. SCP 920, B1↓(100.0% abs.) B2↑(Follower)	-489.4	-390.3	151.41	1.1392

Note:

A typical example of the substantial overestimation of rod worths found with the use of 2D calculations and standard (non-diluted) absorber cross sections is seen in configuration No. 8 of the second series of calculations. Comparing the calculated reactivity worth of rod B1 ($\Delta\rho = 390.3$ pcm) obtained for this configuration with the finally determined experimental MSM value of 298.5 pcm (i.e. 306.5 - 8 pcm, see Table VIII), one observes an overestimation of about 24%!

Further given are the resulting reactivity worths $\Delta\rho$ of B1 relative to the fully raised state, the corresponding products $\rho \cdot C$ and the associated correction factors G . For simplicity the subscripts 'i' were omitted.

Figure 9 gives a graphical presentation of the results of this Table. Zero is suppressed on both axes.

The following observations are made:

- Over the relatively small reactivity range considered here, both series of calculations show an almost linear dependence of the correction factor G on the reactivity of the dropped rod B1, the cross sections of which had been modified within each series of calculations.
- A reactivity worth change of the dropped rod B1 has a much more pronounced influence on G than a reactivity worth change of the SCP bank which occurs when passing from one series of calculations to the other, i.e. by varying the corresponding 'diluted' cross sections of SCP.

Supplementary calculations, the detailed results of which are not presented here, have shown that over the narrow reactivity range in view, G also changes linearly with the SCP bank worth.

In general terms one observes therefore that local reactivity perturbations have a much stronger influence on the product $\rho \cdot C$ than reactivity changes of a more global nature like changes in the axial buckling or in the worth of the whole SCP system.

Based on the presentation of Figure 9, the analysis can be continued using a graphical method as follows:

1. The first and the last points of the two series of calculations illustrated in Figure 9 are connected with each other by a straight line. The left endpoints of these two straight lines thus belong to the first series of calculations, where the critical state (with the rod pair fully raised) was predicted to be 37.1 pcm overcritical, the right endpoints to the second series of calculations which underpredicted this state by -99.1 pcm.
2. As the start-off subcriticality of -8 pcm was considered to have no influence on $\rho \cdot C$, the interpolation of the results of these two series of calculations is performed as if the experiments had started from critical. Both connection lines are thus divided according to the ratio
$$37.1 / (37.1 + 99.1) = 1 / 3.67.$$
3. The division points on the two connecting lines are now joint to each other by a straight line, which gives -as long as the condition of linearity is fulfilled- the new relationship between the subcriticality ρ attained after the rod drop, and the correction factor G .
4. According to Table I, the subcriticality ρ after the first rod drop was 305.4 pcm, giving a B1 worth of $305.4 - 8 = 297.4$ pcm. Using the newly constructed relationship, one finds a corresponding correction factor G of 1.083.
5. Applying this correction factor to the uncorrected Etalon subcriticality $\rho_{cal,i}^{MSA}$ of Table I (829.7 pcm) we obtain the first corrected Etalon value of 898.9 pcm. Strictly, the correction factor should have been applied to $(829.7 - 8)$ pcm only, as the residual 8 pcm were considered to have no influence on $\rho \cdot C$ and the

8 pcm should have been added after the multiplication. Though in principle more precise, this latter procedure would have changed the Etalon value by only 0.7 pcm. For simplicity, the first alternative was therefore used in the present analysis.

The same procedure has been repeated for the remaining 13 rod drop experiments of Table I. The detailed results of all calculations performed in this context are given in Tables A1.1 through A1.14 of Appendix 1.

The following Table V presents a summary of the results obtained from the 14 rod drop experiments for the Etalon subcriticality $\rho_{cal,i}^{MSM}$.

Table V Assessment of the Etalon subcriticality in C1D
---2D correction factor calculations ---

Configuration after drop	$\rho_{cal,i}^{MSA}$	G_i	$\rho_{cal,i}^{MSM}$
1. SCP 920, B1 ↓ B2 ↑	829.7	1.083	898.9 ± 53.9
2. SCP 921, B1 ↑ B2 ↓	835.9	1.083	905.4 ± 54.3
3. SCP 922, B9 ↓ B10 ↑, B1 918	927.6	0.968	897.8 ± 44.9
4. SCP 922, B9 ↑ B10 ↓, B1 918	949.2	0.966	916.8 ± 36.7
5. SCP 921, B10 ↑ B17 ↓, B1 887	951.9	0.971	924.2 ± 46.2
6. SCP 921, B2 ↑ B18 ↓, B1 918	964.5	0.958	924.1 ± 52.4
7. SCP 929, SAC1 ↓, SAC2,3 ↑	925.3	0.996	922.1 ± 73.8
8. SCP 921, B1,B2 ↓	689.7	1.198	826.5 ± 49.6
9. SCP 922, B2,B10 ↓	819.4	1.095	897.4 ± 53.8
10. SCP 921, B2,B18 ↓, B1 914	840.1	1.074	902.4 ± 54.1
11. SCP 921, B9,B10 ↓	924.6	0.980	906.5 ± 54.4
12. SCP 920, B10,B17 ↓, B1 895	976.1	0.934	911.7 ± 54.7
13. SCP 915, B2,B4 ↓, B6 ↑	708.0	1.232	872.6 ± 52.4
14. SCP 918, B10,B15,B20 ↓	1022.5	0.919	939.2 ± 75.1

The experimental uncertainties quoted with the values of $\rho_{cal,i}^{MSM}$ have been taken from earlier documentation (Ref. / 1 /).

In agreement with the first analysis, the mean value of these 14 individual results is formed via reciprocal error-square weighting, using the standard formula:

$$\bar{\rho}_{cal}^{MSM} = \frac{\sum_{i=1}^{i=14} \frac{\rho_{cal,i}^{MSM}}{(\Delta\rho_i)^2}}{\sum_{i=1}^{i=14} \frac{1}{(\Delta\rho_i)^2}}$$

The $\Delta\rho_i$ are the uncertainties quoted in Table V.

The result obtained for $\bar{\rho}_{cal}^{MSM}$ is $901.9 \pm 6\%$ (1σ) and the SAC-worth is accordingly 894 pcm. Comparing this result with the anticipated SAC-worth of 919 pcm, for which the numerator $\rho_{cal} \cdot C_{cal}$ of the correction factors \mathbf{G}_i had initially been calculated (Figure 8), one observes a discrepancy of 25 pcm. In a very exact analysis, the correction factors therefore should be recalculated using a numerator that fits the new SAC-worth.

Taking this new worth, one reads from Figure 8 a calculated product $\rho_{cal} \cdot C_{cal}$ of 172.7 as opposed to the initially used product of 172.4. As all fourteen correction factors \mathbf{G}_i contain the same numerator, the new mean Etalon subcriticality is simply obtained, by scaling the value obtained above by a factor of $172.7 / 172.4 = 1.0017$, giving a revised result of 903 pcm. For this minute change of the Etalon subcriticality, the product $\rho_{cal} \cdot C_{cal}$ remains virtually unchanged and further iterations are unnecessary.

The subcriticality of the calibration configuration SCP 929 SAC ↓ in C1D is therefore obtained as

$$\bar{\rho}_{cal}^{MSM} = 903 \text{ pcm} \pm 6\%(1\sigma)$$

The resulting worth of the SAC system with SCP at critical insertion is

$$\Delta\rho(SAC) = 895 \text{ pcm} \pm 6\%(1\sigma)$$

Comparing these results with those obtained from the first analysis at CEA / 1 /, one observes a reduction of about 6.4 %. As mentioned earlier, 3.95% of this reduction originate from β_{eff} updating. The remaining 2.45% are due to the use of improved MSM correction factors in the present analysis campaign. Unlike the present analysis, where the calculations had been adjusted to reproduce experimental reactivity levels, the original analysis of C1D performed immediately after the completion of the experiments with very little time available, had used unadjusted design level calculations which substantially overestimated the subcriticalities achieved by control rod insertions.

VI.2 The selected configurations of C1D

Table VI summarises the configurations that were specified by the SPX-1 analysis task force, the associated detector count rates eC , and the uncorrected subcriticalities ${}^e\rho^{MSA}$ resulting from an Etalon detector count rate of 876 c/s and an Etalon subcriticality of 903 pcm.

Table VI Configurations to be analysed in C1D

Configuration	eC	${}^e\rho^{MSA}$
1. SCP 929, SAC ↓ ('Etalon-C1D')	876	
2. SCP 920, B1 ↓, B2 ↑	2380	-332.4
3. SCP 922, B9 ↑, B10 ↓, B1 918	4141	-191.0
4. SCP ↓, SAC ↑	96	-8239.9
5. SCP ↓, SAC ↓	87	-9092.3
6. SCP 600, SAC ↑	279	-2835.2
7. SCP 600, SAC ↓	207	-3821.4
8. SCP 915, B2, B4, B6 ↓	600	-1318.4
9. SCP 918, B10, B15, B20 ↓	1317	-600.6

As explained in Sec. III.1, MSM correction factors \mathbf{F} have the form:

$$\mathbf{F} = \frac{\rho \cdot C}{\rho_{cal} \cdot C_{cal}}$$

In the preceding section, the calculated product $\rho_{cal} \cdot C_{cal}$, has been established as 172.7. The denominator of \mathbf{F} was thus known and the remaining task was to determine the numerator for the different control rod arrays of Table VI. This was done using the same strategy and type of calculations (2D geometry, 4 energy groups, M1 mesh) as for the assessment of the correction factors \mathbf{G} in the previous section. For each control rod array, a series of calculations has been run in which the absorber concentration of the inserted rod(s) was modified. Different subcritical levels were thus established giving different products $\rho \cdot C$ and thus different MSM correction factors \mathbf{F} .

In some cases, two series of calculations were run, simulating insertion of the SCP or SAC absorber bank by the use of two different absorber concentrations and thus approximating the realistic reactivity worth of these banks from both, higher and lower reactivity levels (see also Sec. VI.1).

Although for a given control rod array a relationship between \mathbf{F} and the subcriticality had now been established, the correction factor could not be directly read from this relationship as the true subcriticality of the control rod array for which \mathbf{F} should be determined was a-priori unknown. Different procedures can be employed to overcome this problem:

- A graphical iteration procedure which is rather tedious and time consuming.
- A graphical procedure in which the solution point is directly constructed.
- A purely analytical procedure without any graphical support.

The iterative graphical solution

This procedure can start from either the uncorrected experimental subcriticality (assuming in a first step $F = 1.0$) or from an improved first guess if available. The first correction factor F^1 is then applied to ${}^e\rho^{MSA}$ to give a first solution $\rho^{MSM,1}$. A second correction factor F^2 is then read from the calculated relationship and applied to ${}^e\rho^{MSA}$, giving a second guess solution $\rho^{MSM,2}$ and so on until convergence is achieved. Convergence means in this case that a correction factor has been found whose application to ${}^e\rho^{MSA}$ results in a subcriticality that leads back to the same correction factor within an acceptably small deviation of less than 1 %.

A practical example of this procedure is given hereafter for configuration 4 of Table VI (SCP↓, SAC↑). The uncorrected experimental subcriticality is obtained from

$${}^e\rho^{MSA} = \frac{\bar{\rho}_{cal}^{MSM} \cdot {}^eC_{cal}}{{}^eC} \quad (9)$$

The measured detector count rates in configuration 4 and in the calibration configuration were 96 and 876c/s, respectively, and $\bar{\rho}_{cal}^{MSM}$ was found to be 903 pcm.

--- > ${}^e\rho^{MSA} = 8240 \text{ pcm}$

As usual, this subcriticality represents a superposition of the start subcriticality of -8 pcm and the uncorrected SCP worth of 8232 pcm.

To abbreviate the demonstration, we assume that previous studies have suggested a subcriticality of 7400 pcm. From Table VII and Figure 10 we find an associated correction factor $F^1 = 0.9435$.

Table VII 2D-Calculation of "F" for SCP↓, SAC↑

Configuration	ρ	$\Delta\rho$	$\rho \cdot C$	F
1. SCP 929 (1% abs.) SAC↑(Follower)	+5.1	0.0	---	
2. SCP↓(45.0% abs.) SAC↑(Follower)	-7377.6	-7382.7	162.98	0.9437
3. SCP↓(47.5% abs.) SAC↑(Follower)	-7617.0	-7622.1	162.69	0.9420
4. SCP↓(50.0% abs.) SAC↑(Follower)	-7846.5	-7851.6	162.43	0.9405

It should be mentioned that the ↓ signs found in Table VII and in all other Tables of this report presenting calculated results do not mean that an absorber was completely inserted as it was the case in e.g. Table VI presenting experimental results. In the context of calculated results, this sign indicates only that an absorber has been introduced into the indicated rod position(s). The individual absorber 'dilution' used is always indicated in parentheses behind an ↓ sign.

Application of the above indicated correction factor $F^1 = 0.9435$ to ${}^e\rho^{MSA}$ of 8240 pcm gives

$$\rho^{MSM,1} = 7774\text{pcm}$$

Repetition of the procedure gives

$$F^2 = 0.9410 \text{ and } \rho^{MSM,2} = 7754\text{pcm},$$

$$F^3 = 0.9411 \text{ and } \rho^{MSM,3} = 7755\text{pcm}$$

At this point, the accuracy of the graphical method reaches its limit, but as residual changes are small (in the order of some pcm), this result can be considered as being sufficiently accurate.

The direct graphical solution

Provided that one has the results of more than one correction factor calculation available, a much simpler graphical procedure of finding the subcritical solution point ρ^{MSM} than the iterative approach described above is the following one:

Apart from the calculated relationship shown in Table VII and Figure 10 between the correction factor F and the worth $\Delta\rho$ of SCP (which corresponds to the subcriticality ρ if one neglects the 5.1 pcm reactivity offset at critical), the solution must also satisfy Eq.(5) of Sec. III.1:

$$\rho^{MSM} = {}^e\rho^{MSA} \cdot F \quad (5)$$

which characterizes the actual purpose of the correction factor.

This second relationship is also shown in Figure 10. The intersection point of the two functions

$$F(\rho) = \frac{\rho \cdot C}{\rho_{cal} \cdot C_{cal}} \quad \text{and} \quad F(\rho) = \frac{\rho}{{}^e\rho^{MSA}}$$

is the solution point which indicates the corrected subcriticality ρ^{MSM} .

One obtains the same result as with the iterative graphical approach.

The analytical solution

Provided that over the range of the calculated values that enclose the true experimental subcriticality, the correction factor F is a linear function of the subcriticality ρ , the following formula is applicable:

$$F = m \cdot \rho + F_0$$

'm' is the gradient, which is known from the results of the calculations, e.g. from two calculated points $(\rho_1; F_1)$ and $(\rho_2; F_2)$:

$$m = \frac{F_2 - F_1}{\rho_2 - \rho_1}$$

If the solution point (ρ^{MSM}/F) : is also located on this straight line, one can also write:

$$m = \frac{F - F_1}{\rho^{MSM} - \rho_1}$$

and therefore

$$F = m(\rho^{MSM} - \rho_1) + F_1 \quad (10)$$

The still unknown experimental subcriticality ρ^{MSM} can be replaced by ${}^e\rho^{MSA} \cdot F$, where ${}^e\rho^{MSA}$ is the uncorrected subcriticality (or point reactor result), obtained directly from the experiments. Equation (10) thus becomes:

$$F = m({}^e\rho^{MSA} \cdot F - \rho_1) + F_1 \quad (11)$$

After rearrangement of equation (11) one obtains the required correction factor F as:

$$F = \frac{F_1 - m \rho_1}{1 - m {}^e\rho^{MSA}} \quad (12)$$

where all parameters on the right hand side of the equation are known.

Using this analytical procedure, one obtains for the present example: $F = 0.9410$ and $\rho^{MSM} = 7754$ pcm, i.e. a result that is almost identical to the one obtained from the graphical procedures.

Although this analytical solution would have provided an easier tool to assess the required correction factors than the graphical methods, it was not used in the present analysis for the following reasons:

- There were doubts as to whether the assumption of linearity was always valid with sufficient accuracy.
- A graphical presentation of the results was considered helpful in appreciating possible deviations from a linear relationship, and in estimating the errors introduced by a linear interpolation.

All results presented in this report were therefore derived using the graphical methods.

The detailed results of all correction factor calculations for CID are given in Tables A2.1 through A2.8 of Appendix 2.

Table VIII summarises the investigated configurations, the direct (uncorrected) experimental results ${}^e\rho^{MSA}$, the correction factors F and the final corrected results ρ^{MSM} . Rod worths are obtained from these final results by subtracting the start subcriticality of 8 pcm.

Comparing the corrected reactivity values with those of the original analysis (/ 1 /) one observes the same reduction of about 6.5% rel. that had already been observed and discussed in the context of the Etalon assessment at the end of Sec. VI.1.

Concerning the worth of SAC, it is interesting to note that it drops from 895 pcm with SCP at critical insertion (i.e. almost completely raised), to 890 pcm with SCP at level 600 (i.e. 41.4 cm inserted) and to 705 pcm when SCP is fully inserted. This means that over almost the full stroke of SCP corresponding to a reactivity worth introduction of 7747 pcm (i.e. 7755 - 8 pcm), the SAC worth **drops** by 190 pcm or 21% relative. The major part of this reduction (20.8%) takes place between about half and full insertion of SCP corresponding to a worth introduction of 4957 pcm.

This pronounced reduction of the SAC worth upon SCP insertion is observed only in the core version C1D. It will be seen later (see Sec. VII.3). that for a similar SCP worth introduction (≈ 4350 pcm), the SAC worth in the fully loaded CMP core was found to **increase** by 5%.

This indicates that the type and magnitude of interaction between the primary and the secondary control system of SPX-1 changes drastically with the transition from the C1D to the CMP core loading, i.e. with the replacement of the last 33 dummy subassemblies by fuel. As indicated in Figure 1, these dummy subassemblies were all located in the inner core zone (Identifier 'F' for 'faux combustibles'). The origin of this particular behaviour of the SPX-1 core in terms of neutronic coupling between the two core zones, or of eigenvalue separation between the first two harmonics has not yet been clarified.

Table VIII Results of MSM measurements in C1D
-- 2D correction factor calculations --

Control rod configuration	$e\rho^{MSA}$	F	ρ^{MSM}
1. SCP 929, SAC ↓ (Etalon)			903.0
2. SCP 920, B1 ↓ B2 ↑	332.4	0.922	306.5
3. SCP 922, B9↑,B10↓,B1 918	191.0	1.037	198.1
4. SCP ↓ , SAC ↑	8240.0	0.941	7755.0
5. SCP ↓ , SAC ↓	9092.0	0.930	8460.0
6. SCP 600, SAC ↑	2835.0	0.987	2798.0
7. SCP 600, SAC ↓	3821.0	0.965	3688.0
8. SCP 915, B2,B4,B6 ↓	1318.4	0.679	895.0
9. SCP 918, B10,B15,B20 ↓	600.6	1.087	653.2

It seems further noteworthy that in principle two results are available for each of the three configurations No.2, 3, and 9. These configurations had been established by rod drop experiments and the inverse kinetics analyses of these rod drops had -amongst others- served to establish the Etalon subcriticality on which the present MSM results are based. It is therefore possible to test the consistency of subcriticalities obtained from the rod drop experiments and from the MSM analysis:

	$\rho^{Rod\ drop}$	ρ^{MSM}
SCP 920, B1↓,B2↑	305.4	306.5
SCP 922, B9↑,B10↓,B1 918	200.8	198.1
SCP 918, B10,B15,B20 ↓	680.1	653.2

For the third configuration, one observes a difference of $\simeq 4\%$ while for the first two configurations, the results are in much better agreement. These differences are consistent with the observation that could be made in Table V . The first two configurations corresponding to No.1 and No.4 in Table V had given Etalon subcriticalities that were relatively close (898.8 and 916.8 pcm) to the presently used mean value of 903 pcm. In contrast, the result of 939.2 pcm obtained from the third configuration (No.14 in Table V) differed from the mean value by 4%. As the present MSM results are based on this mean value, this difference is found again when comparing the rod drop and the MSM result.

VII Production of MSM correction factors for CMP

VII.1 *Introductory comments on the different adjustment strategies employed for 2D and 3D calculations*

As outlined in Sec. III.2, a global adjustment of the calculations is performed, in which the calculated excess reactivity with all control rod absorbers fully raised is adapted to the measured value.

The CMP core excess reactivity originally quoted in SPX-1 documentation was of +3945 pcm / 2 /. As indicated before, earlier reactivity values always referred to a preliminary value of the delayed neutron fraction β_{eff} of 380 pcm. Using the revised β_{eff} value of 365 pcm, the excess reactivity was anticipated to change accordingly to +3789 pcm. (The excess reactivity later found in the KfK analysis was +3708 pcm when using 2D and +3732 pcm when using 3D MSM correction factor calculations.)

For twodimensional MSM correction factor calculations, an axial buckling value of $5.67 m^{-2}$ was chosen, which in the case with all control rod absorbers fully raised, i.e. with sodium follower in all rod positions, produced an eigenvalue of 1.03847 ($\rho = +3704$ pcm). This was considered to be sufficiently close to the anticipated experimental excess reactivity indicated above. Critical SCP insertion was simulated by a 17.44% SCP absorber (i.e. mixed cross sections of 17.44% absorber and 82.56% sodium follower). The resulting eigenvalue was 0.99999.

It is important to note that the buckling value used here is much larger than the value used in the CID analysis ($5.38 m^{-2}$) which in view of the similarity of the two core versions seems unlogical. The reason for this anomaly is in that CID contained 33 dummy fuel elements which were not present in CMP.

With the present 2D calculations (4 energy groups, mesh M1) the reactivity worth of these dummy elements versus fuel is overestimated by $\simeq 17\%$. (Using the best 3D calculation performed so far at KfK, this discrepancy is reduced to $\simeq 10\%$). To obtain realistic k_{eff} values for CID it was therefore necessary to substantially reduce the buckling value with respect to the one used in CMP and thereby compensate the excessive negative reactivity contribution arising from the dummy worth overprediction by the calculations.

For threedimensional calculations, the adjustment procedure was somewhat more complicated. This had the following reason:

Unlike the 2D calculations where the state with all absorbers fully raised was simulated by simply using sodium follower cross sections in all control rod positions, a 3D calculation of this case still contains the control rod absorbers in the upper axial blanket and reflector. The 3D k_{eff} value of this case is therefore to some extent influenced by the cross sections used for the control rod absorbers -- which are still awaiting adjustment. This means that in 3D calculations, the global core reactivity and absorber cross section adjustment are not as simply separable as in the 2D treatment.

The adjustment procedure was therefore carried out in a slightly different way than described above for the 2D calculations:

A first series of calculations had the objective of identifying in a first crude attempt diluted absorber cross sections whose use in the 3D calculations would allow a close reproduction of the measured worth of the SCP system. A first information on the measured worth of SCP was already available from the analysis with 2D MSM correction factors. Calculations run in this context had shown (Table A4.16) that the

reactivity worth of the fully inserted SCP system was somewhat underpredicted by the use of a 52.5% absorber and somewhat overpredicted by a 55% absorber. These informations were used as a basic guideline.

Using alternatively one or the other SCP absorber concentration, calculations were run in 3D geometry for the situation with (i) the SCP system fully raised, (ii) with SCP at critical insertion and (iii) with SCP fully inserted. SAC remained fully raised. The results of these calculations showed:

- For the transition from fully raised to critical insertion of SCP, the results obtained with the two absorber concentrations enclosed indeed the experimental value of the core excess reactivity obtained from the 2D analysis i.e. $\rho^{excess} = +3708 pcm$.
- For the transition from critical to full insertion, however, the calculated reactivity differences of 4444 and 4562 pcm obtained with the two absorber concentrations were both somewhat larger (2.1 and 4.8%) than the experimental value of 4353 pcm obtained from the 2D analysis.

No unique absorber dilution could therefore be defined that would equally well reproduce both experimental values, or in other words, that would well reproduce the S-curve of the SCP system.

This observation is little surprising if one remembers that the calculations were run on a relatively 'low level', i.e. using diffusion theory with cross sections condensed to 4 energy groups and M1-mesh, i.e. 7 points per subassembly. It is well known that apart from systematic errors in rod worth predictions, provoked by uncertain basic cross section data the quality of rod worth predictions obtained with this type of calculations depends on the particular control rod configuration. In other words, transport, condensation and mesh corrections (also referred to as 'method'-corrections) are array dependent. While basic data errors could to a certain extent be expected to be compensated by the use of adequately modified absorber cross sections or a correlated degree of absorber cross section 'dilution', this is rather unlikely to be the case for the totality of the array dependent 'method'-corrections.

The fact that although 3D calculations are used, different absorber 'dilutions' are needed to reproduce experimental reality confirms therefore the experience made in earlier control rod experiments.

Similar to the 2D analysis of the MSM experiments, it was therefore also necessary in the 3D analysis to use differently 'diluted' absorber cross sections for the different absorber arrays to achieve optimum match of experiments and calculations.

It should be noted, however, that the overall range of different absorber dilutions involved in the analysis to produce optimum match with the experiments was much smaller in the 3D than in the 2D correction factor calculations. This had the following reason:

In the 2D calculations, a first dilution of the originally available cross sections (Sec. V.1) was necessary as with the use of these unmodified cross sections, control rod worths were systematically overpredicted (see also footnote of Table IV in Sec. VI.1). This overprediction was first observed when the full insertion worth of the complete SCP system was calculated, i.e. in the case where in the 2D model, sodium followers were replaced by full density absorbers.

In addition to this first basic cross section adjustment which served for the reproduction of the **full** SCP insertion worth, the 2D analysis required a variety of further dilutions (on top of the first dilution) to reproduce the smaller reactivity insertions obtained for the different **partial** control rod insertions comprised in the SPX-1 mea-

surements, as these could not easily be modelled otherwise in the 2D centre plane representation of the core. The diluted cross sections used to represent partial rod insertions also accounted implicitly for the changing 'method'- corrections mentioned above.

In the 3D analysis, these various subsequent dilutions were obviously not necessary, as the partial insertion of control rod absorbers could be directly modelled. Only a relatively small variation of the absorber dilution was required to cover the range of varying 'method'- corrections.

The adjustment of the 3D correction factor calculations therefore proceeded as follows:

For each control rod array of interest, two correction factor calculations were run, using alternatively a 52.5 and a 55.0% SCP absorber. Depending on the particular array, MSM correction factors were then either linearly interpolated between the two calculated values or linearly extrapolated. The assumption of a linear dependence of \mathbf{F} on the subcriticality ρ was justified since an extension of the investigations with calculations using smaller and greater absorber dilutions than those indicated above showed that over the small reactivity range in question deviations from linearity were negligibly small.

A basic adjustment of the core reactivity was performed by scaling ' ν ' in the production term $\nu\Sigma_f$ with a factor of 0.99913. This manipulation causes a reactivity shift of -84 pcm. The reason for choosing this adjustment has a historical background. Part of the 3D investigations were launched while there were indications that β_{eff} would be updated to 360 pcm (instead of the finally used value of 365 pcm). The core excess reactivity was then expected to drop from the original value of +3945 pcm by a factor of 360/380 to a new value of +3737 pcm. In retrospect this value represented (fortuitously) a better estimation of the experimental core excess reactivity of +3732 pcm found with 3D correction factors than the anticipated value of +3789 pcm based on the presently used $\beta_{eff} = 365$ pcm (see the beginning of this section!)

Using the $\nu\Sigma_f$ adjustment and the two absorber concentrations indicated above, 3D calculations of the state with all SCP absorbers fully raised produced excess reactivities that enclosed the then anticipated excess reactivity: +3743 pcm (52.5% abs.) and +3735 pcm (55.0% abs.).

The same applied to the situation with SCP at critical insertion, where corresponding reactivity values of +90 pcm and -14 pcm were found.

Over the range of cross sections (32.5 to 37.5% abs.), that were tentatively used to reproduce the experimental worth of the SAC rods, the all-follower core k_{eff} value changed by less than 4 pcm - a consequence of the small number of SAC rods and of their small reactivity worth. The choice of the SAC cross sections interferes therefore very little with the reactivity adjustment procedure described above.

Closing this section on the differences between 2D and 3D correction factor calculations for the CMP core, it should be mentioned that for the production of MSM factors with 2D calculations, obviously only one calculated detector count rate (that of the centre plane) was used. In contrast to this, 3D calculations produce an axial distribution of count rates. The detector count rate was in this case obtained by averaging the axial count rates over the full height of the central BOUPHY detector of 12 cm.

VII.2 The calibration state (Etalon) SCP 542 SAC ↓ of CMP

In contrast to the CID analysis, where the complete campaign of MSM factor calculations that served for the establishment of the Etalon subcriticality had been repeated, in the case of the CMP core this was done only for about one third of the configurations that originally served for this purpose. This appeared sufficient to confirm previous results, as unlike CID, the first analysis of CMP had already used correction factors that were adjusted to the measured rod worths ($/ 2 /$).

A survey of the rod drop experiments that have been selected for the present re-analysis, the detector count rates eC_i , the subcriticality ${}^e\rho_i$ of the reactor after the drop, and the uncorrected Etalon subcriticalities $\rho_{cal}^{MSA} = ({}^e\rho_i \cdot {}^eC_i) / {}^eC_{cal}$ are given in Table IX. The detector count rate ${}^eC_{cal}$, recorded in the Etalon configuration of CMP was 757 c/s.

As these rod drop experiments were performed by starting directly from the standard critical situation SCP 542 SAC↑, where all SCP rods were already near half insertion, these drops were called 'half' rod drops. It is recalled that the rod drop experiments discussed in the context of the CID Etalon assessment (Sec. VI.1) involved 'full' rod drops; this means that before a rod drop was executed in CID, the rod or rods to be dropped were fully raised and the resulting positive reactivity was counteracted by compensating insertion of the remaining SCP rods.

Table IX Results of "half" rod drops in CMP

Configuration after drop	eC_i	${}^e\rho_i$	$\rho_{cal,i}^{MSA}$
1. SCP 542, B1 ↓	3383	220.9	987.2
2. SCP 542, B2 ↓	3430	215.2	975.1
3. SCP 542, B10 ↓	5671	140.2	1050.3
4. SCP 542, B18 ↓	5400	148.9	1062.2
5. SCP 542, B9 ↓	5095	156.6	1054.0
6. SCP 542, B17 ↓	5756	141.2	1073.6
7. SCP 542, B1,B2 ↓	1786	401.5	947.3
8. SCP 542, B2,B10 ↓	2351	317.0	984.5
9. SCP 542, B2,B18 ↓	1923	393.8	1000.4
10. SCP 542, B9,B10 ↓	3264	249.7	1076.6
11. SCP 542, B10,B17 ↓	2719	297.8	1069.6

With the exception that the CMP analysis includes 3D correction factor calculations, the analysis proceeded in the same way as described in Sec. VI.1 for the CID core.

Assessment of the numerator of the correction factors G_i

The first step was the determination of the numerator $\rho_{cal} \cdot C_{cal}$ of the correction factors G_i .

The subcriticality of the Etalon state of CMP was anticipated as 1047 pcm, the SAC worth accordingly as 1039 pcm. These values originated from the results of the first analysis of CMP (-1090 pcm for the Etalon subcriticality) reduced by 3.95% to allow for β_{eff} updating.

The results of 2D and 3D calculations, run for the determination of $\rho_{cal} \cdot C_{cal}$ are summarised in Tables X and XI. A graphical presentation of the same results is given in Figures 11 and 12.

As was already indicated in Sec. VII.1, 2D calculations for the Etalon case were run using SCP absorber cross sections diluted to 17.44%. The first line of Table X shows that with this absorber dilution the critical situation is very well reproduced. Subsequently the absorber cross sections used for SAC were tuned to enclose the anticipated SAC worth (lines 2 to 4 of Table X).

Following the comments of Sec. VII.1, 3D calculations had to be run twice using two different SCP absorber dilutions, as no unique cross section dilution could be found that would equally well reproduce the reactivity worth of partial and of full SCP insertion. SAC cross sections were tuned for each of the two SCP concentrations, but in contrast to the 2D calculations of Table X, only two different dilutions (32.5 and 35%) were now used. This appeared sufficient, as the 2D results (see Figure 11) had demonstrated a sufficiently linear dependence of $\rho_{cal} \cdot C_{cal}$ on the SAC worth, so that for SAC worths outside the calculated range, the corresponding values of $\rho_{cal} \cdot C_{cal}$ could have been easily obtained by linear extrapolation.

In contrast to the 2D calculations, where a fully raised absorber was simply represented by a sodium follower (core centre-plane model), a 3D calculation contained this absorber in its realistic position, i.e. in the upper axial blanket and reflector. The same diluted absorber cross sections that were used for an inserted absorber were then consequently also used for the raised absorber.

In agreement with the experience made in the CID analysis, one finds that the product $\rho \cdot C$ changes relatively little with the worth of SAC and thus with the Etalon subcriticality. Using linear interpolation between the calculated points, one finds for the anticipated $\rho_{cal}^{MSM} = 1047$ pcm a value of $\rho \cdot C = 155.9$ for 2D and of $\rho \cdot C = 3.715$ for 3D calculations.

One notes that the products $\rho_{cal} \cdot C_{cal}$ obtained from 2D and 3D calculations differ by approximately a factor of 42. This has the following reason:

The external source strength input in units of neutrons/(second \times cm³) used in 3D calculations was the same in all axial planes within the core height and zero in the blanket regions. This assumption of an axially flat source distribution over the full core height was realistic as the experiments were performed in a relatively 'fresh' core, i.e. a core with very little burn-up. The source distribution was therefore not yet significantly influenced by the build-up of ²⁴²Cm and ²⁴⁴Cm occurring during extended reactor operation, but was still an image of the homogeneous axial fuel distribution established in the subassembly fabrication.

The radial and azimuthal distribution of the source was identical to that used in 2D calculations.

While code input in 2D calculations always assumed a hypothetical core height of 2.0 cm, the true core height used in 3D calculations was 100.114 cm. The strength of the total external source present in 2D and 3D calculations therefore differed by a factor of $100.114 / 2.0 = 50.057$.

Table X 2D-calculation of $\rho_{cal} \cdot C_{cal}$ for CMP

Critical insertion of SCP ('Cote 542') was simulated by a 17.44% absorber

Configuration	ρ_{cal}	$\Delta\rho_{SAC}$	C_{cal}	$\rho_{cal} \cdot C_{cal}$
1. SCP 542, SAC ↑(Follower)	-1.4	---	---	
2. SCP 542, SAC ↓(32.5% abs.)	-989.3	-987.9	0.1577	156.06
3. SCP 542, SAC ↓(35.0% abs.)	-1031.2	-1029.8	0.1512	155.94
4. SCP 542, SAC ↓(37.5% abs.)	-1070.5	-1069.1	0.1456	155.83

Table XI 3D-calculation of $\rho_{cal} \cdot C_{cal}$ for CMP

First series: 52.5% absorber used for SCP

Configuration	ρ_{cal}	$\Delta\rho_{SAC}$	C_{cal}	$\rho_{cal} \cdot C_{cal}$
1. SCP 542 SAC ↑(32.5% abs.)	+92.0	---	---	---
2. SCP 542, SAC ↓(32.5% abs.)	-911.1	-1003.1	4.0919E-3	3.7281
3. SCP 542 SAC ↑(35.0% abs.)	+90.4	---	---	---
4. SCP 542, SAC ↓(35.0% abs.)	-954.5	-1044.9	3.9025E-3	3.7249

Second series: 55.0% absorber used for SCP

Configuration	ρ_{cal}	$\Delta\rho_{SAC}$	C_{cal}	$\rho_{cal} \cdot C_{cal}$
1. SCP 542 SAC ↑(32.5% abs.)	-12.6	---	---	---
2. SCP 542, SAC ↓(32.5% abs.)	-1017.6	-1005.0	3.6522E-3	3.7164
3. SCP 542 SAC ↑(35.0% abs.)	-13.9	---	---	---
4. SCP 542, SAC ↓(35.0% abs.)	-1061.1	-1047.2	3.4990E-3	3.7128

Note:

Calculated detector count rates C_{cal} given for 3D calculations do not represent a direct result of the calculations but were obtained by averaging the calculated axial fission rate distribution of ^{235}U (see Sec. V.2) in the centre of the reactor over the height of 12 cm of the central BOUPHY detector.

As code input demanded a total source normalisation to unity, 2D and 3D core midplane fluxes are expected to show approximately the reciprocal ratio of the two source strengths. The observed deviation from this ratio (≈ 42 as opposed to 50) in $\rho_{cal} \cdot C_{cal}$ is due to the two different ways of producing the neutron fluxes (2D or 3D core representation) and to the different ways of deriving C_{cal} using either centre plane fluxes or average fluxes over the realistic detector height.

Assessment of the denominators of the correction factors G_i

The second step of the Etalon assessment consists in the determination of the denominators $\rho_i \cdot C_i$ of the correction factors G_i . The procedure is analogous to that of the CID analysis. The results of the calculations carried out for this purpose are given in Tables A3.1 through A3.14 of Appendix 3. The individual results $\rho_{cal,i}^{MSM}$ for the Etalon subcriticality as obtained from the 11 rod drop experiments are summarised in Table XII .

Table XII Assessment of the Etalon subcriticality in CMP
---2D and 3D correction factor calculations ---

Configuration after drop	$\rho_{cal,i}^{MSA}$	$G_i(2D)$	$G_i(3D)$	$\rho_{cal,i}^{MSM}$
1. SCP 542, B1 ↓	987.2	1.063		1049.6
2. SCP 542, B2 ↓	975.1	1.061	1.064	1034.7
3. SCP 542, B10 ↓	1050.3	0.989		1039.3
4. SCP 542, B18 ↓	1062.2	0.986		1047.7
5. SCP 542, B9 ↓	1054.0	0.992		1045.2
6. SCP 542, B17 ↓	1073.6	0.987		1059.5
7. SCP 542, B1,B2 ↓	947.3	1.141	1.139	1080.8
8. SCP 542, B2,B10 ↓	984.5	1.066		1049.5
9. SCP 542, B2,B18 ↓	1000.4	1.045		1045.8
10. SCP 542, B9,B10 ↓	1076.6	1.000		1077.0
11. SCP 542, B10,B17 ↓	1069.6	0.969	0.968	1036.3

One observes that the correction factors obtained from 2D and 3D calculations differ very little. As a complete set of results was available in 2D geometry only, only these results were actually used to assess the Etalon subcriticality.

As before, the mean value of these 11 individual results was formed via reciprocal error-square weighting. The individual uncertainties were not explicitly quoted in Table XII. They are found in the documentation of the original analysis in Ref. / 2 /.

The value obtained for $\bar{\rho}_{cal}^{MSM}$ is 1046.5 pcm. Comparing this result with the anticipated Etalon subcriticality of 1047 pcm, i.e. the value to which the calculation that produced the numerator $\rho_{cal} \cdot C_{cal}$ of the correction factors G_i had been adjusted, one observes only a minute difference of 0.5 pcm. A re-assessment of the correction factors G_i is therefore not necessary!

Comparing the result of the present analysis with that obtained in the first analysis at CEA (/ 2 /) using the same selection of rod drops ($\rho_{cal}^{MSM} = 1094.6$ pcm) one observes a reduction of 4.4%. As indicated before, a reduction of 3.95% is due to the changed β_{eff} value. The more elaborated procedure presently employed for the production of MSM correction factors, comprising an adjustment of the calculations to the experimental reactivity scale at critical and a close reproduction of experimental rod worths has in this case lowered the Etalon subcriticality by 0.4% only!

The value presently derived for the Etalon subcriticality was based on a selected number of 11 from a total of 35 rod drop experiments which originally served to establish this parameter. As for the remaining 24 rod drop experiments no revised analysis has been performed, no precise information can at present be given on the 24 Etalon values that would have been obtained using KfK correction factor calculations.

As, however, for the 11 selected configurations considered here the change in Etalon subcriticality with respect to the first analysis was due predominantly to the revision of β_{eff} , it is presently proposed to neglect the small influence (0.4%) of the revised MSM correction factor calculations.

An updated value of the Etalon subcriticality would then be obtained by simply reducing the final result of the first analysis (1090 pcm) by 3.95%. The subcriticality of the calibration configuration SCP 542 SAC ↓ in CMP is therefore obtained as

$$\bar{\rho}_{cal}^{MSM} = 1047 \text{ pcm} \pm 5\%(1\sigma)$$

The resulting worth of the SAC system with SCP at critical insertion is

$$\Delta\rho(SAC) = 1039 \text{ pcm} \pm 5\%(1\sigma)$$

The 1σ uncertainties quoted for the Etalon subcriticality and for the SAC worth were taken from the original analysis of the experiments (Ref. / 2 /).

It is important to note that this result justifies a-posteriori the approach chosen by CEA for the first analysis campaign of CMP.

Unlike the first analysis of the CID experiments, where the MSM correction factors had been directly taken from unadjusted design level calculations, in the case of CMP, the correction factors obtained from such calculations had been linearly interpolated to match experimental reactivity worths:

$$F_{\text{interpolated}} = 1 - [1 - F_{\text{calculated}}] \cdot \frac{\Delta\rho_{\text{measured}}}{\Delta\rho_{\text{calculated}}}$$

(More precisely, the difference between unity and the calculated correction factor was interpolated according to the reactivity ratio!)

As the measured subcriticality was a-priori unknown, an iterative procedure was used to determine $F_{\text{interpolated}}$.

In view of the substantial reactivity scale shift (-1900 pcm) observed in the calculations for the critical situation, not the calculated subcriticality of a given situation was used in the above formula, but the calculated reactivity difference between the in principle critical state and the configuration in question. Correction factors were thus interpolated on the basis of rod worths under neglect of the faulty reactivity scale adjustment at critical.

It should be emphasized that although this approach was found to produce satisfactory results not only for the assessment of the CMP Etalon subcriticality but also for a number of other configurations where correction factors differed little from unity, it can not always be employed with the same reliability. Substantial errors were observed in the case of more complicated control rod arrays involving strong flux distortions and correction factors that differed significantly from unity.

VII.3 The selected configurations of CMP

Table XIII summarises the configurations that had been recommended by the SPX-1 analysis task force to be analysed, the associated detector count rates eC , and the uncorrected subcriticalities ${}^e\rho^{MSA}$ resulting from an Etalon detector count rate of 757.3 c/s and an Etalon subcriticality of 1047 pcm.

Table XIII Configurations to be analysed in CMP

Configuration	eC	${}^e\rho^{MSA}$
1. SCP 542, SAC ↓ ('Etalon-CMP')	757.3	
2. SCP 542, B10 ↓	5671.0	-139.8
3. SCP 542, B2 ↓	3430.0	-231.1
4. SCP 542, SAC1 ↓, SAC2,SAC3 ↑	2825.6	-280.6
5. SCP 542, B1,B2 ↓	1786.0	-443.9
6. SCP 542, B10,B17 ↓	2719.0	-291.6
7. RE 542, RI ↓	439.0	-1806.1
8. RI 900, RE ↓	5297.0	-149.7
9. SCP 520, B2 ↓	1500.8	-528.3
10. SCP 520, B7 ↓	1858.2	-426.7
11. SCP 520, B8 ↓	1845.9	-429.5
12. SCP 520, B9 ↓	1914.0	-414.3
13. SCP 520, B10 ↓	2028.2	-390.9
14. SCP 520, B11 ↓	2111.1	-375.6
15. SCP 465, B2,B4,B6 ↓	437.0	-1814.4
16. SCP 486, B10,B15,B20 ↓	724.0	-1095.2
17. SCP ↓	167.4 (166.2)	-4736.5 (4770.6)
18. SCP ↓, SAC ↓	133.9	-5921.5
19. SCP ↓, B12 ↑	182.8	-4337.5

Whenever the state of the SAC system is not indicated, its absorbers are fully raised.

The count rate given in parentheses for configuration 17 was obtained when the same configuration was established for a second time.

The procedure used to determine the MSM correction factors was analogous to that described in Sec. VI.2 for the analysis of the C1D experiments.

In the preceding section, the calculated product $\rho_{cal} \cdot C_{cal}$, was established as 155.9 for 2D calculations and as 3.715 for 3D calculations. The detailed results of the calculations serving to derive the configuration dependent products $\rho \cdot C$ are given in Tables A4.1 through A4.29 of Appendix 4.

The assessment of the Etalon subcriticality in the previous section had shown that the SAC worth was well (within 10 pcm) reproduced when cross sections of a 35% SCP absorber were used (Tables X and XI). It was therefore decided to economize on computing costs and to use only these cross sections in the 3D calculations rather than running through the usual tuning procedure.

**Table XIV Results of MSM measurements in CMP
---2D and 3D correction factor calculations ---**

Control rod configuration	$\epsilon \rho^{MSA}$	F(2D)	F(3D)	ρ_{2D}^{MSM}	ρ_{3D}^{MSM}
1. SCP 542, SAC ↓ (Etalon)				-1047.0	
2. SCP 542, B10 ↓	-139.8	1.011		-141.3	
3. SCP 542, B2 ↓	-231.1	0.942	0.943	-217.8	-218.0
4. SCP 542,SAC1↓,SAC2,3↑	-280.6	0.982		-275.6	
5. SCP 542, B1,B2 ↓	-443.9	0.876	0.881	-388.9	-391.1
6. SCP 542, B10,B17 ↓	-291.6	1.032	1.032	-300.9	-300.9
7. RE 542, RI ↓	-1806.1	0.655	0.657	-1183.0	-1186.6
8. RI 900, RE ↓	-149.7	1.473	1.483	-220.5	-222.0
9. SCP 520, B2 ↓	-528.3	0.941		-497.1	
10. SCP 520, B7 ↓	-426.7	1.005		-428.8	
11. SCP 520, B8 ↓	-429.5	1.003		-430.8	
12. SCP 520, B9 ↓	-414.3	1.001		-414.7	
13. SCP 520, B10↓	-390.9	1.004		-392.5	
14. SCP 520, B11↓	-375.6	1.005		-377.5	
15. SCP 465, B2,B4,B6 ↓	-1814.4	0.846	0.844	-1534.9	-1530.6
16. SCP 486,B10,B15,B20↓	-1095.2	1.028	1.018	-1125.8	-1114.9
17. SCP ↓	-4736.5	0.919	0.925	-4352.9	-4381.3
17a. SCP ↓ (*)	-4770.7	0.919	0.924	-4383.5	-4409.5
18. SCP ↓ , SAC ↓	-5921.5	0.936	0.941	-5542.4	-5572.0
19. SCP ↓, B12 ↑	-4337.5	0.762	0.774	-3306.8	-3358.0

Remark (*) see following text !

Table XIV summarises the results of the KfK correction factor calculations for CMP. Given are the uncorrected experimental results ${}^e\rho^{MSA}$, the MSM correction factors F(2D) and F(3D) obtained from calculations in 2D and 3D geometry and the resulting experimental subcriticalities ρ_{2D}^{MSM} and ρ_{3D}^{MSM} .

(*) As mentioned above, a slightly different detector count rate was recorded when configuration SCP↓, SAC↑ was established for a second time. This second measurement was performed just before the start of a series of experiments, where rods in one half of the reactor core were raised to approach asymmetrical criticality. The next step in this series of experiments was to fully raise rod B12, thus leading to configuration No.19. Although the count rate change from 167.4 c/s to 166.2 c/s seems relatively small (-0.72%), it has a significant influence on the worth of B12, obtained as the difference in subcriticality between configurations 17 and 19. This is because $\Delta\rho(B12)$ is smaller by a factor of $\simeq 4$ than the subcriticality of configuration 17 from which rod B12 was raised! It was therefore considered useful to distinguish between the first and the second measurement of configuration SCP↓ SAC↑, and it seems plausible to derive the worth of B12 on the basis of the second measurement as it is in closer chronological correspondence to configuration 19.

One observes that for all configurations investigated, 2D and 3D calculations produce very similar results. In most cases the agreement is significantly better than 1% (rel.).

The most pronounced difference (1.6%) between the two calculation paths is found for the 'stuck-rod' configuration SCP↓ B12↑ SAC↑. The occurrence of an extreme flux peak around the position of the raised rod (B12) poses apparently a more serious problem for a twodimensional treatment than the other control rod configurations that have been analysed so far. In view of the complexity of this configuration, the agreement between the two calculations is nevertheless considered satisfactory.

Taking the reactivity difference between configurations 17a and 19, the worth of B12 when raised from shutdown is obtained as 1078 pcm and 1052 pcm when using calculations in 2D and 3D geometry respectively.

The SAC worth with SCP fully inserted is found as 1189.5 pcm with 2D calculations and as 1190.7 pcm with 3D calculations. Differences found when using alternatively 2D and 3D MSM factor calculations to derive the subcriticalities of configurations 17 and 18 cancel out on the SAC worth. The SAC worth with SCP at critical insertion was found as 1039 pcm. When the SCP system is lowered from critical to full insertion, involving a worth introduction of $\simeq 4350$ pcm, the worth of SAC therefore **increases** by 152 pcm or by 5% relative.

It is recalled that a significantly different behaviour had been observed for the first critical core (Sec. VI.2). There, a worth introduction in SCP of 4957 pcm had **reduced** the worth of SAC by almost 21%.

Finally, the excess reactivity of the CMP core with all control rod absorbers fully raised is obtained as follows:

S-curve measurements of the SCP system, performed during the different loading phases of the reactor (there over the full stroke) and in the core variants C1D and CMP (there only below critical insertion) have led to the conclusion that in CMP the worth fractions of SCP above and below critical insertion are 46% and 54% of the full stroke worth, respectively. From this, the CMP core excess reactivity can easily be deduced from the shutdown subcriticalities given for configuration 17 (or 17a):

$$\rho^{excess} = \left(\frac{1}{0.54} - 1 \right) \cdot 4352.8 = 3708 \text{ pcm} \quad (2D)$$

$$\rho^{excess} = \left(\frac{1}{0.54} - 1 \right) \cdot 4381.2 = 3732 \text{ pcm} \quad (3D)$$

Alternative use of 2D and 3D correction factor calculations thus leads to values of the core excess reactivity that differ by only 24 pcm (i.e. less than 0.7%). Comprising a more detailed description of the core geometry, the 3D calculation can probably be assumed to give the more trustworthy MSM correction factor; the value of 3732 pcm is therefore proposed to be used for the experimental core excess reactivity of the CMP (BOL) core.

In this context one should remember that the 2D and 3D calculations serving for the determination of the correction factors did not exactly reproduce this value of the excess reactivity as they had been adjusted to an anticipated value of this parameter. The calculation in 2D geometry had given a core excess reactivity of +3704 pcm. 3D calculations using two different absorber concentrations for the fully raised SCP rods gave +3735 pcm and +3743 pcm. These minute inconsistencies between the adjustment of the calculations and the experimental result produced with the help of these calculations are not considered to have a severe impact on the present re-analysis.

VIII Some remarks on uncertainties of experimental results

VIII.1 *The present state*

Uncertainties on the experimental results as quoted in the original CEA analysis of the control rod experiments in References. / 1 and 2 / are the following (always 1σ):

For the calibration state (Etalon)

1. Detector count rates: $\pm 2\%$
2. MSM correction factors G_i : $\pm 3\%$
3. Subcriticalities after rod drops (inverse kinetics analysis): Individual uncertainties ranging from ± 2 to $\pm 10\%$.

An adequate combination of these individual contributions led to the following combined uncertainties:

Etalon of the C1D - core: $\pm 6\%$

Etalon of the CMP - core: $\pm 5\%$

It is stressed that these uncertainties do not include the uncertainty of the delayed neutron fraction β_{eff} which is usually quoted as $\pm 5\%$ (1σ).

For the subcriticality of the reactor determined by the MSM method.

1. Detector count rates : $\pm 2\%$
2. MSM correction factors F : $\pm 3\%$
3. Uncertainty on the subcriticality of the Etalon-state: $\pm 6\%$ in C1D and $\pm 5\%$ in CMP.

A combination of these contributions gave the following total uncertainties (still excluding β_{eff}) for the subcriticality of any control rod configuration (1σ):

in the C1D - core: $\pm 7\%$

in the CMP - core: $\pm 6\%$

It is evident that the situation becomes more complicated in those cases where not the subcriticality of a given reactor configuration is the subject of interest, but the difference in subcriticality between two configurations.

Such a situation is encountered e.g. in the assessment of the worth of the SAC system when the SCP system is fully inserted. References / 1 and 2 / proposes to combine the uncertainties as follows:

1. In the CID core
 - a. Systematic uncertainty (Etalon + F): $\pm 6.7\%$
 - b. Combined uncertainties of count rates: $\pm 15.9\%$
(Etalon and rod array)
2. In the CMP core
 - a. Systematic uncertainty (Etalon + F): $\pm 5.8\%$
 - b. Combined uncertainties of count rates: $\pm 5.8\%$
(Etalon and rod array)

Quadratic combination of the individual contributions leads to the following combined uncertainties on the SAC - worth:

in the CID - core: $\pm 17.3\%$
in the CMP - core: $\pm 8.2\%$

One concludes that substantial uncertainties can be accumulated on the worths of control rods or rod groups when these worths represent the difference of the subcriticalities of two different rod configurations.

VIII.2 *Recent considerations.*

The assessment of uncertainties has recently been reviewed by Belgonucléaire / 15 / and KfK with the result that some of the uncertainty contributions quoted in the original analysis of CEA (/ 1 and 2 /) are proposed to be reduced or deleted.

As these new considerations are still under discussion, only some very brief indications will be given hereafter.

1. One obvious point that had not been thoroughly considered in the original analysis is that uncertainties on the detector count rate of the Etalon state should not appear in the combined uncertainties of the corrected experimental results.

This can be easily demonstrated:

As outlined before, the subcriticality of a given array can be obtained from Eq.(3) of Sec. III.1:

$$\rho^{MSM} = \frac{{}^e\rho_{cal} \cdot {}^eC_{cal}}{{}^eC} \cdot \mathbf{F} \quad (3)$$

In the SPX-1 analysis, an 'artificial' Etalon was defined as the state SCP-Z_c SAC↓ and its subcriticality ${}^e\rho_{cal}$ was determined using a series of rod drop experiments. Each of these experiments gave one individual result for the Etalon subcriticality (Eq.(6) of Sec. IV.3):

$$\rho_{cal,i}^{MSM} = \frac{{}^e\rho_i \cdot {}^eC_i}{{}^eC_{cal}} \cdot \mathbf{G}_i \quad (6)$$

In the analysis presented in this report, the mean value $\bar{\rho}_{cal}^{MSM}$ of these individual results was used for ${}^e\rho_{cal}$ of Eq.(3).

Alternatively one could have completely avoided the definition of an additional Etalon state by simply defining each of the individual rod drops as an Etalon state.

In this case the quantity ${}^e\rho_{cal}$ in Eq.(3) would have been replaced by the individual results of Eq.(6) and Eq.(3) would have read:

$$\rho_i^{MSM} = \frac{{}^eC_{cal}}{{}^eC} \cdot \frac{{}^e\rho_i \cdot {}^eC_i}{{}^eC_{cal}} \cdot \mathbf{G}_i \cdot \mathbf{F} \quad (13)$$

The mean value of all individual subcriticalities ρ_i^{MSM} would obviously agree with the results presented in this report as only the intermediate introduction of the Etalon state was suppressed and the transition from individual values to the corresponding mean value was shifted from the Etalon to the array subcriticality.

The advantage of this different formulation is in that one can readily see that the measured Etalon detector count rate ${}^eC_{cal}$ cancels out in the determination of the array subcriticality and that its uncertainty should therefore not appear in the general uncertainty assessment.

2. It is evident that the same applies to the calculated quantity $\rho_{cal} \cdot C_{cal}$ which appears twice in the correction factor product $\mathbf{G}_i \cdot \mathbf{F}$ of Eq.(13) :

$$\mathbf{G}_i \cdot \mathbf{F} = \frac{\rho_{cal} \cdot C_{cal}}{\rho_i \cdot C_i} \cdot \frac{\rho \cdot C}{\rho_{cal} \cdot C_{cal}} \quad (14)$$

The only reason why nevertheless substantial work was invested in a reliable determination of this quantity (Secs. VI.1 and VII.2) was in that the present analysis involved the intermediate determination of the subcriticality of the 'arbitrarily' defined Etalon state. The formula used for the assessment of this state contains only the correction factors \mathbf{G}_i and therefore required the determination of $\rho_{cal} \cdot C_{cal}$.

The fact that in principle only the correction factors $\rho \cdot C / \rho_i \cdot C_i$ have an influence on the determination of the control rod array subcriticality, implies that in the general uncertainty assessment the contribution from correction factors should only be counted once. The double appearance of the correction factor uncertainty of $\pm 3\%$ in the original analysis in both the Etalon (\mathbf{G}_i) and in the array subcriticality (\mathbf{F}) assessment was therefore not justified.

3. The next point of discussion is that the 1σ uncertainty of MSM correction factors is still considered to be in the order of $\pm 3\%$. Looking at the consistency of the results of this report produced using alternatively 2D and 3D calculations one finds that even for those configurations where flux shapes were extremely distorted, correction factors still agreed within 1.6%. For the majority of the configurations, the agreement of results from the two calculation paths is even better than $\pm 1\%$. MSM correction factors produced by adjusted calculations - as discussed in the present report - should therefore not be affected by errors greater than ± 1 to $\pm 2\%$.
4. Although this point might appear obsolete after the preceding comments, it seems nevertheless worth noting that the uncertainty of the MSM correction factors used to establish the Etalon is unlikely to be greater than $\pm 1\%$. Apart from one configuration where two inner ring rods had been dropped, 2D correction factors found in this context differed very little from unity and are

therefore not likely to contain any substantial errors. Sample calculations in 3D geometry reproduced the results of the 2D calculations within 0.2% !

5. Uncertainties of $\pm 2\%$ on detector count rates seem too pessimistic as apparently they refer to the largest observed value. In this case it would seem more realistic to attribute these uncertainties to a 2σ rather than to 1σ level. The 1σ uncertainty which is presently being considered would then drop to $\pm 1\%$.

These considerations and some others of smaller importance could lead to a marked reduction of up to 2% in the 1σ uncertainties of the measured subcriticality of control rod configurations using the MSM method. A final decision on these points has, however, not yet been taken by the SPX-1 analysis task-force.

IX Conclusions

As proposed by the SPX-1 analysis task force, MSM correction factors have been produced for a series of control rod configurations established in the first critical core C1D with minimum fissile loading and in the fully loaded core CMP.

The present report gave a complete description of the method used at KfK to produce these correction factors and summarised the evaluated experimental results obtained.

The KfK method is characterized by a 'two-step-adjustment': A basic reactivity scale adjustment and a subsequent rod worth adjustment.

The first adjustment was achieved by 'tuning' either the axial buckling in the leakage term DB^2 or the average number of neutrons per fission ν in the production term $\nu\Sigma_f$ so that the excess reactivity of the so-called 'Follower-core' with all control rods fully raised was properly reproduced. As this excess reactivity could not be directly determined by an experiment, it had to be assessed from the shut-down worth of the main control system in combination with measured fractions of the S-curve of this system (see Secs. III.2, VII.3).

In the second adjustment, the absorber cross sections were tuned to reproduce experimental rod worths.

While for the analysis of the C1D experiments, MSM correction factor calculations were performed in 2D centre-plane geometry only, the analysis of the CMP measurements employed both 2D and 3D calculations.

The results show :

1. For the core C1D, the present analysis leads to a subcriticality of the MSM calibration configuration (Etalon) of 903 pcm. The original CEA analysis had produced a value of 965 pcm. The origin of this significant reduction of 6.4% is twofold:
 - a. A reduction of β_{eff} from the initial value of 380 pcm which was used in the first analysis to a presently recommended value of 365 pcm, caused a reduction of experimental rod worths by 3.9%.
 - b. The residual reduction of 2.5% is caused by the improved reproduction of experimental reactivity levels in the presently used refined correction factor calculations. Performed immediately after the completion of the measurements with very little time available, the original CEA analysis of the C1D experiments used MSM correction factors that were directly taken from unadjusted design level calculations. As rod worths were substantially overestimated by these calculations, the resulting correction factors did not match the experimental reactivity levels.
2. As a consequence of (1), shut-down worths for the situations SCP↓ SAC↑ and SCP↓ SAC↓ drop from the original values of 8295 pcm and 9066 pcm by 6.5% (6.7%) to values of 7755 pcm and 8460 pcm, respectively. Similar changes are observed for the other re-evaluated configurations.
3. For the core CMP, the present analysis leads to a subcriticality of the MSM calibration configuration (Etalon) of 1047 pcm, while the original analysis had given 1090 pcm. The observed reduction of 3.9% is fully explained by the updating of β_{eff} . The consistency of these results underlines two points:

- a. The approach chosen by the SPX-1 start-up group at CEA to produce MSM correction factors in the course of the first determination of the Etalon subcriticality of CMP was justified. Unlike the first analysis of the CID experiments, where the MSM correction factors had been directly taken from unadjusted design level calculations, in the case of CMP, the correction factors obtained from such calculations had been linearly interpolated to match experimental reactivity worths.
 - b. The production of MSM correction factors is insensitive to the data base (CEA used the CARNAVAL-IV, while KfK uses the KFKINR001 library of nuclear cross sections).
4. In agreement with the reduction of the Etalon subcriticality, the reactivity worths of most other configurations are also found to be about 3.9 % smaller than those found in the original analysis. This does e.g. not apply to the configuration where one single control rod was completely raised from shut-down. For this configuration, the linear interpolation approach of the first CEA analysis had produced a strongly aberrant result!
 5. For all configurations investigated in CMP, correction factors produced using 2D and 3D calculations show very close agreement. In most cases this agreement is significantly better than 1%(rel.). The most pronounced difference (1.6%) between the two calculation paths is found for the 'stuck-rod' configuration SCP↓ B12↑ SAC↑. The occurrence of an extreme flux peak around the position of the raised rod (B12) poses apparently a more serious problem for a twodimensional treatment than the other control rod configurations that have been analysed so far. This illustrates the limited applicability of 2D calculations in cases involving extreme flux distortions. In view of the complexity of this configuration, the agreement of the MSM correction factors obtained with the two calculations within less than 2% can nevertheless be considered satisfactory.

Acknowledgements

The author is deeply indebted to Drs. F. Helm and E. Kiefhaber for the stimulating discussions that helped to arrive at a better understanding of the complex implications that arise with the use of the MSM technique in power reactors and for their critical and patient reviewing of this report.

The programming efforts of Mr. B. Stehle in implementing a novel version of the source driven mode of the diffusion theory code D3E to allow the separate input of spontaneous and (α, n) sources with different associated spectra and to automatically calculate the products $\langle S\Phi^+ \rangle$, $\langle \Phi^+ P \Phi^{inh} \rangle$ (see Sec. V.2) and $\langle \Sigma_{det} \bullet \Phi^{inh} \rangle$ (see Sec. III.1) which substantially facilitated the analysis work are gratefully acknowledged.

References:

- / 1 / J.P. WEST, J.C. GAUTHIER
Unpublished CEA report.
- / 2 / J.P. WEST, J.C. GAUTHIER
Unpublished CEA report.
- / 3 / J.L. ROWLANDS, C.R. EATON
'The spatial averaging of cross sections for use in transport theory reactor calculations, with an application to control rod fine structure homogenisation'.
Proc. of the Specialists' Meeting on Homogenisation Methods in Reactor Physics, Lugano, Switzerland, November 13-15, 1978, p. 261-268.
- / 4 / G. PALMIOTTI
'A method to obtain new cross sections transport equivalent'.
Proc. of the IAEA/IWGFR Specialists' Meeting on Methods for Reactor Physics Calculations for Control Rods in Fast Reactors, Winfrith, UK, December 6-8, 1988, p. 33-56.
- / 5 / J.C. CABRILLAT, et al.
'Application of transport equivalent cross sections obtained by the MONSTRE-method to SPX-1 case'.
Proc. of the IAEA/IWGFR Specialists' Meeting on Methods for Reactor Physics Calculations for Control Rods in Fast Reactors, Winfrith, UK, December 6-8, 1988, p. 263-285.
- / 6 / S.G. CARPENTER
'Measurement of Control Rod Worths Using ZPPR'.
Proc. of the Specialists' Meeting on Control Rod Measurement Techniques: Reactivity Worth and Power Distributions, Cadarache, France, April 21-22, 1976.
- / 7 / R. DE WOUTERS
Unpublished BN report.
- / 8 / E. KIEFHABER
'The KFKINR-Set of Group Constants , Nuclear Data Basis, and First Results of its Application to the Recalculation of Fast Zero-Power Reactors'.
KfK-Report KfK-1572 (Kernforschungszentrum Karlsruhe 1972)
- / 9 / R. BOEHME and E.A. FISCHER
'The fast reactor cell code KAPER4'.
KfK-Report KfK-4435 (Kernforschungszentrum Karlsruhe 1988)
- / 10 / E.A. FISCHER
'Neutron Streaming in Fast Reactor Slab Lattices and in Cylindrical Channels'.
Nucl. Sci. Eng., 78, 227-238 (1981)

- / 11 / U.K. WEHMANN, H. GIESE
'Methods for Shutdown Worth Calculations in Fast Reactors
and Their Validation With Help of SPX-1 Absorber Experiment
Evaluations'.
Proc. of the IAEA/IWGFR Specialists' Meeting on Methods for
Reactor Physics Calculations for Control Rods in Fast Reactors,
Winfrith, UK, December 6-8, 1988, p. 341-353.
- / 12 / B. STEHLE
'D3D, Ein Fortran Programm zur Loesung der stationaeren
dreidimensionalen Multigruppendiffusionsgleichungen'.
KfK-Report KfK-2118 (Kernforschungszentrum Karlsruhe 1975)
- / 13 / J. HOMMET et al
Unpublished CEA report.
- / 14 / J.C. CABRILLAT
Unpublished CEA report.
- / 15 / R. DE WOUTERS
Private Communication (17.2.1989)
- / 16 / A. D'ANGELO
Unpublished CEA report.

Appendix 1

Calculations concerning the C1D Etalon

This Appendix presents the detailed results of the KfK calculations, that served to establish the subcriticality ρ_{cal}^{MSM} of the Etalon configuration SCP 929 SAC↓ in C1D.

All calculations were performed in 2D geometry and used a global axial buckling of 5.38 m^{-2} .

Table A1.1 2D-Calculation of "G" for SCP 920, B1↓, B2↑

First series: SCP 920 simulated by a 1% absorber

Configuration	ρ	$\Delta\rho$	$\rho \cdot C$	G
1. SCP 920, B1↑(Follower) B2↑(")	+ 37.1	0.0	---	
2. SCP 920, B1↓(42.5% abs.) B2↑(Follower)	-250.5	-287.6	159.78	1.0795
3. SCP 920, B1↓(45.0% abs.) B2↑(Follower)	-257.6	-294.7	159.17	1.0836
4. SCP 920, B1↓(57.5% abs.) B2↑(Follower)	-287.3	-324.4	156.57	1.1016
5. SCP 920, B1↓(60.0% abs.) B2↑(Follower)	-292.3	-329.4	156.12	1.1048
6. SCP 920, B1↓(62.5% abs.) B2↑(Follower)	-297.1	-334.2	155.70	1.1078
7. SCP 920, B1↓(65.0% abs.) B2↑(Follower)	-301.6	-338.7	155.29	1.1107

Second series: SCP 920 simulated by a 1.5% absorber

Configuration	ρ	$\Delta\rho$	$\rho \cdot C$	G
1. SCP 920, B1↑(Follower) B2↑(")	-99.1	-0.0	---	
2. SCP 920, B1↓(42.5% abs.) B2↑(Follower)	-390.6	-291.5	160.21	1.0766
3. SCP 920, B1↓(45.0% abs.) B2↑(Follower)	-397.9	-298.6	159.61	1.0807
4. SCP 920, B1↓(57.5% abs.) B2↑(Follower)	-427.8	-328.7	157.01	1.0985
5. SCP 920, B1↓(60.0% abs.) B2↑(Follower)	-432.8	-333.7	156.56	1.1017
6. SCP 920, B1↓(62.5% abs.) B2↑(Follower)	-437.7	-338.6	156.13	1.1047
7. SCP 920, B1↓(65.0% abs.) B2↑(Follower)	-442.2	-343.1	155.72	1.1076
8. SCP 920, B1↓(100.0% abs.) B2↑(Follower)	-489.4	-390.3	151.41	1.1392

Table A1.2 2D-Calculation of "G" for SCP 921, B1↑, B2↓

First series: SCP 921 simulated by a 1.0% absorber

Configuration	ρ	$\Delta\rho$	$\rho \cdot C$	G
1. SCP 921, B1↑(Follower) B2↑(")	+37.1	0.0	---	
2. SCP 921, B1↑(Follower) B2↓(42.5% abs.)	-247.8	-284.9	159.86	1.0790
3. SCP 921, B1↑(Follower) B2↓(45.0% abs.)	-254.9	-292.0	159.26	1.0830
4. SCP 921, B1↑(Follower) B2↓(52.5% abs.)	-273.6	-310.7	157.61	1.0944
5. SCP 921, B1↑(Follower) B2↓(55.0% abs.)	-279.2	-316.3	157.14	1.0976
6. SCP 921, B1↑(Follower) B2↓(100.0% abs.)	-345.6	-382.7	151.13	1.1413

Second series: SCP 921 simulated by a 1.5% absorber

Configuration	ρ	$\Delta\rho$	$\rho \cdot C$	G
1. SCP 921, B1↑(Follower) B2↑(")	-99.1	0.0	---	
2. SCP 921, B1↑(Follower) B2↓(42.5% abs.)	-387.8	-288.7	160.29	1.0761
3. SCP 921, B1↑(Follower) B2↓(45.0% abs.)	-395.0	-295.9	159.68	1.0801
4. SCP 921, B1↑(Follower) B2↓(100.0% abs.)	-486.6	-387.5	151.55	1.1381

Table A1.3 2D-Calculation of "G" for SCP 922, B9↓, B10↑, B1 918

First series: SCP 922 simulated by a 1.0% absorber

Configuration	ρ	$\Delta\rho$	$\rho \cdot C$	G
1. SCP 922, B9↑(Follower) B10↑(")	+28.7	0.0	---	
2. SCP 922, B9↓(40.0% abs.) B10↑(Follower)	-156.4	-185.1	178.54	0.9660
3. SCP 922, B9↓(42.5% abs.) B10↑(Follower)	-160.8	-189.5	178.46	0.9665
4. SCP 922, B9↓(45.0% abs.) B10↑(Follower)	-165.1	-193.8	178.37	0.9670

Second series: SCP 922 simulated by a 1.5% absorber

Configuration	ρ	$\Delta\rho$	$\rho \cdot C$	G
1. SCP 922, B9↑(Follower) B10↑(")	-111.2	-0.0	---	
2. SCP 922, B9↓(40.0% abs.) B10↑(Follower)	-301.8	-190.6	178.06	0.9687
3. SCP 922, B9↓(47.5% abs.) B10↑(Follower)	-314.7	-203.5	177.83	0.9699
4. SCP 922, B9↓(50.0% abs.) B10↑(Follower)	-318.5	-207.3	177.76	0.9703

Table A1.4 2D-Calculation of "G" for SCP 922, B9↑, B10↓, B1 918

First series: SCP 922 simulated by a 1.0% absorber

Configuration	ρ	$\Delta\rho$	$\rho \cdot C$	G
1. SCP 922, B9↑(Follower) B10↑(")	+28.7	0.0	---	
2. SCP 922, B9↑(Follower) B10↓(40.0% abs.)	-149.3	-178.0	179.24	0.9623
3. SCP 922, B9↑(Follower) B10↓(42.5% abs.)	-153.4	-182.1	179.17	0.9627
4. SCP 922, B9↑(Follower) B10↓(45.0% abs.)	-157.2	-185.9	179.10	0.9630

Second series: SCP 922 simulated by a 1.5% absorber

Configuration	ρ	$\Delta\rho$	$\rho \cdot C$	G
1. SCP 922, B9↑(Follower) B10↑(")	-111.2	0.0	---	
2. SCP 922, B9↑(Follower) B10↓(40.0% abs.)	-295.1	-183.9	178.77	0.9648
3. SCP 922, B9↑(Follower) B10↓(42.5% abs.)	-299.4	-188.2	178.71	0.9651
4. SCP 922, B9↑(Follower) B10↓(45.0% abs.)	-303.3	-192.1	178.65	0.9655

Table A1.5 2D-Calculation of "G" for SCP 921, B10↑, B17↓, B1 887

First series: SCP 921 simulated by a 1.0% absorber

Configuration	ρ	$\Delta\rho$	$\rho \cdot C$	G
1. SCP 921, B10↑(Follower) B17↑(")	+ 35.3	0.0	---	
2. SCP 921, B10↑(Follower) B17↓(42.5% abs.)	-200.4	-235.7	178.04	0.9688
3. SCP 921, B10↑(Follower) B17↓(45.0% abs.)	-204.4	-239.7	177.87	0.9697

Second series: SCP 921 simulated by a 1.5% absorber

Configuration	ρ	$\Delta\rho$	$\rho \cdot C$	G
1. SCP 921, B10↑(Follower) B17↑(")	-101.4	0.0	---	
2. SCP 921, B10↑(Follower) B17↓(37.5% abs.)	-333.2	-231.8	177.78	0.9702
3. SCP 921, B10↑(Follower) B17↓(45.0% abs.)	-346.3	-244.9	177.30	0.9728
4. SCP 921, B10↑(Follower) B17↓(47.5% abs.)	-350.0	-248.6	177.18	0.9735

Table A1.6 2D-Calculation of "G" for SCP 921, B2↑, B18↓, B1 918

First series: SCP 921 simulated by a 1.0% absorber

Configuration	ρ	$\Delta\rho$	$\rho \cdot C$	G
1. SCP 921, B2↑(Follower) B18↑(")	+36.2	0.0	---	
2. SCP 921, B2↑(Follower) B18↓(45.0% abs.)	-180.7	-216.9	180.04	0.9580
3. SCP 921, B2↑(Follower) B18↓(47.5% abs.)	-184.4	-220.6	179.93	0.9586
4. SCP 921, B2↑(Follower) B18↓(57.5% abs.)	-196.9	-233.1	179.54	0.9607
5. SCP 921, B2↑(Follower) B18↓(60.0% abs.)	-199.6	-235.8	179.45	0.9612
6. SCP 921, B2↑(Follower) B18↓(62.5% abs.)	-202.1	-238.3	179.36	0.9616

Second series: SCP 921 simulated by a 1.5% absorber

Configuration	ρ	$\Delta\rho$	$\rho \cdot C$	G
1. SCP 921, B2↑(Follower) B18↑(")	-101.4	0.0	---	
2. SCP 921, B2↑(Follower) B18↓(42.5% abs.)	-317.2	-216.8	180.17	0.9573
3. SCP 921, B2↑(Follower) B18↓(45.0% abs.)	-321.3	-220.9	180.07	0.9579
4. SCP 921, B2↑(Follower) B18↓(57.5% abs.)	-337.7	-237.3	179.59	0.9604
5. SCP 921, B2↑(Follower) B18↓(60.0% abs.)	-340.4	-240.0	179.51	0.9608
6. SCP 921, B2↑(Follower) B18↓(62.5% abs.)	-342.9	-242.5	179.42	0.9613
7. SCP 921, B2↑(Follower) B18↓(65.0% abs.)	-345.3	-244.9	179.34	0.9617

Table A1.7 2D-Calculation of "G" for SCP 929, SAC1↓, SAC2,3↑

SCP 929 simulated by a 1.0% absorber

Configuration	ρ	$\Delta\rho$	$\rho \cdot C$	G
1. SCP 929, SAC1↑(Follower) SAC2,3↑(")	+ 5.1	0.0	---	
2. SCP 929, SAC1↓(32.5% abs.) SAC2,3↑(Follower)	-231.7	-236.8	173.43	0.9945
3. SCP 929, SAC1↓(35.0% abs.) SAC2,3↑(Follower)	-239.4	-244.5	173.08	0.9965
4. SCP 929, SAC1↓(37.5% abs.) SAC2,3↑(Follower)	-246.4	-251.5	172.75	0.9984

Table A1.8 2D-Calculation of "G" for SCP 921, B1↓, B2↓

First series: SCP 921 simulated by a 1.0% absorber

Configuration	ρ	$\Delta\rho$	$\rho \cdot C$	G
1. SCP 921, B1↑(Follower) B2↑(")	+37.1	0.0	---	
2. SCP 921, B1↓(35.0% abs.) B2↓(")	-428.9	-466.0	145.26	1.1874
3. SCP 921, B1↓(37.5% abs.) B2↓(")	-442.3	-479.4	144.05	1.1974
4. SCP 921, B1↓(57.5% abs.) B2↓(")	-520.0	-557.1	136.66	1.2621
5. SCP 921, B1↓(60.0% abs.) B2↓(")	-527.2	-564.3	135.95	1.2687
6. SCP 921, B1↓(62.5% abs.) B2↓(")	-534.1	-571.2	135.28	1.2750
7. SCP 921, B1↓(65.0% abs.) B2↓(")	-540.5	-577.6	135.64	1.2810

Second series: SCP 921 simulated by a 1.5% absorber

Configuration	ρ	$\Delta\rho$	$\rho \cdot C$	G
1. SCP 921, B1↑(Follower) B2↑(")	-99.1	0.0	---	
2. SCP 921, B1↓(35.0% abs.) B2↓(")	-571.1	-472.0	145.71	1.1837
3. SCP 921, B1↓(37.5% abs.) B2↓(")	-584.5	-485.4	144.49	1.1937
4. SCP 921, B1↓(57.5% abs.) B2↓(")	-663.0	-563.9	137.10	1.2581
5. SCP 921, B1↓(60.0% abs.) B2↓(")	-670.3	-571.2	136.39	1.2646
6. SCP 921, B1↓(62.5% abs.) B2↓(")	-677.1	-578.0	135.71	1.2709
7. SCP 921, B1↓(65.0% abs.) B2↓(")	-683.6	-584.5	135.07	1.2770
8. SCP 921, B1↓(100.0% abs.) B2↓(")	-748.6	-649.5	128.46	1.3427

Table A1.9 2D-Calculation of "G" for SCP 922, B2↓, B10↓

First series: SCP 922 simulated by a 1.0% absorber

Configuration	ρ	$\Delta\rho$	$\rho \cdot C$	G
1. SCP 922, B2↑(Follower) B10↑(")	+32.7	0.0	---	
2. SCP 922, B2↓(42.5% abs.) B10↓(")	-377.3	-410.0	157.98	1.0918
3. SCP 922, B2↓(45.0% abs.) B10↓(")	-385.5	-418.2	157.31	1.0964
4. SCP 922, B2↓(47.5% abs.) B10↓(")	-393.1	-425.8	156.68	1.1008

Second series: SCP 922 simulated by a 1.5% absorber

Configuration	ρ	$\Delta\rho$	$\rho \cdot C$	G
1. SCP 922, B2↑(Follower) B10↑(")	-105.5	0.0	---	
2. SCP 922, B2↓(42.5% abs.) B10↓(")	-522.6	-417.1	158.17	1.0905
3. SCP 922, B2↓(45.0% abs.) B10↓(")	-530.8	-425.3	157.51	1.0950
4. SCP 922, B2↓(47.5% abs.) B10↓(")	-538.5	-433.0	156.88	1.0994

Table A1.10 2D-Calculation of "G" for SCP 921, B2↓, B18↓, B1 914

First series: SCP 921 simulated by a 1.0% absorber

Configuration	ρ	$\Delta\rho$	$\rho \cdot C$	G
1. SCP 921, B2↑(Follower) B18↑(")	+ 36.2	0.0	---	
2. SCP 921, B2↓(42.5% abs.) B18↓(")	-519.7	-555.9	161.47	1.0682
3. SCP 921, B2↓(45.0% abs.) B18↓(")	-533.7	-569.9	160.86	1.0722
4. SCP 921, B2↓(47.5% abs.) B18↓(")	-546.8	-583.0	160.29	1.0761

Second series: SCP 921 simulated by a 1.5% absorber

Configuration	ρ	$\Delta\rho$	$\rho \cdot C$	G
1. SCP 921, B2↑(Follower) B18↑(")	-100.4	0.0	---	
2. SCP 921, B2↓(42.5% abs.) B18↓(")	-661.8	-561.4	161.54	1.0677
3. SCP 921, B2↓(45.0% abs.) B18↓(")	-675.8	-575.4	160.93	1.0717
4. SCP 921, B2↓(47.5% abs.) B18↓(")	-689.0	-588.6	160.36	1.0756

Table A1.11 2D-Calculation of "G" for SCP 921, B9↓, B10↓

First series: SCP 921 simulated by a 1.0% absorber

Configuration	ρ	$\Delta\rho$	$\rho \cdot C$	G
1. SCP 921, B9↑(Follower) B10↑(")	+28.7	0.0	---	
2. SCP 921, B9↓(42.5% abs.) B10↓(")	-271.2	-299.9	176.29	0.9784
3. SCP 921, B9↓(45.0% abs.) B10↓(")	-276.3	-305.0	176.09	0.9795
4. SCP 921, B9↓(47.5% abs.) B10↓(")	-281.0	-309.7	175.91	0.9805

Second series: SCP 921 simulated by a 1.5% absorber

Configuration	ρ	$\Delta\rho$	$\rho \cdot C$	G
1. SCP 921, B9↑(Follower) B10↑(")	-111.2	0.0	---	
2. SCP 921, B9↓(42.5% abs.) B10↓(")	-419.7	-308.5	176.03	0.9798
3. SCP 921, B9↓(45.0% abs.) B10↓(")	-424.8	-313.6	175.85	0.9809
4. SCP 921, B9↓(47.5% abs.) B10↓(")	-429.6	-318.4	175.67	0.9818

Table A1.12 2D-Calculation of "G" for SCP 920, B10↓, B17↓, B1 895

First series: SCP 920 simulated by a 1.0% absorber

Configuration	ρ	$\Delta\rho$	$\rho \cdot C$	G
1. SCP 920, B10↑(Follower) B17↑(")	+35.5	0.0	---	
2. SCP 920, B10↓(42.5% abs.) B17↓(")	-451.2	-486.5	184.81	0.9333
3. SCP 920, B10↓(45.0% abs.) B17↓(")	-462.2	-497.5	184.81	0.9333
4. SCP 920, B10↓(47.5% abs.) B17↓(")	-472.4	-507.7	184.81	0.9333

Second series: SCP 920 simulated by a 1.5% absorber

Configuration	ρ	$\Delta\rho$	$\rho \cdot C$	G
1. SCP 920, B10↑(Follower) B17↑(")	-101.4	0.0	---	
2. SCP 920, B10↓(42.5% abs.) B17↓(")	-597.5	-496.1	184.23	0.9362
3. SCP 920, B10↓(45.0% abs.) B17↓(")	-608.6	-507.2	184.24	0.9362
4. SCP 920, B10↓(47.5% abs.) B17↓(")	-618.9	-517.5	184.24	0.9361

Table A1.13 2D-Calculation of "G" for SCP 915, B2,B4↓, B6↑

First series: SCP 915 simulated by a 1.0% absorber

Configuration	ρ	$\Delta\rho$	$\rho \cdot C$	G
1. SCP 915,B2,B4↑(Follower) B6↑(")	+ 52.5	0.0	---	
2. SCP 915,B2,B4↓(42.5% abs.) B6↑(Follower)	-505.1	-557.6	140.62	1.2265
3. SCP 915,B2,B4↓(45.0% abs.) B6↑(Follower)	-518.6	-571.1	139.49	1.2365
4. SCP 915,B2,B4↓(47.5% abs.) B6↑(Follower)	-531.3	-583.8	138.41	1.2462

Second series: SCP 915 simulated by a 1.5% absorber

Configuration	ρ	$\Delta\rho$	$\rho \cdot C$	G
1. SCP 915,B2,B4↑(Follower) B6↑(")	-76.4	0.0	---	
2. SCP 915,B2,B4↓(42.5% abs.) B6↑(Follower)	-637.9	-561.5	141.65	1.2176
3. SCP 915,B2,B4↓(45.0% abs.) B6↑(Follower)	-651.5	-575.1	140.52	1.2275
4. SCP 915,B2,B4↓(47.5% abs.) B6↑(Follower)	-664.2	-587.8	139.44	1.2369

Table A1.14 2D-Calculation of "G" for SCP 918, B10,B15,B20↓

First series: SCP 918 simulated by a 1.0% absorber

Configuration	ρ	$\Delta\rho$	$\rho \cdot C$	G
1. SCP 918, B10,B15,B20 ↑ (Follower)	+ 39.6	0.0	---	
2. SCP 918, B10,B15,B20 ↓ (42.5% abs.)	-602.0	-641.6	187.72	0.9188
3. SCP 918, B10,B15,B20 ↓ (45.0% abs.)	-618.9	-658.5	187.89	0.9180
4. SCP 918, B10,B15,B20 ↓ (47.5% abs.)	-635.0	-674.6	188.06	0.9172
5. SCP 918, B10,B15,B20 ↓ (57.5% abs.)	-691.2	-730.8	188.62	0.9144
6. SCP 918, B10,B15,B20 ↓ (60.0% abs.)	-703.5	-743.1	188.72	0.9139
7. SCP 918, B10,B15,B20 ↓ (62.5% abs.)	-715.3	-754.9	188.83	0.9134
8. SCP 918, B10,B15,B20 ↓ (65.0% abs.)	-726.6	-766.2	188.94	0.9129

Second series: SCP 918 simulated by a 1.5% absorber

Configuration	ρ	$\Delta\rho$	$\rho \cdot C$	G
1. SCP 918, B10,B15,B20 ↑ (Follower)	-95.2	0.0	---	
2. SCP 918, B10,B15,B20 ↓ (42.5% abs.)	-744.4	-649.2	186.91	0.9228
3. SCP 918, B10,B15,B20 ↓ (45.0% abs.)	-761.5	-666.3	187.10	0.9219
4. SCP 918, B10,B15,B20 ↓ (47.5% abs.)	-777.7	-682.5	187.26	0.9211

Appendix 2

Calculations concerning the selected configurations of CID

This Appendix presents the detailed results of the KfK calculations that served to produce MSM correction factors for those control rod configurations established in CID, that were proposed by the SPX-1 task force group to be analysed by the different task force members.

It is noted that Tables A2.1, A2.2 and A2.8 of this Appendix represent copies of Tables A1.1, A1.4 and A1.14 of Appendix 1 where the same control rod configurations had been used to derive the correction factors **G**. Comparing the corresponding tables with each other, one observes, however, that although the formulas for the correction factors **F** and **G** are reciprocal, this is not exactly true for the quoted values of **F** and **G**. The reason for this anomaly is in the fact that for the numerator of **G**, the first guess product $\rho_{cal} \cdot C_{cal} = 172.4$ had been used, whereas for the denominator of **F**, the "converged" value of 172.7 has been taken.

Corresponding **F** and **G** values in the two sets of Tables therefore differ by 0.17%.

All calculations were performed in 2D geometry and used a global axial buckling of 5.38 m^{-2} .

Table A2.1 2D-Calculation of "F" for SCP 920, B1↓, B2↑

First series: SCP 920 simulated by a 1% absorber

Configuration	ρ	$\Delta\rho$	$\rho \cdot C$	F
1. SCP 920, B1↑(Follower) B2↑(")	+ 37.1	0.0	---	
2. SCP 920, B1↓(42.5% abs.) B2↑(Follower)	-250.5	-287.6	159.78	0.9252
3. SCP 920, B1↓(45.0% abs.) B2↑(Follower)	-257.6	-294.7	159.17	0.9217
4. SCP 920, B1↓(57.5% abs.) B2↑(Follower)	-287.3	-324.4	156.57	0.9066
5. SCP 920, B1↓(60.0% abs.) B2↑(Follower)	-292.3	-329.4	156.12	0.9040
6. SCP 920, B1↓(62.5% abs.) B2↑(Follower)	-297.1	-334.2	155.70	0.9016
7. SCP 920, B1↓(65.0% abs.) B2↑(Follower)	-301.6	-338.7	155.29	0.8992

Second series: SCP 920 simulated by a 1.5% absorber

Configuration	ρ	$\Delta\rho$	$\rho \cdot C$	F
1. SCP 920, B1↑(Follower) B2↑(")	-99.1	-0.0	---	
2. SCP 920, B1↓(42.5% abs.) B2↑(Follower)	-390.6	-291.5	160.21	0.9277
3. SCP 920, B1↓(45.0% abs.) B2↑(Follower)	-397.9	-298.6	159.61	0.9242
4. SCP 920, B1↓(57.5% abs.) B2↑(Follower)	-427.8	-328.7	157.01	0.9091
5. SCP 920, B1↓(60.0% abs.) B2↑(Follower)	-432.8	-333.7	156.56	0.9065
6. SCP 920, B1↓(62.5% abs.) B2↑(Follower)	-437.7	-338.6	156.13	0.9041
7. SCP 920, B1↓(65.0% abs.) B2↑(Follower)	-442.2	-343.1	155.72	0.9017
8. SCP 920, B1↓(100.0% abs.) B2↑(Follower)	-489.4	-390.3	151.41	0.8767

Table A2.2 2D-Calculation of "F" for SCP 922, B9↑, B10↓, B1 918

First series: SCP 922 simulated by a 1.0% absorber

Configuration	ρ	$\Delta\rho$	$\rho \cdot C$	F
1. SCP 922, B9↑(Follower) B10↑(")	+28.7	0.0	---	
2. SCP 922, B9↑(Follower) B10↓(40.0% abs.)	-149.3	-178.0	179.24	1.0379
3. SCP 922, B9↑(Follower) B10↓(42.5% abs.)	-153.4	-182.1	179.17	1.0375
4. SCP 922, B9↑(Follower) B10↓(45.0% abs.)	-157.2	-185.9	179.10	1.0371

Second series: SCP 922 simulated by a 1.5% absorber

Configuration	ρ	$\Delta\rho$	$\rho \cdot C$	F
1. SCP 922, B9↑(Follower) B10↑(")	-111.2	0.0	---	
2. SCP 922, B9↑(Follower) B10↓(40.0% abs.)	-295.1	-183.9	178.77	1.0352
3. SCP 922, B9↑(Follower) B10↓(42.5% abs.)	-299.4	-188.2	178.71	1.0348
4. SCP 922, B9↑(Follower) B10↓(45.0% abs.)	-303.3	-192.1	178.65	1.0344

Table A2.3 2D-Calculation of "F" for SCP↓, SAC↑

Configuration	ρ	$\Delta\rho$	$\rho \cdot C$	F
1. SCP 929 (1% abs.) SAC↑(Follower)	+ 5.1	0.0	---	
2. SCP↓(45.0% abs.) SAC↑(Follower)	-7377.6	-7382.7	162.98	0.9437
3. SCP↓(47.5% abs.) SAC↑(Follower)	-7617.0	-7622.1	162.69	0.9420
4. SCP↓(50.0% abs.) SAC↑(Follower)	-7846.5	-7851.6	162.43	0.9405

Table A2.4 2D-Calculation of "F" for SCP↓, SAC↓

First series: SAC↓ simulated by a 32.5% absorber

Configuration	ρ	$\Delta\rho$	$\rho \cdot C$	F
1. SCP 929 (1% abs.) SAC↑(Follower)	+ 5.1	0.0	---	
2. SCP↓(45.0% abs.) SAC↓(32.5% abs.)	-8121.0	-8126.1	161.04	0.9325
3. SCP↓(47.5% abs.) SAC↓(32.5% abs.)	-8350.0	-8355.1	160.79	0.9310
4. SCP↓(50.0% abs.) SAC↓(32.5% abs.)	-8569.0	-8574.1	160.56	0.9297

Second series: SAC↓ simulated by a 35.0% absorber

Configuration	ρ	$\Delta\rho$	$\rho \cdot C$	F
1. SCP 929 (1% abs.) SAC↑(Follower)	+ 5.1	0.0	---	
2. SCP↓(45.0% abs.) SAC↓(35.0% abs.)	-8149.1	-8154.1	160.89	0.9316
3. SCP↓(47.5% abs.) SAC↓(35.0% abs.)	-8377.7	-8382.8	160.64	0.9302
4. SCP↓(50.0% abs.) SAC↓(35.0% abs.)	-8596.0	-8601.1	160.41	0.9288

Table A2.5 2D-Calculation of "F" for SCP 600 , SAC↑

Configuration	ρ	$\Delta\rho$	$\rho \cdot C$	F
1. SCP 929 (1% abs.) SAC↑(Follower)	+5.1	0.0	---	
2. SCP 600 (7.5% abs.) SAC↑(Follower)	-1688.1	-1693.2	173.34	1.0037
3. SCP 600 (10.0% abs.) SAC↑(Follower)	-2265.2	-2270.3	171.74	0.9944
4. SCP 600 (12.5% abs.) SAC↑(Follower)	-2798.1	-2803.2	170.42	0.9868

Table A2.6 2D-Calculation of "F" for SCP 600 , SAC↓

SAC↓ simulated by a 32.5% absorber

Configuration	ρ	$\Delta\rho$	$\rho \cdot C$	F
1. SCP 929 (1% abs.) SAC↑(Follower)	+5.1	0.0	---	
2. SCP 600 (7.5% abs.) SAC↓(32.5% abs.)	-2579.6	-2584.7	168.68	0.9767
3. SCP 600 (10.0% abs.) SAC↓(32.5% abs.)	-3149.9	-3155.0	167.57	0.9703
4. SCP 600 (12.5% abs.) SAC↓(32.5% abs.)	-3675.7	-3680.8	166.66	0.9650

Table A2.7 2D-Calculation of "F" for SCP 915, B2,B4,B6↓

First series: SCP 915 simulated by a 1.0% absorber

Configuration	ρ	$\Delta\rho$	$\rho \cdot C$	F
1. SCP 915, B2,B4,B6↑ (Follower)	+ 52.5	0.0	---	
2. SCP 915, B2,B4,B6↓ (47.5% abs.)	-820.6	-873.1	118.43	0.6857
3. SCP 915, B2,B4,B6↓ (57.5% abs.)	-885.8	-938.3	113.17	0.6553
4. SCP 915, B2,B4,B6↓ (60.0% abs.)	-899.9	-952.4	112.01	0.6486
5. SCP 915, B2,B4,B6↓ (62.5% abs.)	-913.4	-965.9	110.92	0.6423
6. SCP 915, B2,B4,B6↓ (65.0% abs.)	-926.1	-978.6	109.86	0.6361
7. SCP 915, B2,B4,B6↓ (72.5% abs.)	-961.0	-1013.5	107.01	0.6196

Second series: SCP 915 simulated by a 1.5% absorber

Configuration	ρ	$\Delta\rho$	$\rho \cdot C$	F
1. SCP 915, B2,B4,B6↑ (Follower)	-76.4	0.0	---	
2. SCP 915, B2,B4,B6↓ (45.0% abs.)	-936.5	-860.1	121.04	0.7008
3. SCP 915, B2,B4,B6↓ (47.5% abs.)	-955.5	-879.1	119.53	0.6921
4. SCP 915, B2,B4,B6↓ (50.0% abs.)	-973.3	-896.9	118.10	0.6839

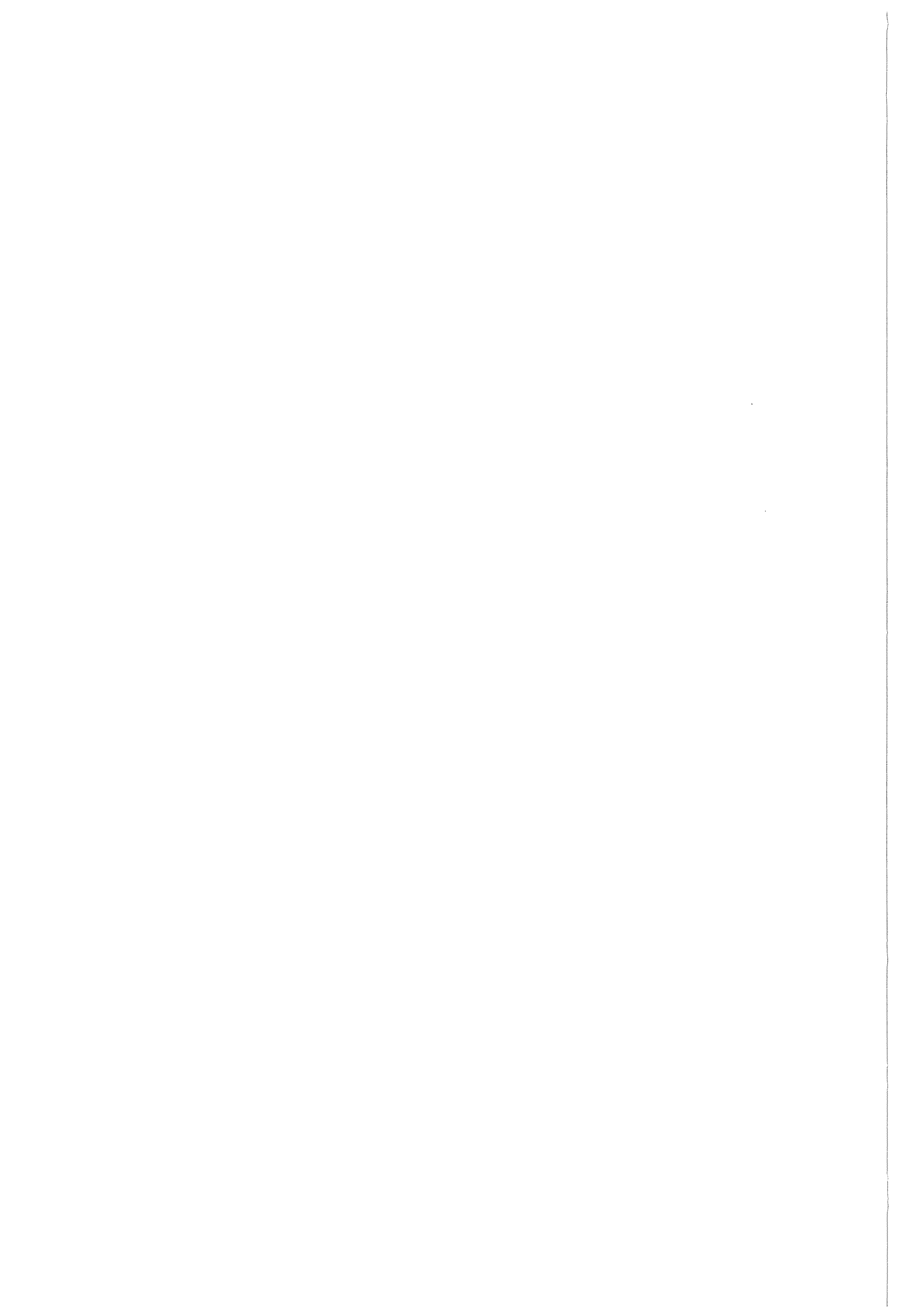
Table A2.8 2D-Calculation of "F" for SCP 918, B10,B15,B20↓

First series: SCP 918 simulated by a 1.0% absorber

Configuration	ρ	$\Delta\rho$	$\rho \cdot C$	F
1. SCP 918, B10,B15,B20↑ (Follower)	+ 39.6	0.0	---	
2. SCP 918, B10,B15,B20↓ (42.5% abs.)	-602.0	-641.6	187.72	1.0870
3. SCP 918, B10,B15,B20↓ (45.0% abs.)	-618.9	-658.5	187.89	1.0880
4. SCP 918, B10,B15,B20↓ (47.5% abs.)	-635.0	-674.6	188.06	1.0889
5. SCP 918, B10,B15,B20↓ (57.5% abs.)	-691.2	-730.8	188.62	1.0922
6. SCP 918, B10,B15,B20↓ (60.0% abs.)	-703.5	-743.1	188.72	1.0928
7. SCP 918, B10,B15,B20↓ (62.5% abs.)	-715.3	-754.9	188.83	1.0934
8. SCP 918, B10,B15,B20↓ (65.0% abs.)	-726.6	-766.2	188.94	1.0941

Second series: SCP 918 simulated by a 1.5% absorber

Configuration	ρ	$\Delta\rho$	$\rho \cdot C$	F
1. SCP 918, B10,B15,B20↑ (Follower)	-95.2	0.0	---	
2. SCP 918, B10,B15,B20↓ (42.5% abs.)	-744.4	-649.2	186.91	1.0823
3. SCP 918, B10,B15,B20↓ (45.0% abs.)	-761.5	-666.3	187.10	1.0834
4. SCP 918, B10,B15,B20↓ (47.5% abs.)	-777.7	-682.5	187.26	1.0843



Appendix 3

Calculations concerning the CMP Etalon

This Appendix presents the detailed results of the KfK calculations in 2D and 3D geometry that served to establish the subcriticality ρ_{cal}^{MSM} of the Etalon configuration SCP 542 SAC↓ in CMP.

All 2D calculations used a global axial buckling of $5.67 m^{-2}$.

Table A3.1 2D-Calculation of "G" for SCP 542, B1↓

SCP 542 simulated by a 17.44% absorber

Configuration	ρ	$\Delta\rho$	$\rho \cdot C$	G
1. SCP 542	-1.4	0.0	---	
2. SCP 542, B1↓(52.5% abs.)	-209.3	-207.9	146.94	1.0611
3. SCP 542, B1↓(55.0% abs.)	-217.6	-216.2	146.48	1.0645

Table A3.2 2D-Calculation of "G" for SCP 542, B2↓

SCP 542 simulated by a 17.44% absorber

Configuration	ρ	$\Delta\rho$	$\rho \cdot C$	G
1. SCP 542	-1.4	0.0	---	
2. SCP 542, B2↓(52.5% abs.)	-209.1	-207.7	146.90	1.0614
3. SCP 542, B2↓(55.0% abs.)	-217.4	-216.0	146.43	1.0648

Table A3.3 2D-Calculation of "G" for SCP 542, B10↓

SCP 542 simulated by a 17.44% absorber

Configuration	ρ	$\Delta\rho$	$\rho \cdot C$	G
1. SCP 542	-1.4	0.0	---	
2. SCP 542, B10↓(55.0% abs.)	-135.0	-133.6	157.58	0.9895
3. SCP 542, B10↓(57.5% abs.)	-139.4	-138.0	157.54	0.9897

Table A3.4 2D-Calculation of "G" for SCP 542, B18↓

SCP 542 simulated by a 17.44% absorber

Configuration	ρ	$\Delta\rho$	$\rho \cdot C$	G
1. SCP 542	-1.4	0.0	---	
2. SCP 542, B18↓(55.0% abs.)	-139.8	-138.4	158.07	0.9864
3. SCP 542, B18↓(57.5% abs.)	-144.3	-142.9	158.04	0.9866

Table A3.5 2D-Calculation of "G" for SCP 542, B9↓

SCP 542 simulated by a 17.44% absorber

Configuration	ρ	$\Delta\rho$	$\rho \cdot C$	G
1. SCP 542	-1.4	0.0	---	
2. SCP 542, B9↓(52.5% abs.)	-144.6	-143.2	157.25	0.9915
3. SCP 542, B9↓(55.0% abs.)	-149.8	-148.4	157.19	0.9919

Table A3.6 2D-Calculation of "G" for SCP 542, B17↓

SCP 542 simulated by a 17.44% absorber

Configuration	ρ	$\Delta\rho$	$\rho \cdot C$	G
1. SCP 542	-1.4	0.0	---	
2. SCP 542, B17↓(55.0% abs.)	-132.2	-130.8	158.03	0.9867
3. SCP 542, B17↓(57.5% abs.)	-136.3	-134.9	158.00	0.9868

Table A3.7 2D-Calculation of "G" for SCP 542, B1↓, B2↓

SCP 542 simulated by a 17.44% absorber

Configuration	ρ	$\Delta\rho$	$\rho \cdot C$	G
1. SCP 542	-1.4	0.0	---	
2. SCP 542, B1↓(52.5% abs.) B2↓(")	-384.0	-382.6	137.31	1.1355
3. SCP 542, B1↓(55.0% abs.) B2↓(")	-397.8	-396.4	136.46	1.1426

Table A3.8 2D-Calculation of "G" for SCP 542, B2↓, B10↓

SCP 542 simulated by a 17.44% absorber

Configuration	ρ	$\Delta\rho$	$\rho \cdot C$	G
1. SCP 542	-1.4	0.0	---	
2. SCP 542, B2↓(52.5% abs.) B10↓(")	-306.6	-305.2	146.45	1.0647
3. SCP 542, B2↓(55.0% abs.) B10↓(")	-316.9	-315.5	145.91	1.0686

Table A3.9 2D-Calculation of "G" for SCP 542, B2↓, B18↓

SCP 542 simulated by a 17.44% absorber

Configuration	ρ	$\Delta\rho$	$\rho \cdot C$	G
1. SCP 542	-1.4	0.0	---	
2. SCP 542, B2↓(52.5% abs.) B18↓(")	-375.8	-374.4	149.42	1.0435
3. SCP 542, B2↓(55.0% abs.) B18↓(")	-391.5	-390.1	149.04	1.0462

Table A3.10 2D-Calculation of "G" for SCP 542, B9↓, B10↓

SCP 542 simulated by a 17.44% absorber

Configuration	ρ	$\Delta\rho$	$\rho \cdot C$	G
1. SCP 542	-1.4	0.0	---	
2. SCP 542, B9↓(55.0% abs.) B10↓(")	-240.0	-238.6	155.97	0.9997
3. SCP 542, B9↓(57.5% abs.) B10↓(")	-246.5	-245.1	155.81	1.0007

Table A3.11 2D-Calculation of "G" for SCP 542, B10↓, B17↓

SCP 542 simulated by a 17.44% absorber

Configuration	ρ	$\Delta\rho$	$\rho \cdot C$	G
1. SCP 542	-1.4	0.0	---	
2. SCP 542, B10↓(52.5% abs.) B17↓(")	-284.6	-283.2	160.87	0.9692
3. SCP 542, B10↓(55.0% abs.) B17↓(")	-295.7	-294.3	160.96	0.9687

Table A3.12 3D-Calculation of "G" for SCP 542, B2↓

*First series: 52.5% absorber used for SCP,
35.0% absorber used for SAC (fully raised).*

Configuration	ρ	$\Delta\rho$	$\rho \cdot C$	G
1. SCP 542	+90.4	0.0	---	
2. SCP 542, B2↓	-135.1	-225.5	3.5040	1.0602

*Second series: 55.0% absorber used for SCP,
35.0% absorber used for SAC (fully raised).*

Configuration	ρ	$\Delta\rho$	$\rho \cdot C$	G
1. SCP 542	-13.9	0.0	---	
2. SCP 542, B2↓	-243.9	-230.0	3.4859	1.0657

Table A3.13 3D-Calculation of "G" for SCP 542, B1↓, B2↓

*First series: 52.5% absorber used for SCP,
35.0% absorber used for SAC (fully raised).*

Configuration	ρ	$\Delta\rho$	$\rho \cdot C$	G
1. SCP 542	+90.4	0.0	---	
2. SCP 542, B1,B2↓	-321.3	-411.7	3.2729	1.1351

*Second series: 55.0% absorber used for SCP,
35.0% absorber used for SAC (fully raised).*

Configuration	ρ	$\Delta\rho$	$\rho \cdot C$	G
1. SCP 542	-13.9	0.0	---	
2. SCP 542, B1,B2↓	-432.9	-419.0	3.2529	1.1421

Table A3.14 3D-Calculation of "G" for SCP 542, B10↓, B17↓

*First series: 52.5% absorber used for SCP,
35.0% absorber used for SAC (fully raised).*

Configuration	ρ	$\Delta\rho$	$\rho \cdot C$	G
1. SCP 542	+90.4	0.0	---	
2. SCP 542, B10,B17↓	-207.0	-297.4	3.8457	0.9660

*Second series: 55.0% absorber used for SCP,
35.0% absorber used for SAC (fully raised).*

Configuration	ρ	$\Delta\rho$	$\rho \cdot C$	G
1. SCP 542	-13.9	0.0	---	
2. SCP 542, B10,B17↓	-318.0	-304.1	3.8322	0.9694

Appendix 4

Calculations concerning the selected configurations of CMP

This Appendix presents the detailed results of the KfK calculations in 2D and 3D geometry that served to produce MSM correction factors for those control rod configurations established in CMP, that were proposed by the SPX-1 task force group to be analysed by the different task force members.

It is remarked that Tables A4.1, A4.2, A4.4, A4.5, A4.21, A4.22, and A4.23 of this Appendix represent copies of Tables A3.3, A3.2, A3.7, A3.11, A3.12, A3.13, and A3.14 of Appendix 3 where the same control rod configurations had been used to derive the correction factors **G**. Comparing these tables with each other, one finds that corresponding values of **G** and **F** are reciprocal.

All 2D calculations used a global axial buckling of 5.67 m^{-2} .

Table A4.1 2D-Calculation of "F" for SCP 542, B10↓

SCP 542 simulated by a 17.44% absorber

Configuration	ρ	$\Delta\rho$	$\rho \cdot C$	F
1. SCP 542	-1.4	0.0	---	
2. SCP 542, B10↓(55.0% abs.)	-135.0	-133.6	157.58	1.0107
3. SCP 542, B10↓(57.5% abs.)	-139.4	-138.0	157.54	1.0104

Table A4.2 2D-Calculation of "F" for SCP 542, B2↓

SCP 542 simulated by a 17.44% absorber

Configuration	ρ	$\Delta\rho$	$\rho \cdot C$	F
1. SCP 542	-1.4	0.0	---	
2. SCP 542, B2↓(52.5% abs.)	-209.1	-207.7	146.90	0.9421
3. SCP 542, B2↓(55.0% abs.)	-217.4	-216.0	146.43	0.9392

Table A4.3 2D-Calculation of "F" for SCP 542, SAC1↓,SAC2,SAC3↑

SCP 542 simulated by a 17.44% absorber

Configuration	ρ	$\Delta\rho$	$\rho \cdot C$	F
1. SCP 542	-1.4	0.0	---	
2. SCP 542, SAC1↓(32.5% abs.)	-257.4	-256.0	153.40	0.9839
3. SCP 542, SAC1↓(35.0% abs.)	-265.6	-264.2	153.14	0.9822
4. SCP 542, SAC1↓(37.5% abs.)	-273.1	-271.7	152.89	0.9806

Table A4.4 2D-Calculation of "F" for SCP 542, B1↓, B2↓

SCP 542 simulated by a 17.44% absorber

Configuration	ρ	$\Delta\rho$	$\rho \cdot C$	F
1. SCP 542	-1.4	0.0	---	
2. SCP 542, B1↓(52.5% abs.) B2↓(")	-384.0	-382.6	137.31	0.8807
3. SCP 542, B1↓(55.0% abs.) B2↓(")	-397.8	-396.4	136.46	0.8752

Table A4.5 2D-Calculation of "F" for SCP 542, B10↓, B17↓

SCP 542 simulated by a 17.44% absorber

Configuration	ρ	$\Delta\rho$	$\rho \cdot C$	F
1. SCP 542	-1.4	0.0	---	
2. SCP 542, B10↓(52.5% abs.) B17↓(")	-284.6	-283.2	160.87	1.0317
3. SCP 542, B10↓(55.0% abs.) B17↓(")	-295.7	-294.3	160.96	1.0323

Table A4.6 2D-Calculation of "F" for RE 542, RI ↓

SCP 542 simulated by a 17.44% absorber

Configuration	ρ	$\Delta\rho$	$\rho \cdot C$	F
1. SCP 542	-1.4	0.0	---	
2. RE 542 , RI ↓(52.5% abs.)	-1173.7	-1172.3	102.70	0.6587
3. RE 542 , RI ↓(55.0% abs.)	-1216.6	-1215.2	100.53	0.6447
4. RE 542 , RI ↓(57.5% abs.)	-2566.2	-2564.8	98.47	0.6316

Table A4.7 2D-Calculation of "F" for RI 900, RE ↓

First series: RI 900 simulated by a 1.0% absorber

Configuration	ρ	$\Delta\rho$	$\rho \cdot C$	F
1. SCP 542	-1.4	0.0	---	
2. RI 900 , RE ↓(52.5% abs.)	-87.0	-85.6	231.06	1.4819
3. RI 900 , RE ↓(55.0% abs.)	-151.9	-150.5	231.23	1.4830

Second series: RI 900 simulated by a 1.5% absorber

Configuration	ρ	$\Delta\rho$	$\rho \cdot C$	F
1. SCP 542	-1.4	0.0	---	
2. RI 900 , RE ↓(52.5% abs.)	-190.5	-189.1	229.58	1.4724
3. RI 900 , RE ↓(55.0% abs.)	-256.6	-255.2	229.80	1.4738

Table A4.8 2D-Calculation of "F" for SCP 520, B2↓

First series: SCP 520 simulated by a 17.5% absorber

Configuration	ρ	$\Delta\rho$	$\rho \cdot C$	F
1. SCP 542	-1.4	0.0	---	
2. SCP 520, B2↓(50.0% abs.)	-247.4	-246.0	147.31	0.9448
3. SCP 520, B2↓(52.5% abs.)	-256.2	-254.8	146.82	0.9417
4. SCP 520, B2↓(55.0% abs.)	-264.6	-263.2	146.36	0.9387

Second series: SCP 520 simulated by a 20.0% absorber

Configuration	ρ	$\Delta\rho$	$\rho \cdot C$	F
1. SCP 542	-1.4	0.0	---	
2. SCP 520, B2↓(50.0% abs.)	-638.7	-637.3	146.72	0.9410
3. SCP 520, B2↓(52.5% abs.)	-647.8	-646.4	146.24	0.9380
4. SCP 520, B2↓(55.0% abs.)	-656.3	-654.9	145.79	0.9350

Supplementary information on B2 worth

First series: SCP 520 simulated by a 17.5% absorber

Configuration	ρ	$\Delta\rho(B2)$
1. SCP 520, B2↑(Follower)	+ 232.5	0.0
2. SCP 520	-50.7	-283.2
3. SCP 520, B2↓(50.0% abs.)	-247.4	-479.9
4. SCP 520, B2↓(52.5% abs.)	-256.2	-488.7
5. SCP 520, B2↓(55.0% abs.)	-264.6	-497.1

Second series: SCP 520 simulated by a 20.0% absorber

Configuration	ρ	$\Delta\rho(B2)$
1. SCP 520, B2↑(Follower)	-139.9	0.0
2. SCP 520	-460.2	-320.3
3. SCP 520, B2↓(50.0% abs.)	-638.7	-498.8
4. SCP 520, B2↓(52.5% abs.)	-647.8	-507.9
5. SCP 520, B2↓(55.0% abs.)	-656.3	-516.4

Table A4.9 2D-Calculation of "F" for SCP 520, B7↓

First series: SCP 520 simulated by a 17.5% absorber

Configuration	ρ	$\Delta\rho$	$\rho \cdot C$	F
1. SCP 542	-1.4	0.0	---	
2. SCP 520, B7↓(50.0% abs.)	-171.3	-169.9	157.68	1.0113
3. SCP 520, B7↓(52.5% abs.)	-176.1	-174.7	157.65	1.0111
4. SCP 520, B7↓(55.0% abs.)	-180.5	-179.1	157.62	1.0109

Second series: SCP 520 simulated by a 20.0% absorber

Configuration	ρ	$\Delta\rho$	$\rho \cdot C$	F
1. SCP 542	-1.4	0.0	---	
2. SCP 520, B7↓(25.0% abs.)	-489.8	-488.4	155.49	0.9972
3. SCP 520, B7↓(30.0% abs.)	-513.2	-511.8	155.75	0.9989
4. SCP 520, B7↓(35.0% abs.)	-532.1	-530.7	155.89	0.9998
5. SCP 520, B7↓(40.0% abs.)	-547.8	-546.4	155.96	1.0003
6. SCP 520, B7↓(45.0% abs.)	-561.0	-559.6	155.99	1.0004
7. SCP 520, B7↓(50.0% abs.)	-572.3	-570.9	155.98	1.0004
8. SCP 520, B7↓(52.5% abs.)	-577.3	-575.9	155.97	1.0003
9. SCP 520, B7↓(55.0% abs.)	-582.0	-580.6	155.95	1.0002

Supplementary information on B7 worth

First series: SCP 520 simulated by a 17.5% absorber

Configuration	ρ	$\Delta\rho(B7)$
1. SCP 520, B7↑(Follower)	+188.7	0.0
2. SCP 520	-50.7	-239.4
3. SCP 520, B7↓(50.0% abs.)	-171.3	-360.0
4. SCP 520, B7↓(52.5% abs.)	-176.1	-364.8
5. SCP 520, B7↓(55.0% abs.)	-180.5	-369.2

Second series: SCP 520 simulated by a 20.0% absorber

Configuration	ρ	$\Delta\rho(B7)$
1. SCP 520, B7↑(Follower)	-177.4	0.0
2. SCP 520	-460.2	-282.8
3. SCP 520, B7↓(25.0% abs.)	-489.8	-312.4
4. SCP 520, B7↓(30.0% abs.)	-513.2	-335.8
5. SCP 520, B7↓(35.0% abs.)	-532.1	-354.7
6. SCP 520, B7↓(40.0% abs.)	-547.8	-370.4
7. SCP 520, B7↓(45.0% abs.)	-561.0	-383.6
8. SCP 520, B7↓(50.0% abs.)	-572.3	-394.9
9. SCP 520, B7↓(52.5% abs.)	-577.3	-399.9
10. SCP 520, B7↓(55.0% abs.)	-582.0	-404.6

Table A4.10 2D-Calculation of "F" for SCP 520, B8↓

First series: SCP 520 simulated by a 17.5% absorber

Configuration	ρ	$\Delta\rho$	$\rho \cdot C$	F
1. SCP 542	-1.4	0.0	---	
2. SCP 520, B8↓(50.0% abs.)	-178.2	-176.8	157.53	1.0104
3. SCP 520, B8↓(52.5% abs.)	-183.3	-181.9	157.50	1.0101
4. SCP 520, B8↓(55.0% abs.)	-188.1	-186.7	157.46	1.0099

Second series: SCP 520 simulated by a 20.0% absorber

Configuration	ρ	$\Delta\rho$	$\rho \cdot C$	F
1. SCP 542	-1.4	0.0	---	
2. SCP 520, B8↓(50.0% abs.)	-578.3	-576.9	155.86	0.9996
3. SCP 520, B8↓(52.5% abs.)	-583.7	-582.3	155.84	0.9995
4. SCP 520, B8↓(55.0% abs.)	-588.8	-587.4	155.82	0.9994

Supplementary information on B8 worth

First series: SCP 520 simulated by a 17.5% absorber

Configuration	ρ	$\Delta\rho(B8)$
1. SCP 520, B8↑(Follower)	+193.2	0.0
2. SCP 520	-50.7	-243.9
3. SCP 520, B8↓(50.0% abs.)	-178.2	-371.4
4. SCP 520, B8↓(52.5% abs.)	-183.3	-376.5
5. SCP 520, B8↓(55.0% abs.)	-188.1	-381.3

Second series: SCP 520 simulated by a 20.0% absorber

Configuration	ρ	$\Delta\rho(B8)$
1. SCP 520, B8↑(Follower)	-173.9	0.0
2. SCP 520	-460.2	-286.3
3. SCP 520, B8↓(50.0% abs.)	-578.3	-404.4
4. SCP 520, B8↓(52.5% abs.)	-583.7	-409.8
5. SCP 520, B8↓(55.0% abs.)	-588.8	-414.9

Table A4.11 2D-Calculation of "F" for SCP 520, B9↓

First series: SCP 520 simulated by a 17.5% absorber

Configuration	ρ	$\Delta\rho$	$\rho \cdot C$	F
1. SCP 542	-1.4	0.0	---	
2. SCP 520, B9↓(50.0% abs.)	-187.0	-185.6	157.11	1.0076
3. SCP 520, B9↓(52.5% abs.)	-192.7	-191.3	157.06	1.0073
4. SCP 520, B9↓(55.0% abs.)	-198.0	-196.6	157.00	1.0069

Second series: SCP 520 simulated by a 20.0% absorber

Configuration	ρ	$\Delta\rho$	$\rho \cdot C$	F
1. SCP 542	-1.4	0.0	---	
2. SCP 520, B9↓(50.0% abs.)	-585.7	-584.3	155.47	0.9971
3. SCP 520, B9↓(52.5% abs.)	-591.6	-590.2	155.44	0.9969
4. SCP 520, B9↓(55.0% abs.)	-597.1	-595.7	155.41	0.9967

Supplementary information on B9 worth

First series: SCP 520 simulated by a 17.5% absorber

Configuration	ρ	$\Delta\rho(B9)$
1. SCP 520, B9↑(Follower)	+189.4	0.0
2. SCP 520	-50.7	-240.1
3. SCP 520, B9↓(50.0% abs.)	-187.0	-376.4
4. SCP 520, B9↓(52.5% abs.)	-192.7	-382.1
5. SCP 520, B9↓(55.0% abs.)	-198.0	-387.4

Second series: SCP 520 simulated by a 20.0% absorber

Configuration	ρ	$\Delta\rho(B9)$
1. SCP 520, B9↑(Follower)	-182.3	0.0
2. SCP 520	-460.2	-277.9
3. SCP 520, B9↓(50.0% abs.)	-585.7	-403.3
4. SCP 520, B9↓(52.5% abs.)	-591.6	-409.3
5. SCP 520, B9↓(55.0% abs.)	-597.1	-414.8

Table A4.12 2D-Calculation of "F" for SCP 520, B10↓

First series: SCP 520 simulated by a 17.5% absorber

Configuration	ρ	$\Delta\rho$	$\rho \cdot C$	F
1. SCP 542	-1.4	0.0	---	
2. SCP 520, B10↓(50.0% abs.)	-173.7	-172.3	157.45	1.0098
3. SCP 520, B10↓(52.5% abs.)	-178.7	-177.3	157.41	1.0096
4. SCP 520, B10↓(55.0% abs.)	-183.4	-182.0	157.38	1.0094

Second series: SCP 520 simulated by a 20.0% absorber

Configuration	ρ	$\Delta\rho$	$\rho \cdot C$	F
1. SCP 542	-1.4	0.0	---	
2. SCP 520, B10↓(50.0% abs.)	-574.0	-572.6	155.76	0.9990
3. SCP 520, B10↓(52.5% abs.)	-579.3	-577.9	155.75	0.9989
4. SCP 520, B10↓(55.0% abs.)	-584.2	-582.8	155.73	0.9988

Supplementary information on B10 worth

First series: SCP 520 simulated by a 17.5% absorber

Configuration	ρ	$\Delta\rho(B10)$
1. SCP 520, B10↑(Follower)	+178.9	0.0
2. SCP 520	-50.7	-229.6
3. SCP 520, B10↓(50.0% abs.)	-173.7	-352.6
4. SCP 520, B10↓(52.5% abs.)	-178.7	-357.6
5. SCP 520, B10↓(55.0% abs.)	-183.4	-362.3

Second series: SCP 520 simulated by a 20.0% absorber

Configuration	ρ	$\Delta\rho(B10)$
1. SCP 520, B10↑(Follower)	-191.4	0.0
2. SCP 520	-460.2	-268.8
3. SCP 520, B10↓(50.0% abs.)	-574.0	-382.6
4. SCP 520, B10↓(52.5% abs.)	-579.3	-387.9
5. SCP 520, B10↓(55.0% abs.)	-584.2	-392.8

Table A4.13 2D-Calculation of "F" for SCP 520, B11↓

First series: SCP 520 simulated by a 17.5% absorber

Configuration	ρ	$\Delta\rho$	$\rho \cdot C$	F
1. SCP 542	-1.4	0.0	---	
2. SCP 520, B11↓(50.0% abs.)	-165.9	-164.5	157.62	1.0109
3. SCP 520, B11↓(52.5% abs.)	-170.5	-169.1	157.60	1.0108
4. SCP 520, B11↓(55.0% abs.)	-174.8	-173.4	157.57	1.0106

Second series: SCP 520 simulated by a 20.0% absorber

Configuration	ρ	$\Delta\rho$	$\rho \cdot C$	F
1. SCP 542	-1.4	0.0	---	
2. SCP 520, B11↓(50.0% abs.)	-567.0	-565.6	155.91	0.9999
3. SCP 520, B11↓(52.5% abs.)	-571.9	-570.5	155.90	0.9999
4. SCP 520, B11↓(55.0% abs.)	-576.5	-575.1	155.89	0.9998

Supplementary information on B11 worth

First series: SCP 520 simulated by a 17.5% absorber

Configuration	ρ	$\Delta\rho(B11)$
1. SCP 520, B11↑(Follower)	+168.7	0.0
2. SCP 520	-50.7	-219.4
3. SCP 520, B11↓(50.0% abs.)	-165.9	-334.6
4. SCP 520, B11↓(52.5% abs.)	-170.5	-339.2
5. SCP 520, B11↓(55.0% abs.)	-174.8	-343.5

Second series: SCP 520 simulated by a 20.0% absorber

Configuration	ρ	$\Delta\rho(B11)$
1. SCP 520, B11↑(Follower)	-202.4	0.0
2. SCP 520	-460.2	-257.8
3. SCP 520, B11↓(50.0% abs.)	-567.0	-364.6
4. SCP 520, B11↓(52.5% abs.)	-571.9	-369.5
5. SCP 520, B11↓(55.0% abs.)	-576.5	-374.1

Table A4.14 2D-Calculation of "F" for SCP 465, B2,B4,B6↓

First series: SCP 465 simulated by a 22.5% absorber

Configuration	ρ	$\Delta\rho$	$\rho \cdot C$	F
1. SCP 542	-1.4	0.0	---	
2. SCP 465,B2,B4,B6↓ (27.5%)	-970.0	-968.6	148.48	0.9523
3. SCP 465,B2,B4,B6↓ (32.5%)	-1075.6	-1074.2	144.16	0.9246
4. SCP 465,B2,B4,B6↓ (37.5%)	-1166.9	-1165.5	140.36	0.9002
5. SCP 465,B2,B4,B6↓ (42.5%)	-1246.9	-1245.5	136.98	0.8785
6. SCP 465,B2,B4,B6↓ (47.5%)	-1317.5	-1316.1	133.95	0.8591
7. SCP 465,B2,B4,B6↓ (50.0%)	-1349.9	-1348.5	132.55	0.8501
8. SCP 465,B2,B4,B6↓ (52.5%)	-1380.5	-1379.1	131.22	0.8416
9. SCP 465,B2,B4,B6↓ (55.0%)	-1409.4	-1408.0	129.95	0.8334

Second series: SCP 465 simulated by a 25.0% absorber

Configuration	ρ	$\Delta\rho$	$\rho \cdot C$	F
1. SCP 542	-1.4	0.0	---	
2. SCP 465,B2,B4,B6↓ (50.0%)	-1660.9	-1659.5	133.99	0.8593
3. SCP 465,B2,B4,B6↓ (52.5%)	-1692.1	-1690.7	132.67	0.8509
4. SCP 465,B2,B4,B6↓ (55.0%)	-1721.7	-1720.3	131.42	0.8429

Supplementary information on B2,B4,B6 worth

First series: SCP 465 simulated by a 22.5% absorber

Configuration	ρ	$\Delta\rho(B2,B4,B6)$
1. SCP 465, B2,B4,B6↑(Follower)	+136.3	0.0
2. SCP 465	-846.5	-982.8
3. SCP 465, B2,B4,B6↓ (27.5% abs.)	-970.0	-1106.3
4. SCP 465, B2,B4,B6↓ (32.5% abs.)	-1075.6	-1211.9
5. SCP 465, B2,B4,B6↓ (37.5% abs.)	-1166.9	-1303.2
6. SCP 465, B2,B4,B6↓ (42.5% abs.)	-1246.9	-1383.2
7. SCP 465, B2,B4,B6↓ (47.5% abs.)	-1317.5	-1453.8
8. SCP 465, B2,B4,B6↓ (50.0% abs.)	-1349.9	-1486.2
9. SCP 465, B2,B4,B6↓ (52.5% abs.)	-1380.5	-1516.8
10. SCP 465, B2,B4,B6↓ (55.0% abs.)	-1409.4	-1545.7

Second series: SCP 465 simulated by a 25.0% absorber

Configuration	ρ	$\Delta\rho(B2,B4,B6)$
1. SCP 465 ,B2,B4,B6↑(Follower)	-140.8	0.0
2. SCP 465	-1212.1	-1171.3
3. SCP 465 ,B2,B4,B6↓ (50.0% abs.)	-1660.9	-1520.1
4. SCP 465 ,B2,B4,B6↓ (52.5% abs.)	-1692.1	-1551.3
5. SCP 465 ,B2,B4,B6↓ (55.0% abs.)	-1721.7	-1580.9

Table A4.15 2D-Calculation of "F" for SCP 486, B10,B15,B20 ↓

First series: SCP 486 simulated by a 20.0% absorber

Configuration	ρ	$\Delta\rho$	$\rho \cdot C$	F
1. SCP 542	-1.4	0.0	---	
2. SCP 486,B10,B15,B20↓(50.0%)	-851.7	-850.3	160.56	1.0298
3. SCP 486,B10,B15,B20↓(52.5%)	-872.7	-871.3	160.82	1.0314
4. SCP 486,B10,B15,B20↓(55.0%)	-892.5	-891.1	161.06	1.0330

Second series: SCP 486 simulated by a 22.5% absorber

Configuration	ρ	$\Delta\rho$	$\rho \cdot C$	F
1. SCP 542	-1.4	0.0	---	
2. SCP 486,B10,B15,B20↓(27.5%)	-934.0	-932.6	154.73	0.9924
3. SCP 486,B10,B15,B20↓(32.5%)	-1008.6	-1007.2	155.81	0.9993
4. SCP 486,B10,B15,B20↓(37.5%)	-1073.2	-1071.8	156.70	1.0050
5. SCP 486,B10,B15,B20↓(42.5%)	-1129.7	-1128.3	157.46	1.0099
6. SCP 486,B10,B15,B20↓(47.5%)	-1179.7	-1178.3	158.11	1.0140
7. SCP 486,B10,B15,B20↓(50.0%)	-1202.6	-1201.2	158.40	1.0159
8. SCP 486,B10,B15,B20↓(52.5%)	-1224.2	-1222.8	158.67	1.0176
9. SCP 486,B10,B15,B20↓(55.0%)	-1244.7	-1243.3	158.92	1.0193

Supplementary information on B10,B15,B20 worth

First series: SCP 486 simulated by a 20.0% absorber

Configuration	ρ	$\Delta\rho(B10,B15,B20)$
1. SCP 486, B10,B15,B20↑(Follower)	+175.5	0.0
2. SCP 486	-460.2	-635.7
3. SCP 486, B10,B15,B20↓ (50.0% abs.)	-851.7	-1027.2
4. SCP 486, B10,B15,B20↓ (52.5% abs.)	-872.7	-1048.2
5. SCP 486, B10,B15,B20↓ (55.0% abs.)	-892.5	-1068.0

Second series: SCP 486 simulated by a 22.5% absorber

Configuration	ρ	$\Delta\rho(B10,B15,B20)$
1. SCP 486, B10,B15,B20↑(Follower)	-136.2	0.0
2. SCP 486	-846.5	-710.3
3. SCP 486, B10,B15,B20↓ (50.0% abs.)	-1202.6	-1066.4
4. SCP 486, B10,B15,B20↓ (52.5% abs.)	-1224.2	-1088.0
5. SCP 486, B10,B15,B20↓ (55.0% abs.)	-1244.7	-1108.5

Table A4.16 2D-Calculation of "F" for SCP ↓, SAC ↑

Configuration	ρ	$\Delta\rho$	$\rho \cdot C$	F
1. SCP 542	-1.4	0.0	---	
2. SCP ↓ (17.5% abs.),SAC ↑	-50.7	-49.3	156.88	1.0062
3. SCP ↓ (20.0% abs.),SAC ↑	-460.2	-458.8	155.03	0.9943
4. SCP ↓ (22.5% abs.),SAC ↑	-846.5	-845.1	153.42	0.9840
5. SCP ↓ (25.0% abs.),SAC ↑	-1212.1	-1210.7	152.02	0.9750
6. SCP ↓ (27.5% abs.),SAC ↑	-1558.8	-1557.4	150.78	0.9670
7. SCP ↓ (52.5% abs.),SAC ↑	-4268.4	-4267.0	143.51	0.9204
8. SCP ↓ (55.0% abs.),SAC ↑	-4483.3	-4481.9	143.08	0.9176
9. SCP ↓ (57.5% abs.),SAC ↑	-4690.5	-4689.1	142.67	0.9150

Table A4.17 2D-Calculation of "F" for SCP ↓, SAC ↓

First series: SAC ↓ simulated by a 35.0% absorber

Configuration	ρ	$\Delta\rho$	$\rho \cdot C$	F
1. SCP 542	-1.4	0.0	---	
2. SCP ↓ (52.5% abs.),SAC ↓	-5390.4	-5389.0	146.19	0.9376
3. SCP ↓ (55.0% abs.),SAC ↓	-5609.4	-5608.9	145.89	0.9357
4. SCP ↓ (57.5% abs.),SAC ↓	-5820.6	-5819.2	145.62	0.9339

Second series: SAC ↓ simulated by a 37.5% absorber

Configuration	ρ	$\Delta\rho$	$\rho \cdot C$	F
1. SCP 542	-1.4	0.0	---	
2. SCP ↓ (52.5% abs.),SAC ↓	-5431.5	-5430.1	146.22	0.9378
3. SCP ↓ (55.0% abs.),SAC ↓	-5650.6	-5649.2	145.93	0.9359
4. SCP ↓ (57.5% abs.),SAC ↓	-5861.7	-5860.3	145.66	0.9342

Table A4.18 2D-Calculation of "F" for SCP ↓, SAC ↑, B12 ↑

Configuration	ρ	$\Delta\rho$	$\rho \cdot C$	F
1. SCP 542	-1.4	0.0	---	
2. SCP ↓ (52.5% abs.), B12 ↑	-3232.7	-3231.3	119.55	0.7667
3. SCP ↓ (55.0% abs.), B12 ↑	-3381.2	-3379.8	118.22	0.7582

Table A4.19 3D-Calculation of "F" for SCP 542, B2↓

*First series: 52.5% absorber used for SCP,
35.0% absorber used for SAC (fully raised).*

Configuration	ρ	$\Delta\rho$	$\rho \cdot C$	F
1. SCP 542	+90.4	0.0	---	
2. SCP 542, B2↓	-135.1	-225.5	3.5040	0.9432

*Second series: 55.0% absorber used for SCP,
35.0% absorber used for SAC (fully raised).*

Configuration	ρ	$\Delta\rho$	$\rho \cdot C$	F
1. SCP 542	-13.9	0.0	---	
2. SCP 542, B2↓	-243.9	-230.0	3.4859	0.9383

Table A4.20 3D-Calculation of "F" for SCP 542, B1↓, B2↓

*First series: 52.5% absorber used for SCP,
35.0% absorber used for SAC (fully raised).*

Configuration	ρ	$\Delta\rho$	$\rho \cdot C$	F
1. SCP 542	+90.4	0.0	---	
2. SCP 542, B1,B2↓	-321.3	-411.7	3.2729	0.8810

*Second series: 55.0% absorber used for SCP,
35.0% absorber used for SAC (fully raised).*

Configuration	ρ	$\Delta\rho$	$\rho \cdot C$	F
1. SCP 542	-13.9	0.0	---	
2. SCP 542, B1,B2↓	-432.9	-419.0	3.2529	0.8756

Table A4.21 3D-Calculation of "F" for SCP 542, B10↓, B17↓

*First series: 52.5% absorber used for SCP,
35.0% absorber used for SAC (fully raised).*

Configuration	ρ	$\Delta\rho$	$\rho \cdot C$	F
1. SCP 542	+90.4	0.0	---	
2. SCP 542, B10,B17↓	-207.0	-297.4	3.8457	1.0352

*Second series: 55.0% absorber used for SCP,
35.0% absorber used for SAC (fully raised).*

Configuration	ρ	$\Delta\rho$	$\rho \cdot C$	F
1. SCP 542	-13.9	0.0	---	
2. SCP 542, B10,B17↓	-318.0	-304.1	3.8322	1.0315

Table A4.22 3D-Calculation of "F" for RE 542, RI ↓

*First series: 52.5% absorber used for SCP,
35.0% absorber used for SAC (fully raised).*

Configuration	ρ	$\Delta\rho$	$\rho \cdot C$	F
1. SCP 542	+90.4	0.0	---	
2. RE 542, RI ↓	-1156.1	-1246.5	2.4463	0.6585

*Second series: 55.0% absorber used for SCP,
35.0% absorber used for SAC (fully raised).*

Configuration	ρ	$\Delta\rho$	$\rho \cdot C$	F
1. SCP 542	-13.9	0.0	---	
2. RE 542, RI ↓	-1282.7	-1268.8	2.4184	0.6510

Table A4.23 3D-Calculation of "F" for RI 900, RE ↓

*First series: 52.5% absorber used for SCP,
35.0% absorber used for SAC (fully raised).*

Configuration	ρ	$\Delta\rho$	$\rho \cdot C$	F
1. SCP 542	+90.4	0.0	---	
2. RI 900, RE ↓	-176.7	-267.1	5.5098	1.4831

*Second series: 55.0% absorber used for SCP,
35.0% absorber used for SAC (fully raised).*

Configuration	ρ	$\Delta\rho$	$\rho \cdot C$	F
1. SCP 542	-13.9	0.0	---	
2. RI 900, RE ↓	-259.9	-246.0	5.5094	1.4830

Table A4.24 3D-Calculation of "F" for SCP 465, B2,B4,B6 ↓

*First series: 52.5% absorber used for SCP,
35.0% absorber used for SAC (fully raised).*

Configuration	ρ	$\Delta\rho$	$\rho \cdot C$	F
1. SCP 542	+90.4	0.0	---	
2. SCP 465, B2,B4,B6 ↓	-1444.6	-1534.9	3.1243	0.8410

*Second series: 55.0% absorber used for SCP,
35.0% absorber used for SAC (fully raised).*

Configuration	ρ	$\Delta\rho$	$\rho \cdot C$	F
1. SCP 542	-13.9	0.0	---	
2. SCP 465, B2,B4,B6 ↓	-1586.8	-1572.9	3.1043	0.8356

Supplementary information on B2,B4,B6 worth

*First series: 52.5% absorber used for SCP,
35.0% absorber used for SAC (fully raised).*

Configuration	ρ	$\Delta\rho(B2,B4,B6)$
1. SCP 465, B2,B4,B6 ↑	+104.3	0.0
2. SCP 465, B2,B4,B6 ↓	-1444.6	-1548.9

*Second series: 55.0% absorber used for SCP,
35.0% absorber used for SAC (fully raised).*

Configuration	ρ	$\Delta\rho(B2,B4,B6)$
1. SCP 465, B2,B4,B6 ↑	+2.3	0.0
2. SCP 465, B2,B4,B6 ↓	-1586.8	-1589.1

Table A4.25 3D-Calculation of "F" for SCP 486, B10,B15,B20 ↓

*First series: 52.5% absorber used for SCP,
35.0% absorber used for SAC (fully raised).*

Configuration	ρ	$\Delta\rho$	$\rho \cdot C$	F
1. SCP 542	+90.4	0.0	---	
2. SCP 486, B10,B15,B20 ↓	-1021.3	-1111.7	3.8045	1.0241

*Second series: 55.0% absorber used for SCP,
35.0% absorber used for SAC (fully raised).*

Configuration	ρ	$\Delta\rho$	$\rho \cdot C$	F
1. SCP 542	-13.9	0.0	---	
2. SCP 486, B10,B15,B20 ↓	-1154.1	-1140.2	3.7914	1.0206

Supplementary information on B10,B15,B20 worth

*First series: 52.5% absorber used for SCP,
35.0% absorber used for SAC (fully raised).*

Configuration	ρ	$\Delta\rho(B10,B15,B20)$
1. SCP 486, B10,B15,B20 ↑	+41.4	0.0
2. SCP 486, B10,B15,B20 ↓	-1021.3	-1062.7

*Second series: 55.0% absorber used for SCP,
35.0% absorber used for SAC (fully raised).*

Configuration	ρ	$\Delta\rho(B10,B15,B20)$
1. SCP 486, B10,B15,B20 ↑	-60.1	0.0
2. SCP 486, B10,B15,B20 ↓	-1154.1	-1094.0

Table A4.26 3D-Calculation of "F" for SCP ↓, SAC ↑

*First series: 52.5% absorber used for SCP,
35.0% absorber used for SAC (fully raised).*

Configuration	ρ	$\Delta\rho$	$\rho \cdot C$	F
1. SCP 542	+90.4	0.0	---	
2. SCP ↓, SAC ↑	-4353.9	-4444.3	3.4371	0.9252

*Second series: 55.0% absorber used for SCP,
35.0% absorber used for SAC (fully raised).*

Configuration	ρ	$\Delta\rho$	$\rho \cdot C$	F
1. SCP 542	-13.9	0.0	---	
2. SCP ↓, SAC ↑	-4576.5	-4562.6	3.4249	0.9219

Table A4.27 3D-Calculation of "F" for SCP ↓, SAC ↓

*First series: 52.5% absorber used for SCP,
35.0% absorber used for SAC*

Configuration	ρ	$\Delta\rho$	$\rho \cdot C$	F
1. SCP 542	+90.4	0.0	---	
2. SCP ↓, SAC ↓	-5499.7	-5590.1	3.5000	0.9421

*Second series: 55.0% absorber used for SCP,
35.0% absorber used for SAC*

Configuration	ρ	$\Delta\rho$	$\rho \cdot C$	F
1. SCP 542	-13.9	0.0	---	
2. SCP ↓, SAC ↓	-5726.9	-5713.0	3.4909	0.9397

Table A4.28 3D-Calculation of "F" for SCP ↓, SAC ↑, B12 ↑

*First series: 52.5% absorber used for SCP,
35.0% absorber used for SAC (fully raised).*

Configuration	ρ	$\Delta\rho$	$\rho \cdot C$	F
1. SCP 542	+90.4	0.0	---	
2. SCP↓, SAC ↑, B12 ↑	-3322.4	-3412.8	2.8834	0.7762

*Second series: 55.0% absorber used for SCP,
35.0% absorber used for SAC (fully raised).*

Configuration	ρ	$\Delta\rho$	$\rho \cdot C$	F
1. SCP 542	-13.9	0.0	---	
2. SCP ↓, SAC ↑, B12 ↑	-3479.7	-3465.8	2.8514	0.7675

Table A4.29 3D-Calculation of the CMP core excess reactivity

*First series: 52.5% absorber used for SCP,
35.0% absorber used for SAC (fully raised).*

Configuration	ρ	$\Delta\rho(SCP)$
1. SCP 542, SAC ↑	+90.4	0.0
2. SCP ↑, SAC ↑	+3743.3	+3652.9

*Second series: 55.0% absorber used for SCP,
35.0% absorber used for SAC (fully raised).*

Configuration	ρ	$\Delta\rho(SCP)$
1. SCP 542, SAC ↑	-13.9	0.0
2. SCP ↑, SAC ↑	+3735.4	+3749.3

- B1 ... B21 : Individual control rods of the SCP system
- SAC1 ... SAC3 : Individual control rods of the SAC system
- D : Diluent positions
- B : BOUPHY position
- F : Dummy fuel element positions
- GDN : Neutron guide tube positions for under vessel reactor operation instrumentation

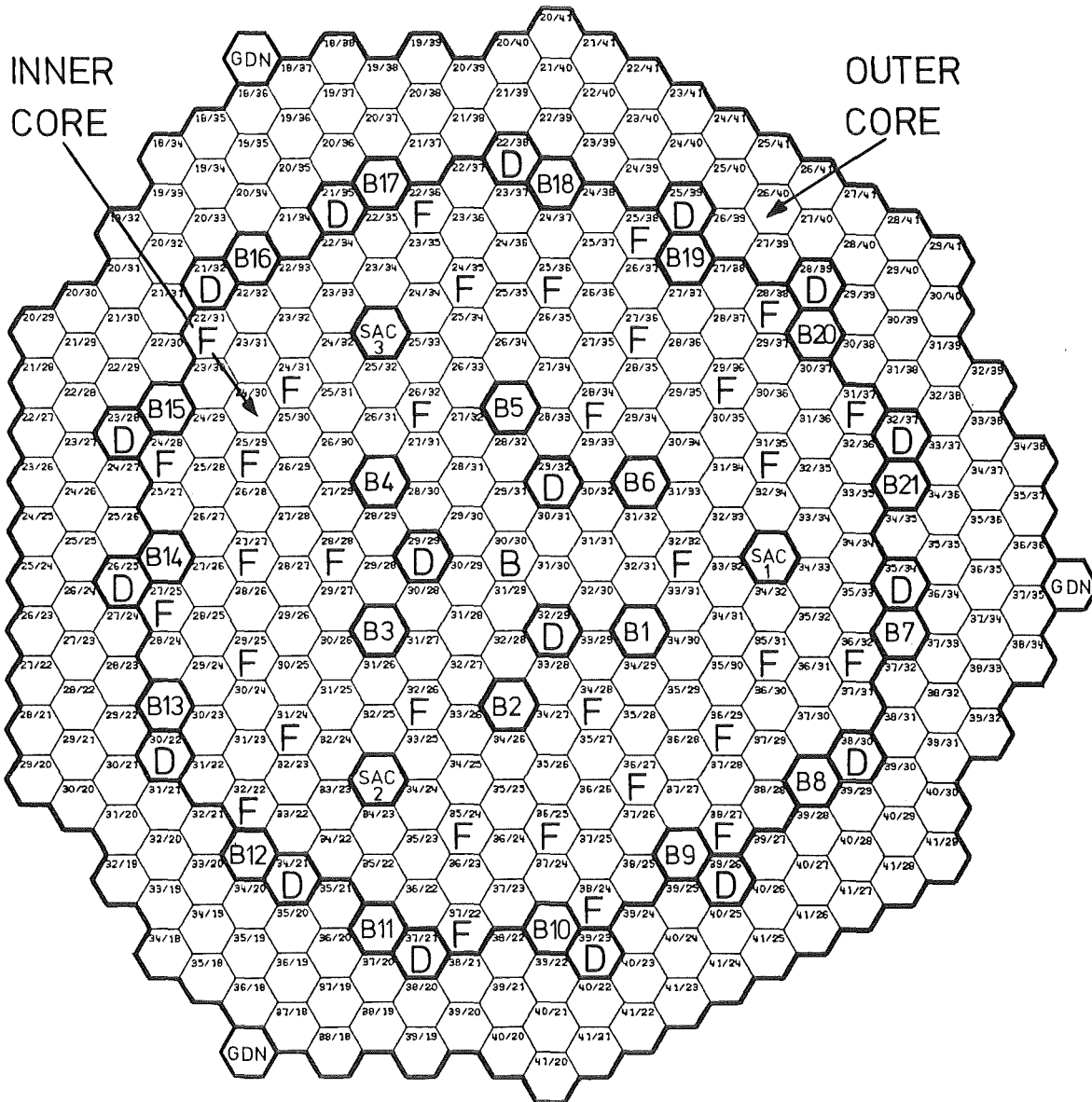


Figure 1 Core loading of SUPER-PHENIX-1
Core version C1D

- B1 ... B21 : Individual control rods of the SCP system
- SAC1 ... SAC3 : Individual control rods of the SAC system
- D : Diluent positions
- B : BOUPHY position
- GDN : Neutron guide tube positions for under vessel reactor operation instrumentation

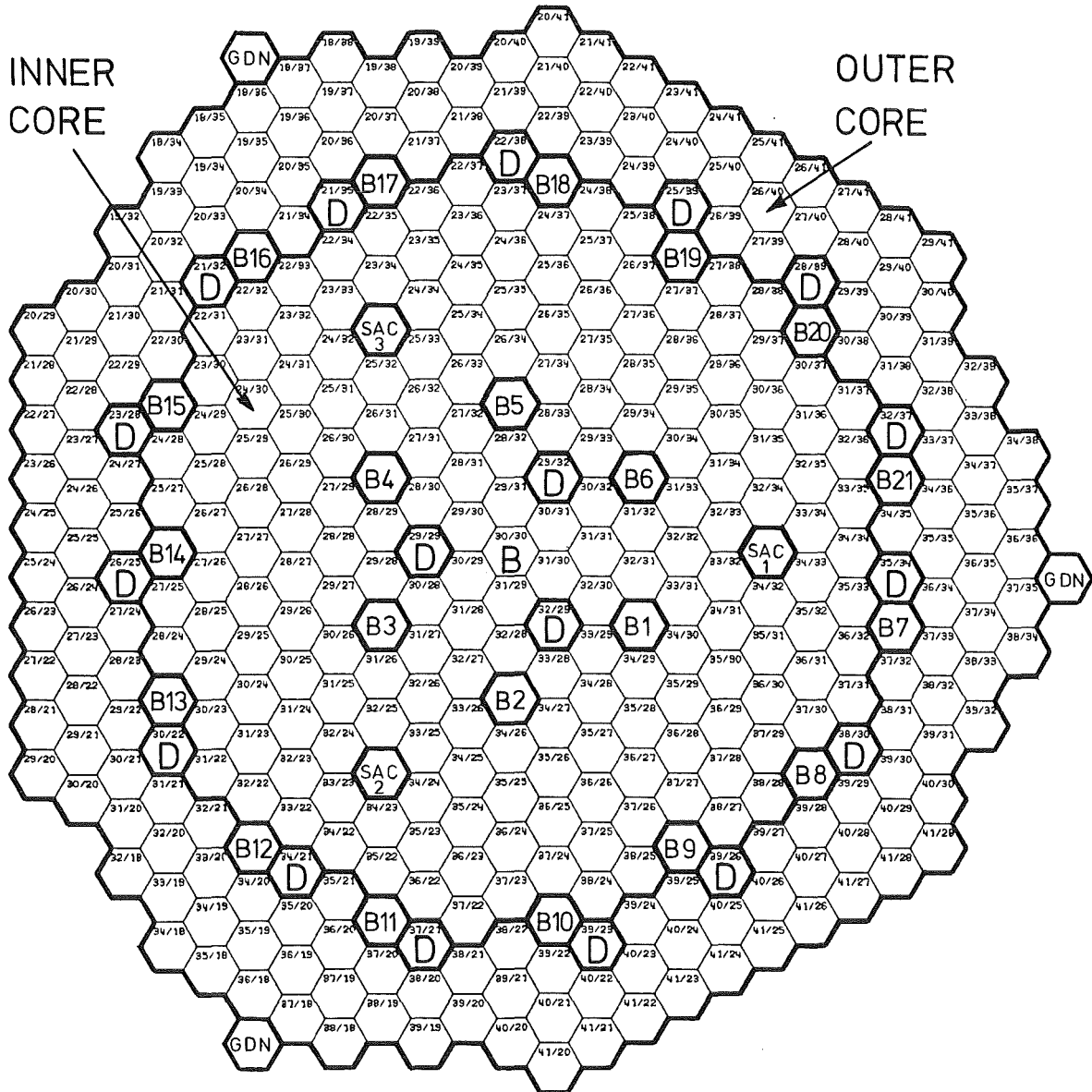


Figure 2 Core loading of SUPER-PHENIX-1
Core version CMP

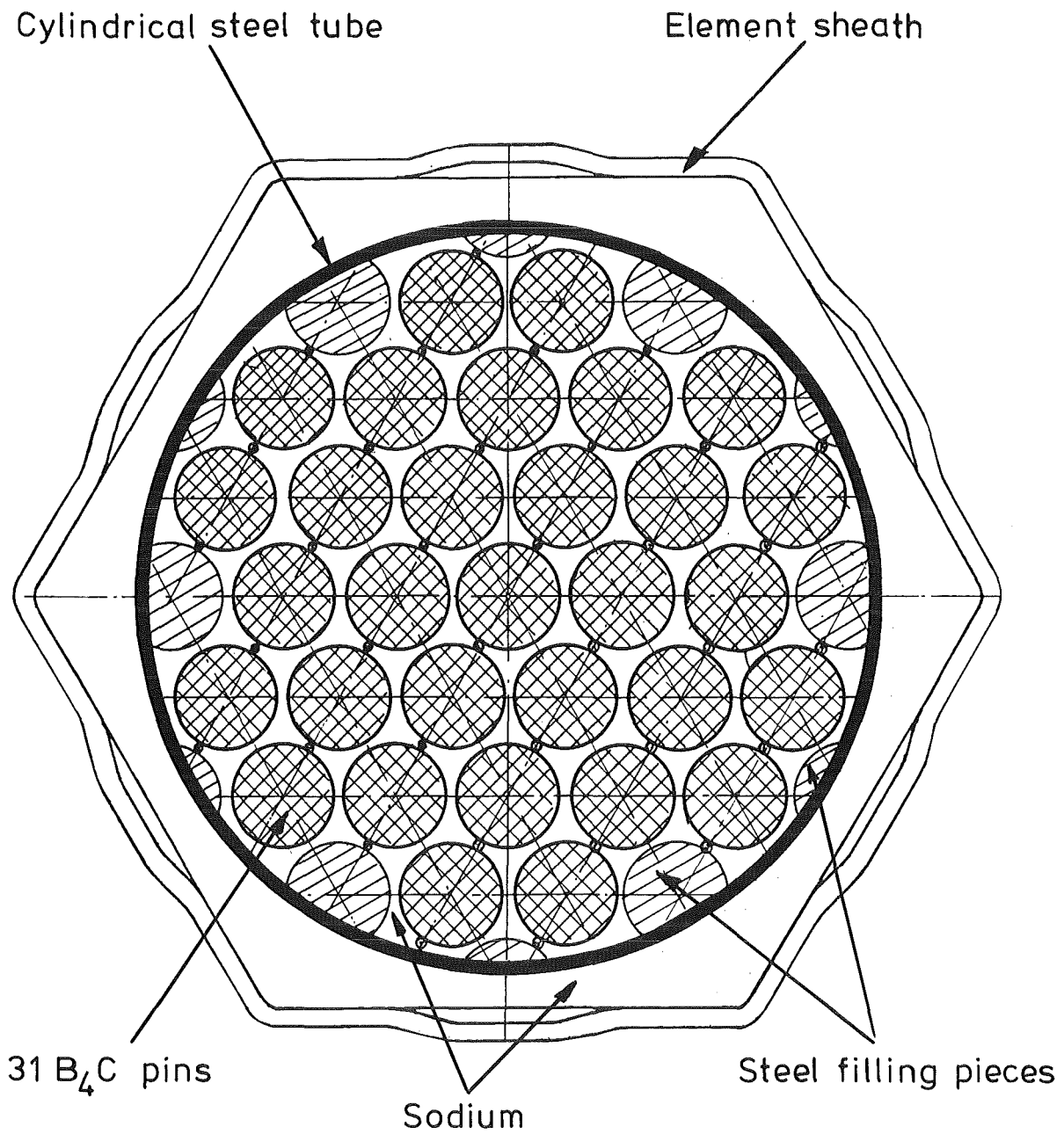


Figure 3 Layout of an SCP absorber

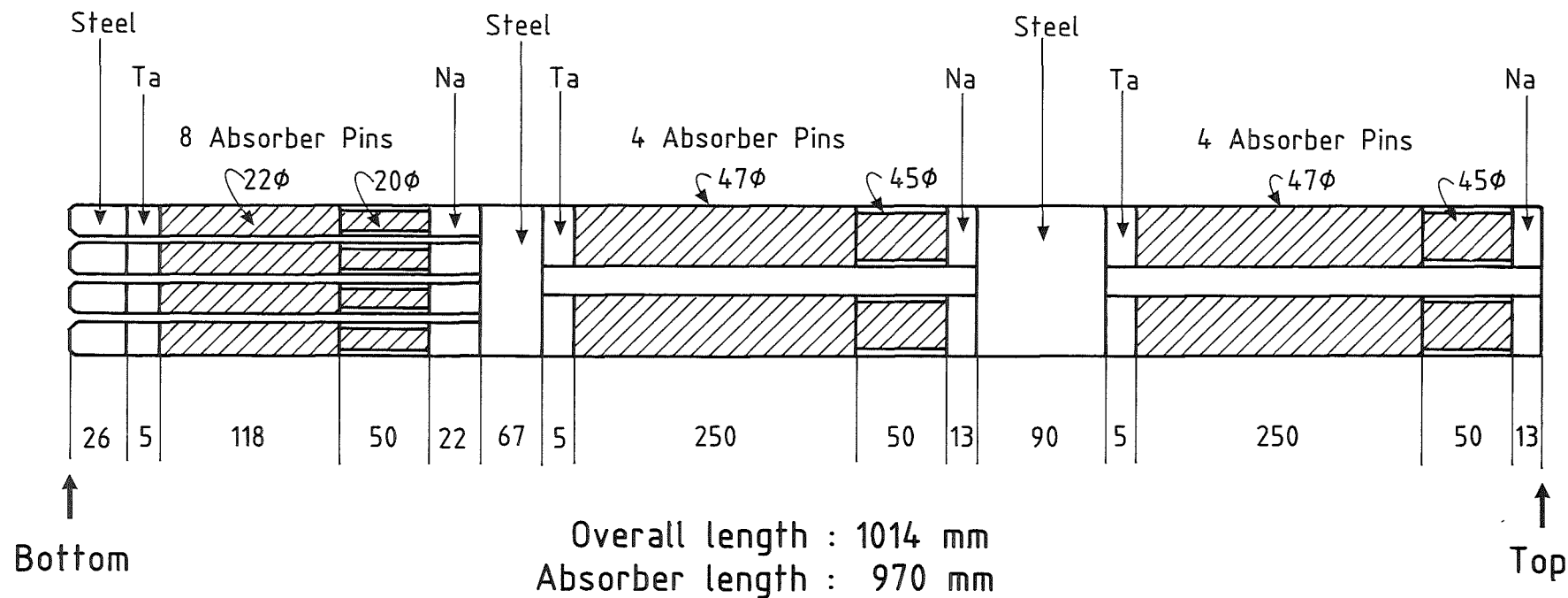
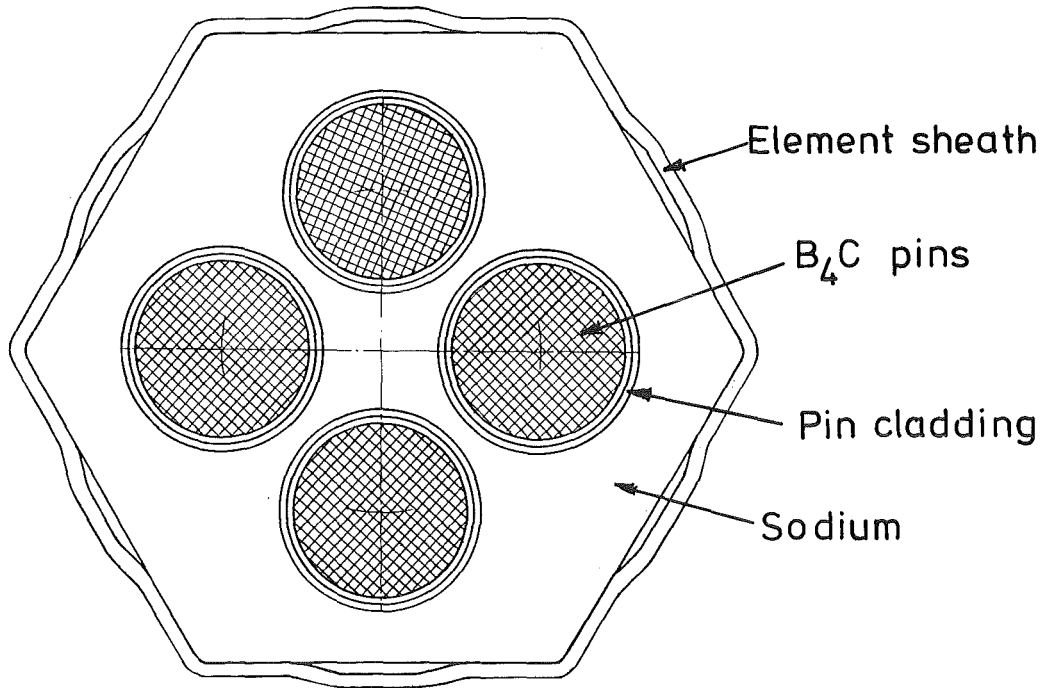


Figure 4 Schematic construction of a SAC absorber assembly
 (All dimensions are given in [mm] and refer to T=20°C)

ATTENTION: DRAWING IS NOT TO SCALE!

Upper and central absorber unit



Lower absorber unit

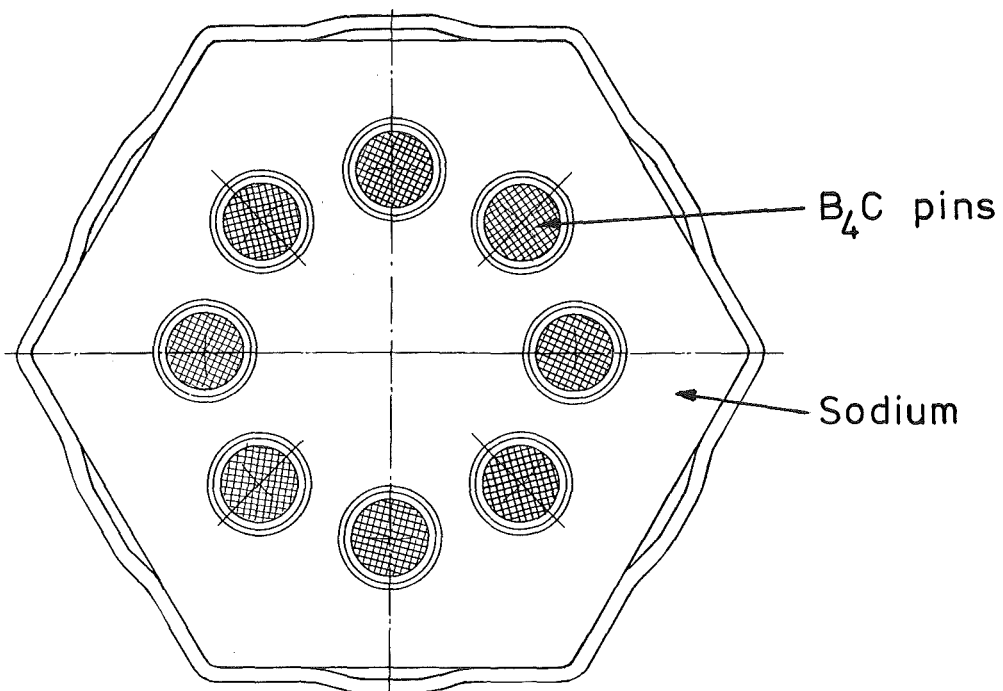


Figure 5 Layout of the SAC absorbers

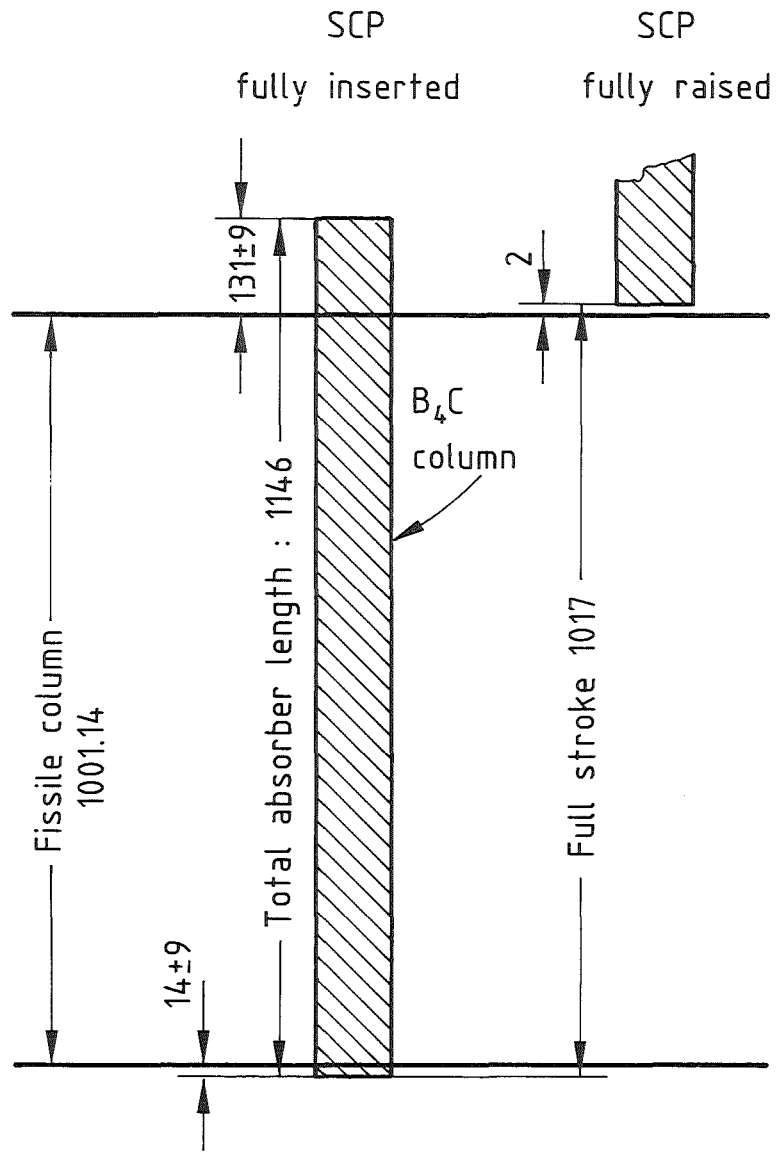


Figure 6
 Axial position of the B_4C column of SCP control rods with respect to the fissile loading at 180°C
 (Dimensions are in [mm])

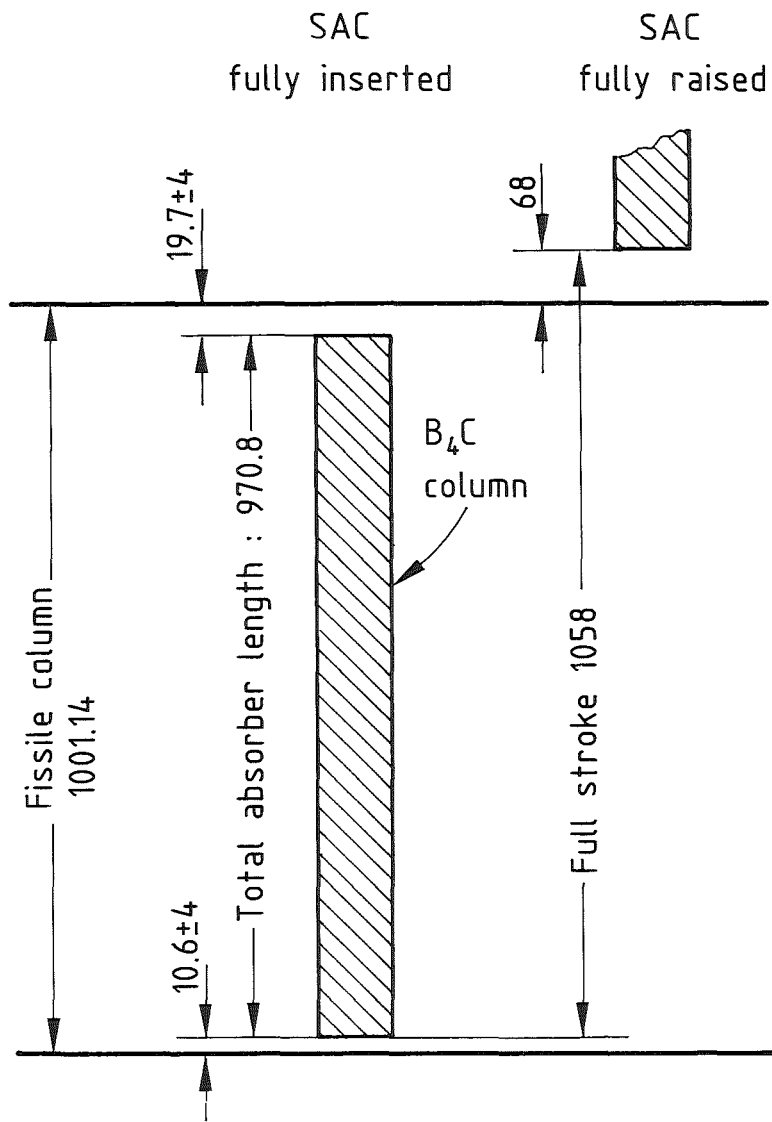


Figure 7
 Axial position of the B_4C
 column of SAC control rods
 with respect to the fissile
 loading at 180°C
 (Dimensions are in [mm])

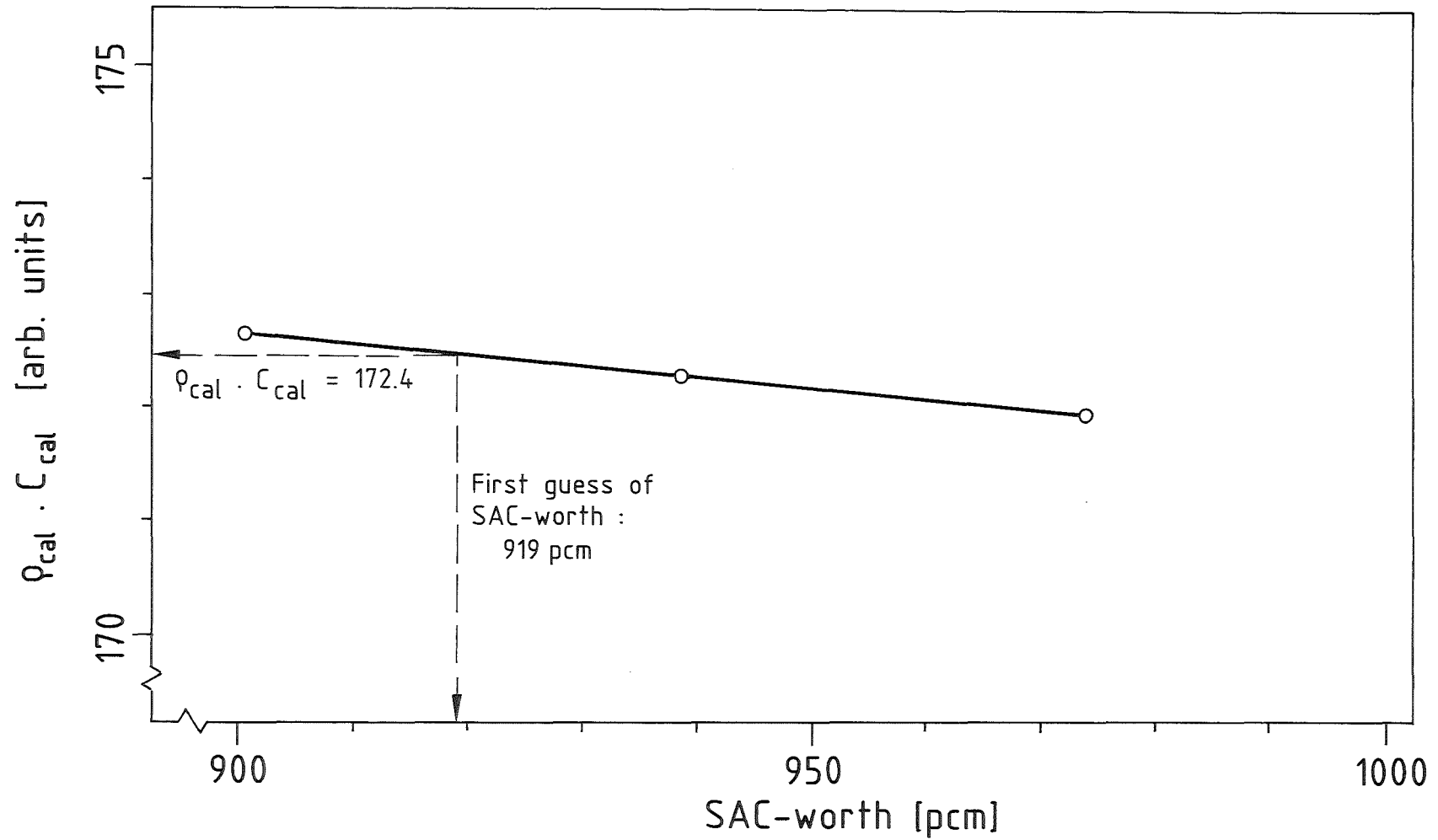


Figure 8 The determination of " $\rho_{\text{cal}} \cdot C_{\text{cal}}$ " for the C1D Etalon
(Calculation : 2D, 4 energy groups, mesh M1)

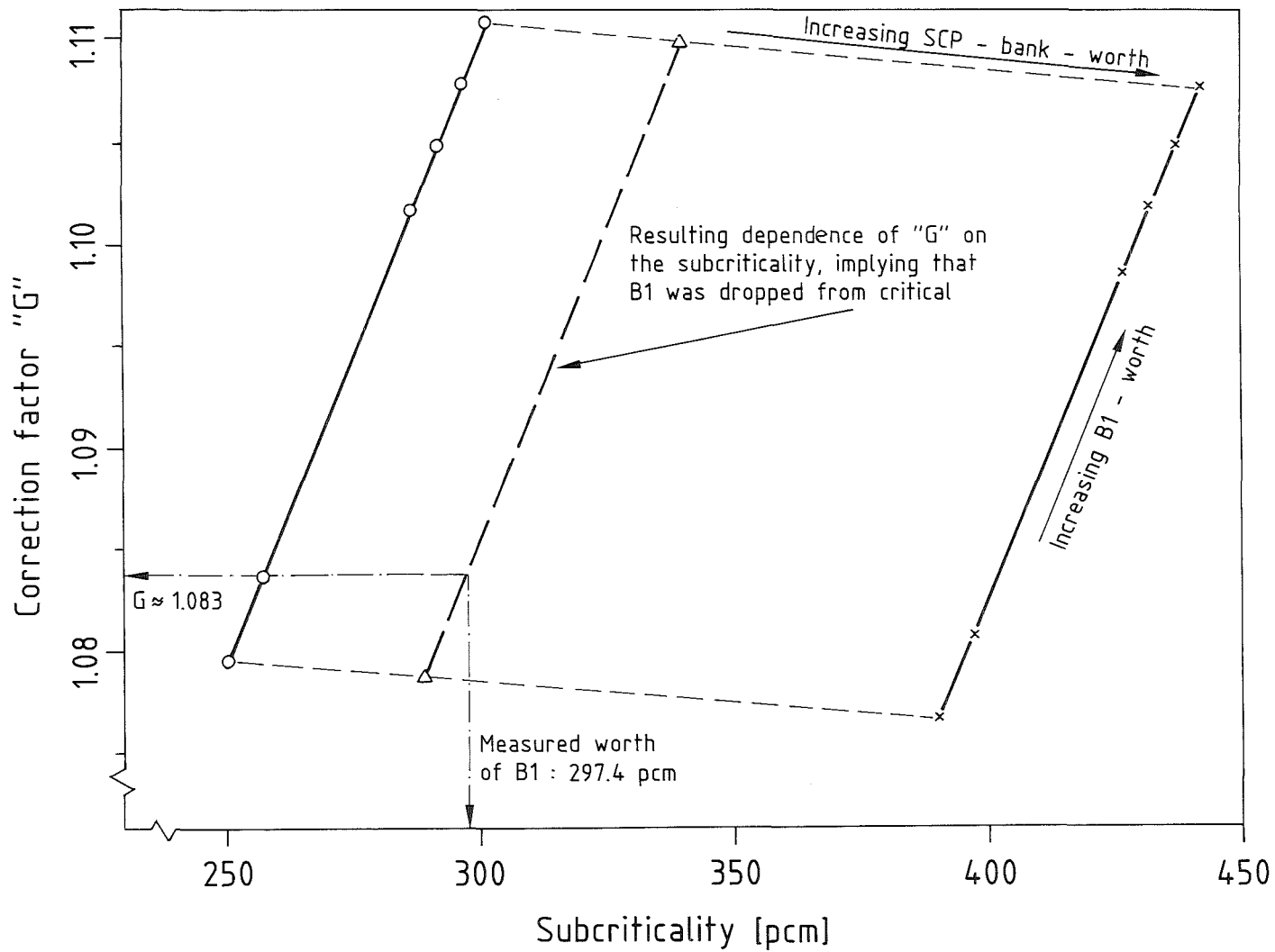


Figure 9 Correction factor "G" for SCP 920 B1↓B2↑ in C1D
(Calculation : 2D, 4 energy groups, mesh M1)

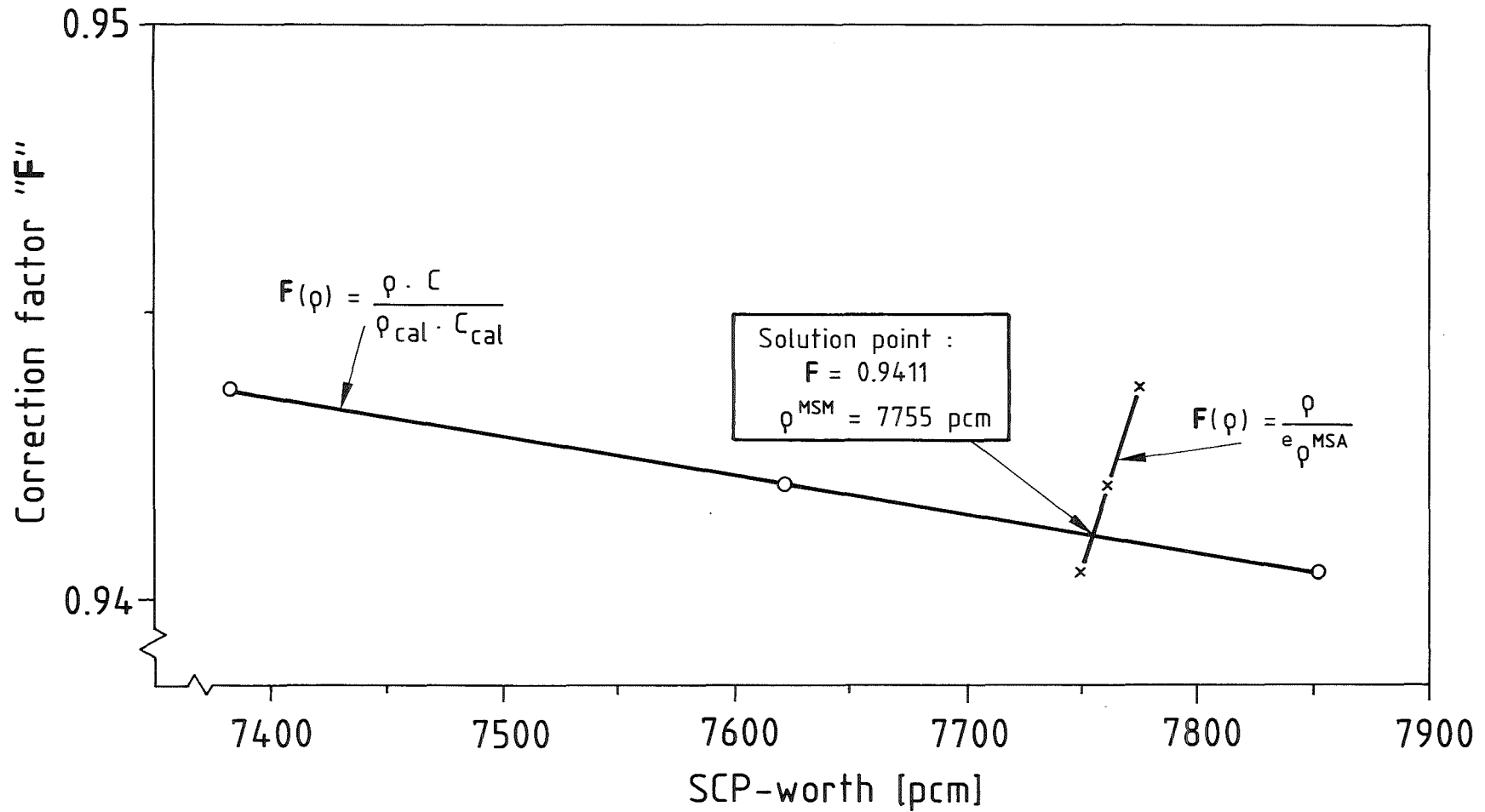


Figure 10 Correction factor "F" for SCP↓ SAC↑ in C1D
 (Calculation : 2D, 4 energy groups, mesh M1)

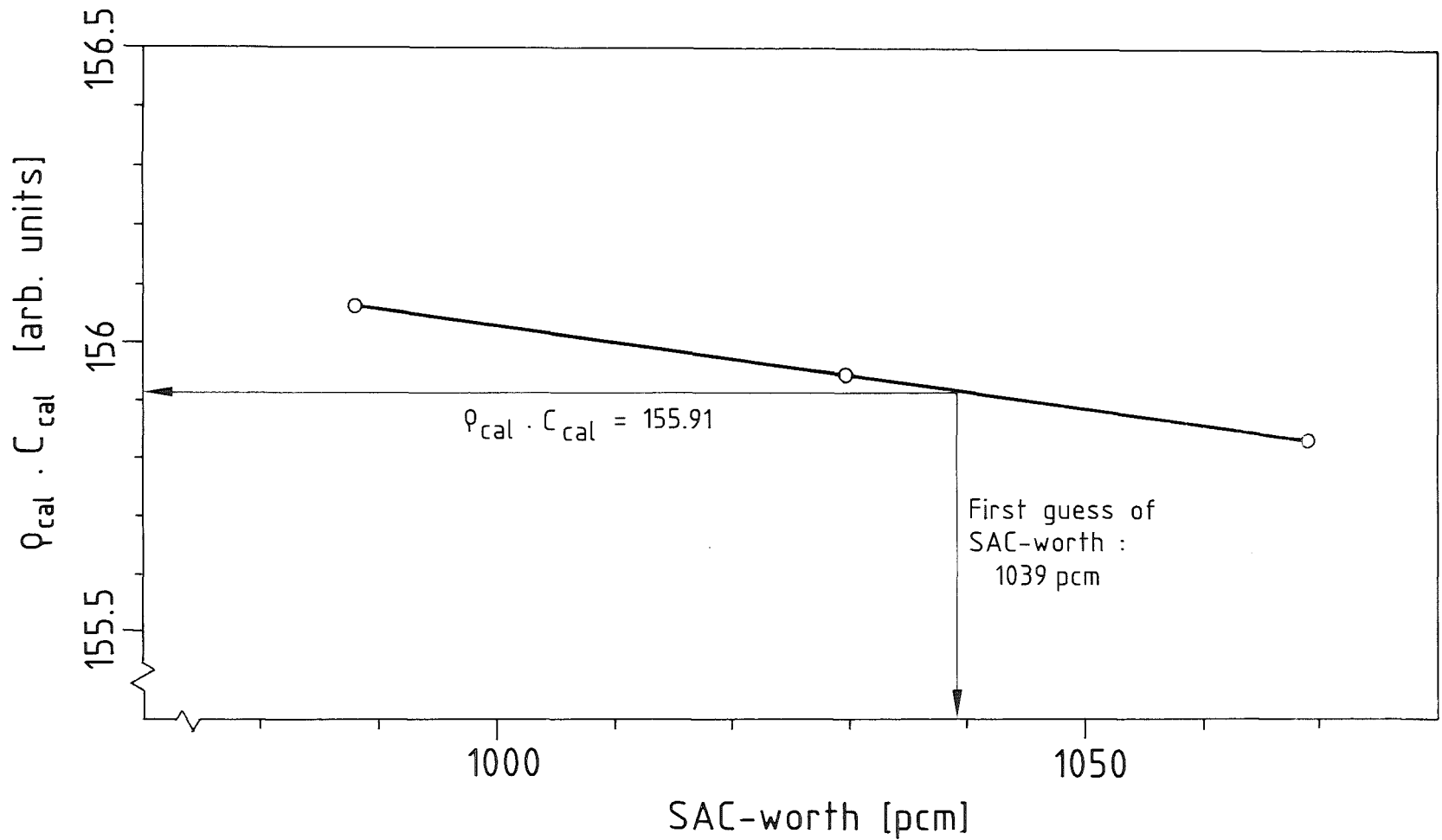


Figure 11 The determination of " $\rho_{cal} \cdot C_{cal}$ " for the CMP Etalon (Calculation : 2D, 4 energy groups, mesh M1)

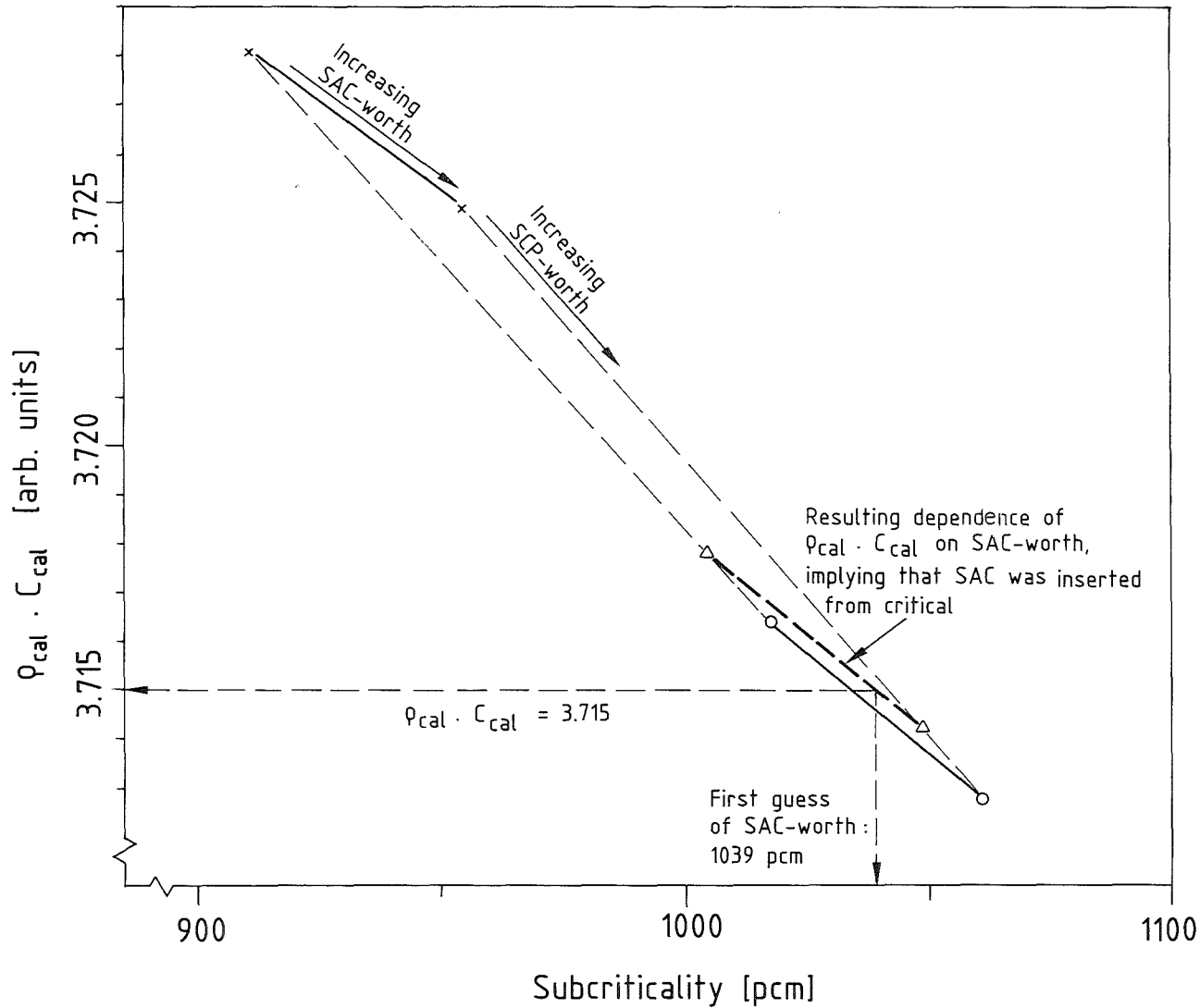


Figure 12 The determination of " $\rho_{cal} \cdot C_{cal}$ " for the CMP Etalon (Calculation : 3D, 4 energy groups, mesh M1)